Missouri S&T Library and Learning Resources

Scholars' Mine

Doctoral Dissertations | Student Theses and Dissertations

Summer 2010

Phase equilibria in iron phosphate system

Liying Zhang

Follow this and additional works at: https://scholarsmine.mst.edu/doctoral_dissertations

 Part of the Ceramic Materials Commons

Department: Materials Science and Engineering

Recommended Citation

Zhang, Liying, "Phase equilibria in iron phosphate system" (2010). *Doctoral Dissertations*. 1952.
https://scholarsmine.mst.edu/doctoral_dissertations/1952

This thesis is brought to you by Scholars' Mine, a service of the Missouri S&T Library and Learning Resources. This work is protected by U. S. Copyright Law. Unauthorized use including reproduction for redistribution requires the permission of the copyright holder. For more information, please contact scholarsmine@mst.edu.

PHASE EQUILIBRIA IN IRON PHOSPHATE SYSTEM

by

LIYING ZHANG

A DISSERTATION

Presented to the Faculty of the Graduate School of the

MISSOURI UNIVERSITY OF SCIENCE AND TECHNOLOGY

In Partial Fulfillment of the Requirements for the Degree

DOCTOR OF PHILOSOPHY

in

CERAMIC ENGINEERING

2010

Approved by

Mark E. Schlesinger, Advisor

Richard K. Brow, Co-advisor

William G. Fahrenholtz

Jeffrey D. Smith

William J. James

PUBLICATION DISSERTATION OPTION

The Introduction and Background sections of this dissertation provide information about the research topic, and a review of the literature. The body of this dissertation has been compiled in the format for publication in peer-reviewed journals. Four papers have been included. The first paper, "Phase Equilibria in the Fe_2O_3-P_2O_5 System," was submitted to the *Journal of the American Ceramic Society* in April 2010. The second paper, "Glass Formation from Iron-Rich Phosphate Melts," has appeared in the *Journal of Non-Crystalline Solids,* volume 356, pages 1252-1257, May 2010. The third paper, "Thermal Studies of Glasses Melted in $Fe_4(P_2O_7)_3$-$Fe(PO_3)_3$ System," was accepted by *Journal of Non-Crystalline Solids* in April 2010. The fourth paper, "A Raman Study of Iron-Phosphate Compounds and Glasses," will be submitted to the *Journal of the American Ceramic Society* in June 2010.

The appendices include experimental results and discussion that are not covered in the main body of this dissertation. This information is presented in the form of manuscripts that must be modified, or expanded, before submitting for publication. The first manuscript, "Preparation and Characterizations of Iron Phosphate Compounds," was prepared to provide detailed information about the preparation, successful and not, of the seventeen iron phosphate compounds reported in literature that form the foundation of this research project. The second manuscript, "The Liquidus Surface of the $Fe_2P_2O_7$-$Fe(PO_3)_2$ System," was prepared to summarize the results of the initial equilibrium study of the ferrous phosphate system.

ABSTRACT

The main objectives of this research were to synthesize iron phosphate compounds, study phase equilibria in the iron phosphate system, focusing on the glass forming area, and investigate glass formability and properties based on the liquidus regions. Twelve iron phosphate compounds were successfully prepared and studied in terms of liquidus temperature or decomposition behavior. The liquidus surface of the Fe_3PO_7- $Fe(PO_3)_3$ system was re-determined and found to be significantly different from that originally presented by Wentrup in 1935. Eutectic points exist at 58.0 mole% Fe_2O_3 (1070°C), 42.7 mole% Fe_2O_3 (925°C), and 37.0 mole% Fe_2O_3 (907°C). The latter two eutectic points bracket the conventional iron phosphate glass-forming range. The liquidus surface of the $Fe_2P_2O_7$-$Fe(PO_3)_2$ system was also determined. A eutectic point exists at 52.8±0.5 mole% FeO and 935°C in the $Fe_2P_2O_7$-$Fe(PO_3)_3$ system. Glass formation of iron-rich phosphate glasses (nominal Fe/P ratios between 1.0 and 1.6) requires a critical cooling rate in the range 10^3-10^4 ºC/sec, compared to 1-10ºC/sec for conventional iron phosphate melts (nominal Fe/P ratios near 0.50). The structures of the iron-rich phosphate glasses are based on isolated orthophosphate tetrahedra, similar to those found in α-$FePO_4$. The stability of melts (with nominal Fe/P compositions between 0.50 and 0.67) against crystallization, described by the Angell and Weinberg parameters, generally decreases with increasing O/P and Fe/P ratios. The structures of crystalline and glassy iron phosphates were studied using Raman spectroscopy. The correlation of the structure of iron phosphate compounds and the Raman modes was summarized and established. The structural parameters (like P-O bond length) of glassy iron phosphates were predicted and discussed.

ACKNOWLEDGMENTS

I am very grateful to my advisor- Dr. Mark E. Schlesinger. It is his encouragement, commitment and support from the initial to the final makes this thesis possible. I also own my deepest gratitude to my co-advisor- Dr. Richard K. Brow, who offered his support and guidance all the time all the ways during this study.

I sincerely appreciate my committee members- Dr. William G. Fahrenholtz, Dr. Jeffrey D. Smith, and Dr. William J. James for their very helpful discussions and constructive suggestions. My appreciation also goes to Dr. Wenhai Huang at Tongji University for introducing me to studying in the USA.

My sincere thanks also go to Dr. Edgar D. Zanotto for his expert comments and suggestions; and Luciana Ghussn for her help with my experiments and life in Brazil; Gustavo, Anne, Oscar, Marcio, Guilherme, Jose and the other members in LaMaV (Sao Carlos, Brazil) for making my study in Brazil fruitful and colorful.

I am so glad to have Melodie L. Schmitt as my colleague in this project. I appreciate her help and the friendship; I want thank all the others in Dr. Brow's group- Signo, Chistopher, Nathaniel, Teng, Jong Wook, Zhongzhi, Lina, Jamie, Xiaoming, Rick (Hen Hsien) and Sagnik. Many thanks to the technicians and staff in MRC, and also to my other friends who have made me enjoy the studies in Rolla.

Last but not least, I want to thank those who made my study and life possible: my parents- Zhengji Zhang and Shufen Qin, and my beloved husband- Qiang Fu. It is their love, care and encouragement that keep me moving forward with my research and my life as well.

TABLE OF CONTENTS

LIST OF ILLUSTRATIONS

Page

LIST OF TABLES

Page

SECTION

1. PURPOSE OF THIS DISSERTATION

Iron phosphate glasses and crystals have a variety of technological applications, including hosts for nuclear wastes, and electrodes for Li-batteries. However, the volatility of P_2O_5 at high temperatures, and the sensitivity of the iron valence to changes in conditions (temperature, oxygen partial pressure, material composition) have limited the number of studies of the equilibrium phases in iron phosphate systems, and those few studies available provide contradictory information. Therefore, the main purpose of this PhD research is to determine the phase equilibria, especially the liquidus surface, of the ferric and ferrous phosphate system, and to then use this information to evaluate the glass-forming tendency of iron phosphate melts.

The first step in this research was to prepare and characterize the 17 iron phosphate compounds reported to form in the system. Most of these compounds, ferric, ferrous and mixed valent phosphates, are not commercially available, and so preparation techniques obtained from the literature and developed in the lab were used to synthesize each stoichiometry. Five of the 17 reported compounds could not be prepared, raising questions about the reported phase equilibria in these systems.

With the compounds that form in the respective systems, the phase equilibria in the ferric phosphate and ferrous phosphate systems were studied. A variety of techniques were developed to minimize changes in iron valence and to prevent P_2O_5-loss from samples heated to different temperatures. Such compositional changes are the likely reasons for differences in the phase equilibria determined in this study, compared with

reports in the literature. In particular, it was found that sealing samples in silica ampoules with air minimized P_2O_5 loss and the reduction of Fe(III) to Fe(II) for melts in the $Fe_4(P_2O_7)_3$-$Fe(PO_3)_3$ system, and sealing ferrous phosphate samples in silica under vacuum minimized the oxidation of Fe(II) and phosphate loss. Analyses of samples quenched from different temperatures were used to determine liquidus surfaces.

The resulting determination of an accurate liquidus surface provided useful information for extending the iron phosphate glass forming regions, and for characterizing the crystallization behavior of different iron phosphate melts. The first systematic study of the structure and properties of iron-rich phosphate glasses, with compositions around the eutectic composition of the $FePO_4$-Fe_3PO_7 system, was conducted. These compositions produce glasses based on orthophosphate anions, and require rapid quenching techniques to avoid crystallization. Glass forming tendency for compositions from the $Fe(PO_3)_3$-$Fe_4(P_2O_7)_3$ system were determined using characteristic temperatures measured by differential scanning calorimetry. In this system, compositions with lower O/P ratios and so produce longer polyphosphate anions are generally easier to quench from melts to produce glasses. Raman spectroscopy proved to be a valuable tool for characterizing the phosphate anions that constitute iron phosphate glasses. Similarities in the Raman spectra of crystalline compounds and related glasses were critical for understanding the structure-composition relationships for the glasses, including the development of a correlation to predict structural parameters like P-O bond lengths from the Raman spectra of iron phosphate glases.

In the end, the liquidus surfaces of the $Fe(PO_3)_3$-Fe_2O_3 and the $Fe(PO_3)_2$-$Fe_2P_2O_7$ systems were determined and shown to be useful for identifying new iron phosphate

glasses, as well as for understanding the glass-forming characteristics of the more well-known iron phosphate melts. Information obtained from Raman spectroscopy on the relatively simple iron phosphate glasses, including the orthophosphate compositions, should prove useful for those studying for complex compositions, including those designed for nuclear waste storage.

2. BACKGROUND

2.1. APPLICATION OF IRON PHOSPHATE SYSTEM

2.1.1. Iron Phosphate Glasses for Nuclear Waste Vitrification. Nuclear wastes are hazardous materials with radioactivity and must be handled carefully under certain regulations. There are several different types of nuclear waste. Table 2.1 shows the nuclear waste classification in the DOE nuclear weapon complex [1]. High-level (HLW) and low-level nuclear (LLW) wastes are the major part of nuclear waste, among which, HLW is responsible for 95% of the entire radioactive nuclear waste in terms of radiation. The radioactivity of the nuclear waste decays with time. Some of the elements in the HLW decay slowly and remain radioactive for hundreds or thousands of years. Each year, nuclear power generation facilities worldwide produce about 200,000 m^3 of low- and intermediate-level radioactive waste, and about 10,000 m^3 of high-level wastes including used fuel designated as waste [2].

The HLW can be vitrified into glass materials and solidified in stainless steel canisters. The advantages of turning wastes into glasses include the immobilization of most heavy metal ions by chemically bonding them in the glass structure, cost savings for transport and storage and the diversity of the waste that can be vitrified due to the dissolution capability of many glass melts [3,4]. DOE currently only approves borosilicate glass for the vitrification of nuclear waste [5]. However, some waste feeds are poorly soluble or chemically incompatible in borosilicate glass. Iron phosphate glasses with Fe/P ratios between 1:3 and 2:3 are a promising alternative for vitrifying nuclear waste [6-12].

Table 2.1 Nuclear waste classification in DOE complex [1]

Waste category	Definition	Total radioactivity (million curies)
High-level waste (HLW)	Highly radioactive waste resulting from chemical processing of SNF and irradiated target assemblies (DOE 1988,1997a, NWPA 1982)	960
TRU waste	Contains alpha-emitting TRU elements with half-lives >20 years whose combined activity level is at least 100 nCi/g of waste at the time of assay (DOE 1988,1997a)	4
Low-level waste (LLW)	Radioactive waste not classified as HLW, TRU waste, SND or natural uranium and thorium by-product defined under 11e(2) of the Atomic Energy Act (DOE 1997)	50
11e(2) by-product material	Produced by the extraction or concentration of uranium or thorium from any ore processed primarily for its source material content (DOE 1997a)	National figures not available, but can exceed 1000 pCi/g
Mixed low-level waste	Contains both hazardous waste subject to RCRA (1976), and source, special nuclear, or by-product material subject to the Atomic Energy Act (DOE 1997a)	<2.4
Hazardous waste	Either listed in the regulations as a hazard waste or exhibits corrosivity, ignitability, reactivity, or toxicity (DOE 1997a)	Not radioactive

Abbreviation: NWPA: Nuclear Waste Policy Act; RCRA: Resource Conservation and Recovery Act; SNF: spent nuclear fuel; TRU: transuranic.

Table 2.2 compares borosilicate glass and iron phosphate glass in terms of the four major factors mentioned above. From the comparison, we can see the advantages of using an iron phosphate matrix compared with a borosilicate glass matrix. And meanwhile, compared to the borosilicate glass, iron phosphate glasses are less expensive considering additional capacity of waste loading, lower melting temperature and shorter melting time, and are now being used for the vitrification of certain types of HLW [13].

Table 2.2 Comparison of borosilicate glass with iron phosphate glass [14]

Glass	Waste loading (wt%)	Chemical durability* ($g/cm^2/min$)	Melting temperature (°C)	Melting time (hr)
Borosilicate	<30%	$10^{7.35}$	1150	≥2
Iron phosphate	Up to 50%	$10^{7.7}$	950-1100	1-2

* Dissolution rate at 90°C in distilled water

It is reported that the HLW in Hanford WA can be vitrified directly by adding 25-30 wt% phosphate [15]. Day and co-workers completed simulation experiments, corrosion tests and glass studies especially on the pyrophosphate composition [6-9,11-15].

2.1.2. Application of Iron Phosphate Compounds. Crystalline iron phosphate compounds have potential applications in catalysis, ionic exchange, optical and electrochemical fields [16-20]. $FePO_4$ can be used in the steel and glass industries [21,22]. At normal pressure, it has a berlinite structure with iron and phosphorus both in tetrahedral coordination with oxygens [23]. $LiFePO_4$ and $LiCoPO_4$, which are phosphor-olivine structures, have been developed and widely studied as cathode materials for Li-electrochemical devices [24,25]. Orthorhombic $FePO_4$ has better reversible capacity than

the $FePO_4$ in a trigonal crystalline structure [26]. Fe_3PO_7 is also classified as an electrode material for lithium secondary batteries due to its interesting electrochemical properties such as high first discharge capacity (800 $mAhg^{-1}$) [27]. The compounds FeP_3O_9, Fe_9PO_{12}, Fe_3PO_7, $Fe_4P_6O_{21}$, Fe_2PO_5, $FePO_4$ and $Fe_7P_6O_{24}$ are reported to have possible cathodic activity due to the Fe(III)/Fe(II) redox couple, and for the same reason, all the ferric phosphates are potential electrode materials due to the multi-valences of iron [27].

The hydrate of $Fe_3(PO_4)_2$ has a non-collinear anti-ferromagnetic structure, and has possible application in ion exchange and single-ion anisotropy (i.e. magnetocrystalline anisotropy) [28-30]. $Fe(PO_3)_3$ is anti-ferromagnetic below 10 K due to its structure [31]. The ferrous compound $Fe_2 P_2O_7$ exhibits anti-ferromagnetic properties at about 12.5 K [32]. The interesting magnetic properties of the iron phosphates can broaden the applications for these materials.

The phosphates have drawn much attention due to their interesting physicochemical and catalytic properties [33]. $FePO_4$ can be used for oxidative dehydrogenation due to the multi-valence of the iron [34,35]. It is reported that the best catalysts in the iron phosphate system contain face-sharing FeO_6 octahedra trimers [36]. Phases that contain both Fe(II) and Fe(III) cations were reported to be the active phases which make the necessary electron transfer possible in the catalystic reaction of the oxidative dehydrogenation of isobutyric acid in the temperature range of 650-680 K [37,38]. The iron phosphates from the FeO-Fe_2O_3-P_2O_5 system and their hydroxyl/oxy complements have FeO_6 octahedra in chains separated by cationic vacancies and bound by PO_4 tetrahedra [37,38]. The selectivity of the catalysts is related to the way that FeO_6 edges are shared [36]. Catalysts having structure (a) are more selective than those having

structure (b) in Fig. 2.1. The catalysts could be active for some oxidation reactions due to the limit of their surface oxygen diffusion [36].

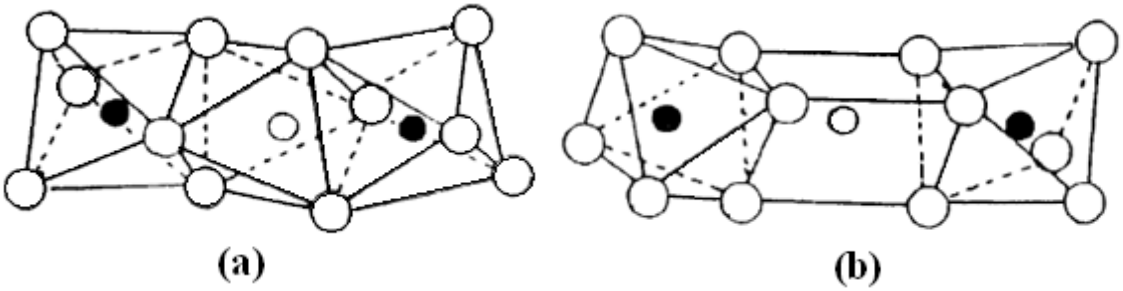

Figure 2.1 Two arrangements of FeO_6 octahedra (•)- Fe(III), (o)-Fe(II) [36].

2.2. PHASE DIAGRAM OF IRON PHOSPHATE SYSTEM

The knowledge of the liquidus surface of the iron phosphate system is beneficial to the preparation and study of glasses and compounds. Iron undergoes valence changes during melting even if the starting materials contains only Fe^{3+} due to the reaction between iron redox couple in the melt [39]. $Fe(II)/Fe_{tot}$ ratio in glasses is affected by melting temperature, time and atmosphere, and the glass composition. The knowledge of the phase equilibira in the iron phosphate system is of interest for Fe^{2+}/Fe^{3+} ratio control in iron phosphate glass making [39]. Meanwhile, the liquidus temperature coupled with glass transition and crystallization temperatures can be used to evaluate glass thermal stability and formability [39-41]. The crystallization behavior can be explained further by understanding the phase equilibria in the iron phosphate system. And based on the studies of the phase diagram, the glass forming area might be extended, by studying the glass forming tendency in each system, especillay around the eutectic areas.

In 1935, Wentrup studied the liquidus behavior of the Fe-P-O system [42], and reported some phase equilibria for the Fe_2O_3–$Fe_4(P_2O_7)_3$, FeO–$Fe_3(PO_4)_2$ and $Fe_3(PO_4)_2$–

$Fe_4(P_2O_7)_3$ systems. Wentrup determined the liquidus surface by recording the heating and cooling curves of the compositions. He used platinum crucibles for the experiments, which increased the potential of reduction reaction of Fe(III) in the melt. He used $FePO_4$, $Fe_4(P_2O_7)_3$ and Fe_2O_3 for ferric phosphate studies, and $Fe_3(PO_4)_2$ for ferrous phosphate studies, which was not homogeneous but the only one available at that time. Figure 2.2 shows the phase digram reported by Wentrup. Wentrup reported a eutectic at 968°C between $FePO_4$ and an iron oxy-phosphate, $2Fe_2O_3{\cdot}P_2O_5$. However, Korinth and Royen reported that the iron oxy-phosphate should be Fe_3PO_7, and that $2Fe_2O_3{\cdot}P_2O_5$ can not be obtained [43]. Gleitzer and his colleagues investigated solid-state equilibria in the Fe-P-O system at 900°C under a range of oxygen partial pressures, and did not report the formation of $2Fe_2O_3{\cdot}P_2O_5$ [44,45]. Another controversy concerns the $FePO_4$–$Fe_4(P_2O_7)_3$ system. Wentrup reports that the melting temperature of the pyrophosphate is greater than 1200°C, However, in a recent report, pyrophosphate glass can be melted at a lower temperature [6,8,39].

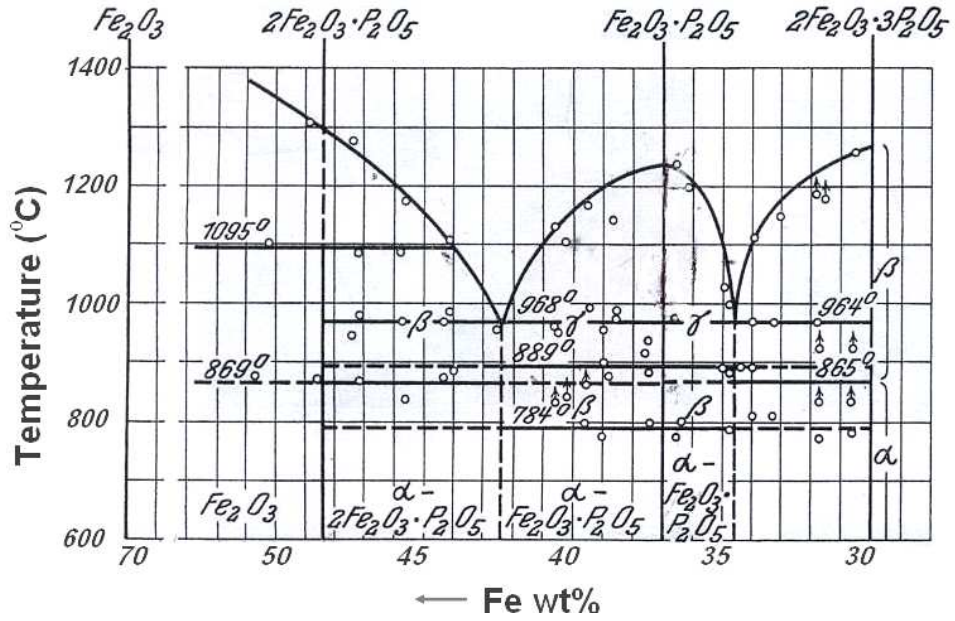

(a)

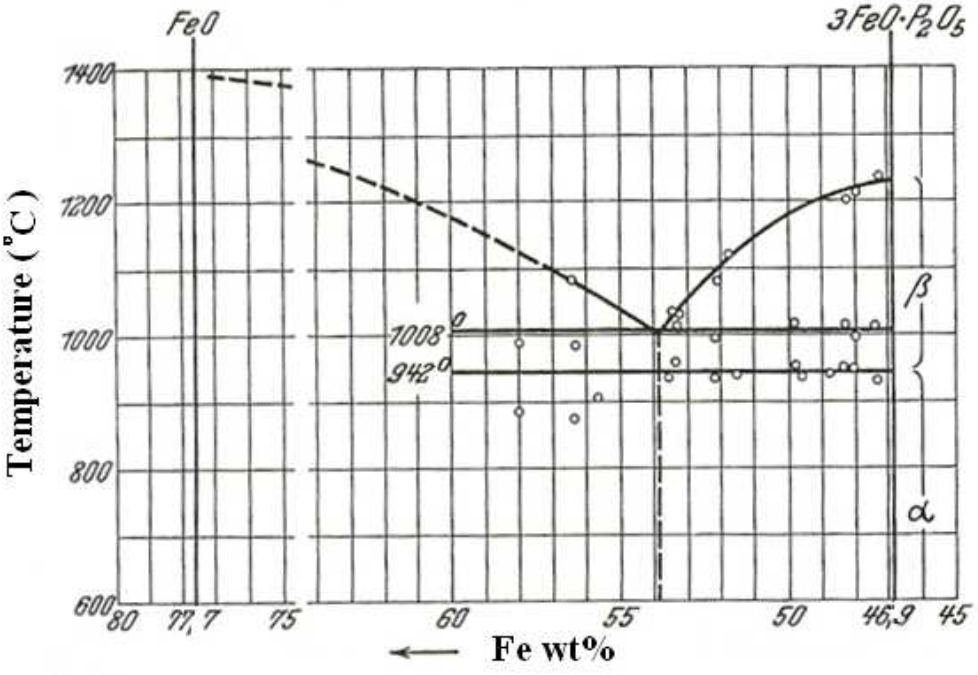

(b)

Figure 2.2 Phase diagrams reported by Wentrup [42], (a)- ferric phosphate system; (b)- ferrous phosphate system; and (c)-mixed valent iron phosphate system.

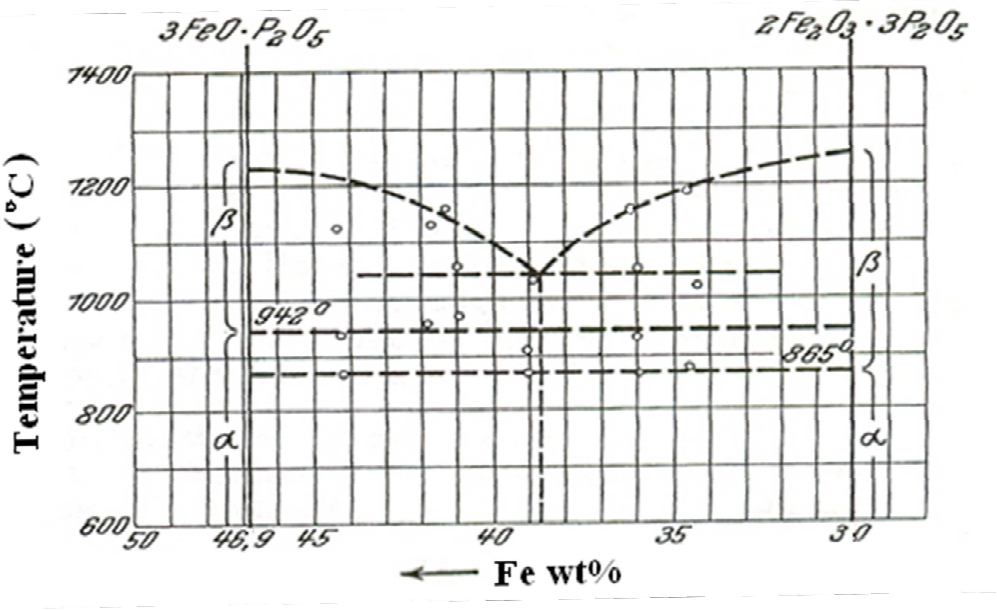

(c)

Figure 2.2 Phase diagrams reported by Wentrup [42], (a)- ferric phosphate system; (b)- ferrous phosphate system; and (c)-mixed valent iron phosphate system. (cont.)

Trömel and his coworkers studied the phase equilibria of one part of the FeO-P_2O_5 system in 1963 [46] (see Fig. 2.3), which is helpful for the phase equlibria study of Fe-P-O slags in the metallurgical industry. They reported that ferrous-rich phosphate melt ($P_2O_5 \leq 32$wt%) has a peritectic reaction at 960°C to Q phase (containing 10% P_2O_5) and wüstite, and then at 940°C has a eutectic reaction between $Fe_3(PO_4)_2$ and Q phase. Meanwhile, they did some isothermal studies on ferrous-rich phosphate melts. Trömel and Wentrup did not indicate experimental melting temperature of the compound $Fe_3(PO_4)_2$. Extrapolation of the liquidus surfaces reported by Trömel and Wentrup gave 1050° and 1250°C, respectively. Meanwhile, the phase diagrams, which are focused on the iron-rich end of the system, do not satisfy the demands of current interest about P_2O_5-rich part.

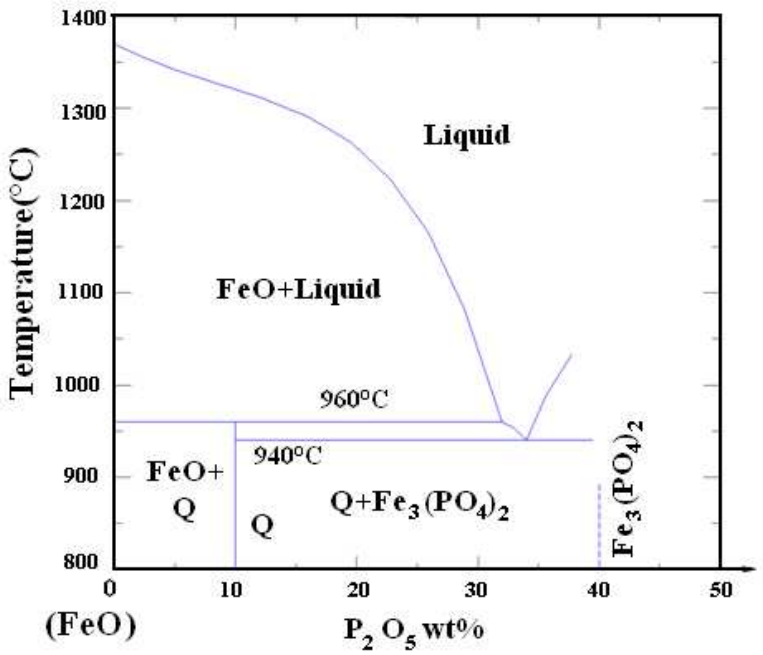

Figure 2.3 Phase diagram reported by Trömel [46]

Some data on the melting behavior and temperatures of iron phosphate compounds have been reported. The melting temperature of $FePO_4$ is reported to be 1230°C–1240°C using quenching experiments [42,47]. The decomposition of Fe_3PO_7 at temperatures above 1100°C to $FePO_4$ and Fe_2O_3 was mentioned without detailed description [43,48]. The incongruent melting temperature of Fe_3PO_7 is estimated to be 1375°C, with uncertainty due to the baseline drift of DTA. Three endothermic DTA peaks between 1000°C and 1150°C when Fe_3PO_7 is heated were reported [49]. Investigation has been carried out on the iron redox reaction in glass melt, and demonstrates that iron (II) formation is more favorable with increasing temperature [39,50-52]. The dissociation of $FePO_4$ into $Fe_2P_2O_7$ and O_2 was reported by Teterevkov [53].

Gorbunov reported that $Fe_7(PO_4)_6$ has a melting temperature of 996°C [54]. For the other compounds, no exact melting temperatures were reported. Glass-melting work has been reported in the iron phosphate system [6,8,39,55,56], which provides some information about the liquidus surface of this system. However, the reported information covers only a small fraction of the system.

2.3. PREPARATION OF IRON PHOSPHATE COMPOUNDS

Establishing the phase equilibria in the iron phosphate system requires preparation of pure iron phosphate compounds. Thirteen iron phosphate compounds are included in Powder Diffraction File (PDF) database [57]. Among them, four are ferric-phosphates, four are ferrous phosphates, and the others are mixed valence compounds. In addition, four compounds are mentioned in literature but without preparation procedures or good characterization, and with no XRD data. They are $Fe_4P_6O_{21}$, $Fe_5P_3O_{13}$, $Fe_5P_2O_{11}$, and $Fe_5P_4O_{16}$. Those compounds were also investigated in this Ph.D research.

2.3.1. Ferric Phosphate Preparation. Hong et. al used Fe_2O_3 and $(NH_4)_2HPO_4$ as starting materials to prepare Fe_3PO_7 by solid-state reactions [58]. $FePO_4$ was made at 950°C by the reaction of Fe_2O_3 and $(NH_4)_2HPO_4$, and then Fe_3PO_7 was synthesized from the reaction of $FePO_4$ and Fe_2O_3 at 1050°C for twelve hours. $Fe_4(P_2O_7)_3$ was discovered by D'Yvoire [59] by heating a mixture of $FePO_4$ and $Fe(PO_3)_3$ to 950°C. $Fe_4(P_2O_7)_3$ was made by solid reaction of $FePO_4$ and $Fe(PO_3)_3$ at 940°C [60,61]. $Fe(PO_3)_3$ can be synthesized by heating a mixture of $Fe(NO_3)_3 \cdot 9H_2O$ and $NH_4H_2PO_4$ at 800°C or $Fe(NO_3)_3 \cdot 9H_2O$ and HNO_3 at 900°C [62,63]. The preparation of ferric phosphates is undertaken in air or oxygen.

2.3.2. Ferrous Phosphate Preparation. $Fe_4P_2O_9$ ($Fe_4(PO_4)_2O$) was prepared by Gleitzer and his colleagues in a vacuum sealed silica tube heated at 900°C or by reducing a mixture of Fe_2O_3-$FePO_4$ or Fe_3PO_7-$FePO_4$ in a H_2-containing atmosphere at 900°C [64]. Gleitzer also mentioned that under these experimental conditions, it was difficult to obtain pure $Fe_4P_2O_9$ because it was stable only in a narrow range of oxygen partial pressure. Parada, et al. prepared γ-$Fe_2P_2O_7$ by solid state reaction between FeC_2O_4 and $NH_4H_2PO_4$ through a strict and complex process [65]. Parada heat-treated the stoichiometric mixture in a closed porcelain crucible to 700°C followed by a 10°C/h cooling to 200°C and then 50°C/h to room temperature, and intermediate grindings were carried out at 250 and 350°C, and samples were held at each temperature for three hours. $Fe_2P_2O_7$ has also been prepared by reducing $FePO_4$ in H_2-containing atmosphere [65-67].

2.3.3. Mixed-Valence Iron Phosphate Preparation. The compounds with mixed valence can be prepared in sealed ampoules at 900°C or by careful reduction of the Fe-P-O batch mixture. Gleitzer prepared $Fe_9(PO_4)O_8$, Fe_2PO_5, $Fe_5P_3O_{13}$, $Fe_7(PO_4)_6$, $Fe_3(P_2O_7)_2$ and $Fe_7(P_2O_7)_4$ by the former methods and crystallized the compounds by annealing with a trace of $FeCl_2$ [67-70]. The preparation of iron phosphates with mixed valence must be carried out in a closed system when the raw materials contain the same Fe/P/O ratio.

2.4. STUDIES OF IRON PHOSPHATE GLASSES

Based on the understanding of the phase equilibria in iron phosphate system, the researchers can look further into the glass structure, crystallization, thermal properties and even chemical durability. As mentioned above, iron undergoes valence change during glass-making, which affects the glass properties and stabilities. The structure of

iron phosphate glasses is complicated due to the different roles of Fe(II) and Fe(III) [71]. Moustafa studied iron oxychloride potassium phosphate glasses and showed that Fe(III) in octahedral coordination can be viewed as a network former, while Fe(II) in octahedral coordination can be viewed as a network modifier [71]. The roles of the Fe(II) and Fe(III) are still uncertain. It is reported that iron content improves the aqueous durability, since the Fe(III)-O-P or Fe(II)-O-P bond is more hydration-resistant than P-O-P bonds [71-73]. For pure P_2O_5, all PO_4 units are attached to three PO_4 neighbors. The cross-links (PO_4 units bonded to three PO_4 units instead of two) are very reactive. Trivalent cations like Fe(III) and Al(III) can produce cross-linking structure in phosphate glass (see Fig. 2.4).

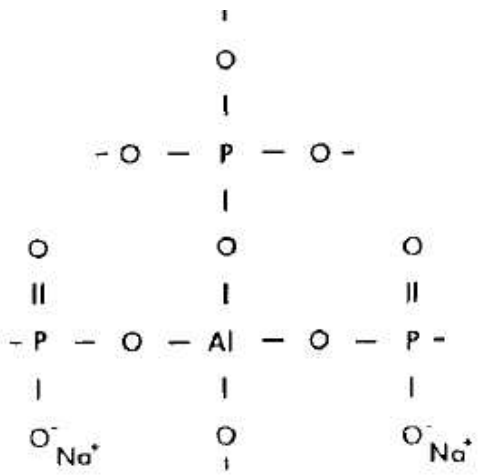

Figure 2.4 Cross-linking agents in phosphate glasses [70].

Fe(II)/Fe(III) ratio in the glass changes with glass melting conditions (including melting temperature, time and atmosphere). The reaction can be written as,

$$Fe^{3+} + ½\ O^{2-} \leftrightarrow Fe^{2+} + ¼\ O_2 \qquad (1)$$

The reduction reaction is an endothermic process. With increasing temperature, Fe(II) formation gets more favorable. Fang and co-workers [39] studied the iron redox equilibrium in nominal $40Fe_2O_3$-$60P_2O_5$ (mol%) glasses melted at different temperatures, and reported that the $Fe(II)/Fe_{total}$ ratio increases from 17% to 50% as the melting temperature increased from 1150° to 1400°C. They also reported that $Fe(II)/Fe_{total}$ ratio is less dependent on the oxygen content of the melting atmosphere than the melting temperature and time [72]. For $40Fe_2O_3$-$60P_2O_5$ (mol%) glasses, the structure and properties do not change significantly with $Fe(II)/Fe_{total}$ ratio. $40Fe_2O_3$-$60P_2O_5$ (mol%) glasses crystallize during heating in DTA to form $Fe_3(P_2O_7)_2$ and $Fe_4(P_2O_7)_3$. The glasses have a similar structure with crystalline $Fe_3(P_2O_7)_2$ in terms of iron coordination and bonding of the phosphate groups [39].

In addition to the glasses that can be made by quenching in air, glasses with Fe/P ratios between 0.33 and 1.83 can be prepared by quenching microwave- or joule-heated melts between pre-cooled copper plates [74]. Both Fe(II) and Fe(III) are in octahedral coordination environments. All glasses made by microwave are crystallized to $FePO_4$, $Fe_3(PO_4)_2$, $Fe(PO_3)_3$, $Fe(PO_3)_2$ and $Fe_7(PO_4)_6$, and the amount of the crystallized phases depends on glass composition and glass preparation procedure. However, the glass structure and glass formability were not investigated.

Phosphate-rich ferrous ultraphosphate glasses (FeO/P_2O_5<1:1) can be made in sealed silica tubes under vacuum [75,76]. The $Fe(II)/Fe_{total}$ ratios in the glasses were determined to be in the range of 82%-94%. Addition of FeO causes Q^3 units (linked to three other P-tetrahehra) to transform to a two dimensional network which is dominated

by Q^2 tetrahedra (linked to two other P-tetrahedra). Both Fe(II) and Fe(III) are also in octahedral coordination environments in those glasses.

Iron-rich phosphate glasses (with Fe/P ratios between 1.0 and 2.3) were made by twin-roller quenching [77]. Cyrstals of Fe_2O_3, $FePO_4$, Fe_3PO_7 or $Fe(PO_3)_2$ crystals precipitate during heat-treatment of the galsses at different temperatures between their glass transition temperature and melting temeprature. The effects of crystallization on the magnetic properties of one glass (Fe/P =2.3) were studied. It is reported that the coordination state around iron in the glasses is less symmetrical than that in the precipitated crystal.

Based on the reported Fe(II)/Fe_{total} ratios in iron phosphate glasses [39,74-79], most of the glass compositions were located in the region marked in Fig. 2.5.

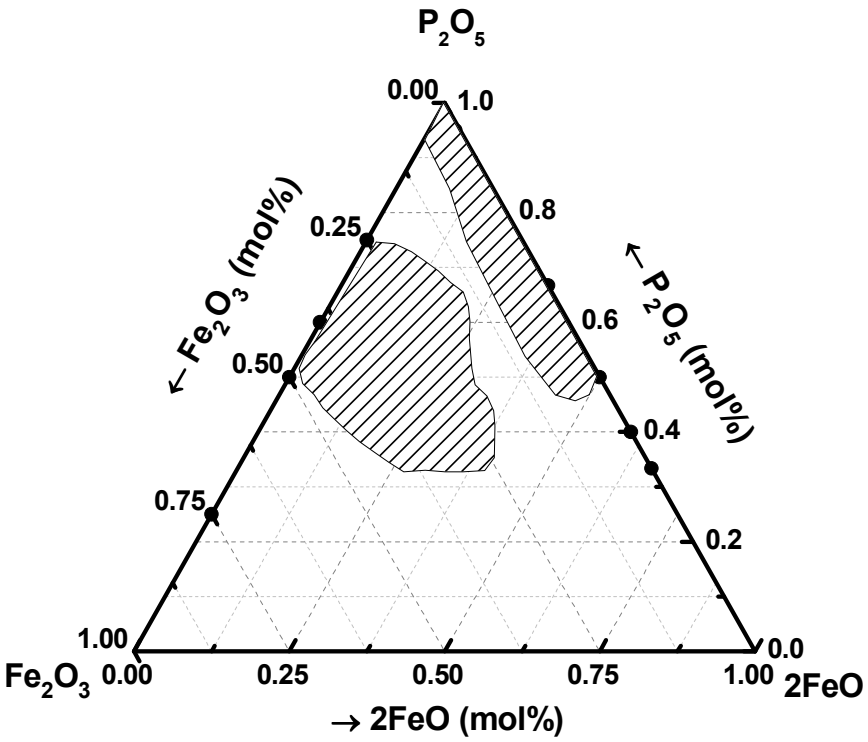

Figure 2.5 The glass forming regions reported [39,74-79].

2.5. REFERENCES

[1] A. Andrews, "Radioactive waste Streams: Waste Classification for Disposal," CRS Report for Congress (2006).

[2] Figures taken from International Atomic Energy Agency Managing Radioactive Waste Factsheet. (http://www.world-nuclear.org/info/inf04.html#ManageHLW).

[3] P. Colombo, G. Brusatin, E. Bernardo, G. Scarinci, "Inertization and Reuse of Waste Materials by Vitrification and Fabrication of Glass-based Products," Curr. Opin. Solid State Mater. Sci. 7 (2003) 225-239.

[4] R. Gutman, "Thermal Technologies to Convert Solid Waste Residuals into Technical Glass Products," Glass Sci. Technol. 69 (1996) 285-299.

[5] Personal Communication, J.D. Vienna, Pacific Northwest National Laboratory (2004).

[6] S.T. Reis, M. Karabulut, D.E. Day, "Structural Features and Properties of Lead Iron Phosphate Nuclear Waste Forms (I)," J. Nuclear Materials 304 (2002) 87-95.

[7] W. Huang, C. W. Kim, C.S. Ray, D.E. Day, "Solubility of High Chrome Nuclear Wastes in Iron Phosphate Glasses," Ceramic Transactions 143 (2003) 347-354.

[8] C.W. Kim, D.E. Day, "Immobilization of Hanford LAW in Iron Phosphate Glasses," J. Non. Cryst. Solids 331 (2003) 20-31.

[9] W.Huang, D.E. Day, C.S. Ray, C.W. Kim, A. Mogus-Milankovic, "Vitrification of High Chrome Oxide Nuclear Waste in Iron Phosphate Glasses," J. Non. Cryst. Solids 327 (2004) 46-57.

[10] B.C. Sales, L.A. Boatner, "Lead-iron Phosphate Glass: A Stable Storage Medium for High-level Nuclear Waste," Science, 226(4670) 45-48 (1984).

[11] X. Yu, D.E. Day, G.J. Long, R.K. Brow, "Properties and Structure of Sodium-iron Phosphate. Glasses," J. Non-Cryst. Solids 215 (1997) 21-31.

[12] D.E. Day, "Iron Phosphate Composition for Containment of Hazardous Metal Waste," U.S. Patent 5750824 (1998).

[13] W. Huang, D.E. Day, C.S. Ray, C.W. Kim, "High temperature properties of an iron phosphate melt containing high chrome nuclear waste," J. Nuclear Mater. 346 (2005) 298-305.

[14] D.E. Day, C.S. Ray, C-W Kim, "Iron Phosphate Glasses: an Alternative for Vitrifying Certain Nuclear Wastes," Final Report for DE-FG07-96ER45618 (2004).

[15] W. Huang, C.W. Kim, D.E. Day, in: S.K. Sundaram, D.R. Spearing, J.D. Vienna (Eds.), "Environmental Issues and Waste Management Technologies in Ceramic and Nuclear Industries VIII" (Ceramic Transaction 143), American Ceramic Society, Westerville, OH, 2003, p. 347.

[16] R. C. Haushalter, L. A. Mundi, "Reduced Molybdenum Phosphates: Octahedral-tetrahedral Framework Solids with Tunnels, Cages, and Micropores," Chem. Mater. 4 (1992) 31-48.

[17] A. Clearfield, "Role of Ion Exchange in Solid-state Chemistry," Chem. Rev. 88, (1988) 125-148.

[18] K. Zaghib, C.M. Julien, "Structure and Electrochemistry of FePO4 ·2H_2O hydrate," J. Power Sources 142 (2005) 279-284.

[19] M. Ai, K. Ohdan, "Effects of the Method of Preparing Iron Orthophosphate Catalyst on the Structure and the Catalytic Activity," Appl. Catal. A 180 (1999), 47-52.

[20] N. Aliouane, T. Badechet, Y. Gagou, E. Nigrelli, P. Saint-Gregoire, "Synthesis and Phase Transitions of Iron Phosphate," Ferroelectrics 241 (2000) 255-262.

[21] C.A. Boras, R. Romagnoli, R.O. Lezna, "In Situ Spectroelectrochemistry (UV-visible and Infrared) of Anodic Films on Iron in Neutral Phosphate Solutions," Electrochem. Acta 45 (2000) 1717-1725.

[22] A. Mogus-Milankovic, D.E. Day, G.J.Long, G.K. Marasinghe, "Structural and Magnetic Properties of Fe_2O_3–P_2O_5–Na_2O Glasses. Part. I. Oxygen Heat Treatment," Phys. Chem. Glasses 37 (1996) 57-61.

[23] H.N. Ng, C. Calvo, "Refinement of the Crystal Structure of the Low-quartz Modification of Ferric Phosphate," Can. J. Chem. 53 (1975) 2064.

[24] A.K. Padhi, K.S. Nanjundaswamy, J.B. Goodenough, "Phospho-olivines as Positive-electrode Materials for Rechargeable Lithium Batteries," J. Electrochem. Soc. 144 (1997) 1188-1194.

[25] A.K. Padhi, K.S. Nanjundaswamy, C. Masquelier, S. Okada, J.B. Goodenough, "Effect of Structure on the Fe3+/Fe2+ Redox Couple in Iron Phosphates," J. Electrochem. Soc. 144 (1997) 1609-1613.

[26] S. Okada, T. Yamamoto, Y. Okazaki, Jun-ichi Yamaki, M. Tokunaga, T. Nishida, "Cathode properties of amorphous and Crystalline $FePO_4$," J. Power Sources 146 (2005) 570-574.

[27] Y-S, Hong, Y.J. Park, K.S. Ryu, S.H Chang, "Crystalline Fe3PO7 as an Electrode Material for Lithium Secondary Batteries," Solid State Ionics 156 (2003) 27-33.

[28] J.B. Forsyth, C.E. Johnson, C. Wilkinson, "The magnetic structure of vivianite, $Fe_3(PO_4)_2.8H_2O$," J. Phys. C: Solid State Phys. 3 (1970) 1127-1139.

[29] J.B. Forsyth, C. Wilkinson, Proc. 7th Int. Conf. on Magnetism (Grenoble, 1970); J. Physique Suppl. 32 (1971).

[30] S.C. Abraham and J.L. Bernstein, "Crystal Structure of Paramagnetic Ludlamite, $Fe_3(PO_4)_2*4(H_2O)$, at 298 K, Sample: T = 298 K," J. Chem. Phys. 44 (1966) 2223-2229.

[31] L.K. Elbouaanani, B. Malaman, Gérardin, R. "Structure Refinement and Magnetic Properties of C-$Fe(PO_3)_3$ Studied by Neutron Diffraction and Mössbauer Techniques," J. Solid State Chem. 148 (1999) 455-463.

[32] C. Parada, J. Perles, R. Saez-Puche, C. Ruiz-Valero, N. Snejko, "Crystal Growth, Structure, and Magnetic Properties of a New Polymorph of $Fe_2P_2O_7$," Chem. Mater. , 2003, 15, 3347-3351.

[33] J.B. Moffat, Catal. "Phosphates as Catalysts," Rev. Sci. Eng. 18 (1978) 199-.

[34] E. Muneyama, A. Kunishige, K. Ohdan, M. Ai, "Effects of Water Vapor in the Oxidative Dehydrogenation of Isobutyric Acid to Methacrylic Acid over Iron Phosphate Catalyst," Cata. Letters, 31 (1995) 209-220.

[35] M. Jin, X. Chui, W. Xu, M. Liu, "Mössbauer study of ferric phosphate catalysts," Hyp. Int. 41 (1988) 645-648.

[36] J.C. Védrine, "Partial Oxidation Reaction on Phosphate-based Catalysts," Topics in Catal. 11/12 (2000) 147-152.

[37] J.-M.M. Millet, J.C. Védrine, G. Hecquet, "Proposal for Active Sites of Iron Phosphates in Isobutyric Oxidative Dehydrogenation Reaction," Stud. Surf. Sci. Catal. 55 (1990) 833-840.

[38] C. Virely, M. Forissier, J.-M.M. Millet, J.C. Védrine, "Kinetic Study of Isobutyric Acid Oxydehydrogenation on Various Fe-P-O Catalysts: Proposal for the Reaction Mechanism," J. Mol. Catal. 71 (1992) 199-213.

[39] X. Fang, C.S. Ray, A. Mogus-Milankovic, D.E. Day, "Iron Redox Equilibrium, Structure and Properties of Iron Phosphate Glasses". J. Non-Cryst. Solids, 283 (2001) 162-172.

[40] A. Hruby, "Evaluation of Glass-forming Tendency by Means of DTA" Czech J. Phys. B, 22 (1972) 1187-1193.

[41] M.L.F. Nacimento, L.A. Souza, E.B. Ferreira, E.D. Zanotto, "Can glass stability parameters infer glass forming ability," J. Non-Cryst. Solids, 351 (2005) 3296-3308.

[42] H. Wentrup. "Contribution on the System Iron-Phosphorus-Oxygen" (in Ger.), Arch. Eisenhüttemwes., 9(7) (1935) 57-60.

[43] J. Korinth, P. Royen. "Reaction in the system $Fe_2O_3/FePO_4$" (in Ger.), Z. Anorg. Allg. Chem, 313 (3-4) (1961) 121-37.

[44] J. C Kaell, F. Jeannot, C. Gleitzer, "Study of the Progressive Reduction of $Fe_3(PO_4)_2$ and $Fe_9(PO_4)O_8$ " (in Fr.), Ann. Chim. (Paris), 9(2) (1984) 169-80.

[45] A. Modaressi, J.C. Kaell, B. Malaman, R. Gérardin, and C. Gleitzer. "Study of the system Fe-P-O (for Fe/P $\geq$1) and its compounds: the Oxyphosphates of Iron" (in Fr.), Mater. Res. Bull, 18 (1983) 101-109.

[46] G. Trömel, K. Schwerdtfeger, "A study of the system iron-phosphorous oxygen," Arch. Eisenhüt., 34 (1963) 55-59.

[47] E.C. Shafer, M.W. Shafer and R. Roy, "Studies of Silica Structure Phases II: Data on $FePO_4$, $FeAsO_4$, $MnPO_4$, BPO_4, $AlVO_4$ and others," Z. Krist., 108 (1956) 263-275.

[48] V. Caglioti. "The Structure of Ferric Phosphate," Atti accad. Lincei, 22 (1935) 146-149.

[49] M.R. De Guire, T.R.S. Prasanna, G. Kalonji, and R.C. O'Handley., "Phase Equilibria in the Iron Oxide-Cobalt Oxide-Phosphorus Oxide System," J. Am. Ceram. Soc., 70(11) (1987) 831-37.

[50] B. Kumar, S. Lin, "Redox State of Iron and Its Related Effects in the $CaO-P_2O_5-Fe_2O_3$ Glasses" 74 (1991) 226-228.

[51] S.T. Reis, A. Moguš-Milanković, V. Ličina, J.B. yang, M. Karabulut, D.E. Day, R.K. Brow, "Iron Redox Equilibrium, Structure and Properties of Zinc Iron Phosphate Glasses," J. Non-cryst. Solids, 353 (2007) 151-158.

[52] N. Métrich, J. Susini, E. Foy, F. Farges, D. Massare, L. Sylla, S. Lequien, M. Bonnin-Mosbah. "Redox State of Iron in Peralkaline Rhyolitic Glass/Melt: X-ray Absorption Micro-spectroscopy Experiments at High Temperature," Chem. Geol., 231 (2006) 350-363.

[53] A.I. Teterevkov, V.V. Pechkovskii, V.V. Tumanov, "Summary of Papers Presented at the Conference of Chemistry of Vaporous Inorganic Compounds and Vapor Generating Process" [in Russian]. Minsk (1973).

[54] Y.A. Gorbunov, B.A. Maksimov, Y.K. Kabalov, A.N. Ivashchenko, O.K. Mel'nikov, N.V. BeloV, "Crystal Structure of $Fe^{2+}{}_3Fe^{3+}{}_4[PO_4]_6$," Dokl. Akad. Nauk SSSR, 254 873-877 (1980).

[55] D.E. Day, Z. Wu, C.S. Ray, and P. Hrm, "Chemically Durable Iron Phosphate Glass Wasteforms," J. Non-Cryst. Solids, 241[1] (1998) 1-12.

[56] K. Tanaka, N. Soga, R. Ota, K. Hirao, "ESR and Mössbauer Studies of Crystallization Process of Iron Phosphate Glass," Bull. Chem. Soc. Jpn., 59 (1986) 1079-1085.

[57] Y. Wang, X.X. Wang, Z. Su, Q. Guo, Q. Tang, Q. Zhang, H. Wan, "SBA-15-supported iron phosphate catalyst for partial oxidation of methane to formaldehyde," Catal. Today, 155 (2004) 93–95.

[58] Y-S Hong, Y.J. Park, K.S. Ryu, S.H. Chang, "Crystalline Fe_3PO_7 as an electrode Material for Lithium Secondary Batteries," Solid State Ionics, 156 (2003) 27-33.

[59] F. D'Yvoire, "Etudes des phosphates d'aluminum et fer trivalent IV. Les di- et triphosphates. Pouvoir d'echange cationique des triphosphates acides $H(AIP_3O_{10})_{2-3}HO$ et $H_2(FeP_3O_{10})\ 2H_2O$," Bull. Soc. Chim. Fr. (1962) 1224-1236.

[60] L.K. Elbouaanai, B. Malaman, R. Gérardin, M. Ijjaali, "Crystal Structure Refinement and Magnetic Properties of $Fe_4(P_2O_7)_3$ Studied by Neutron Diffraction and Mössbauer Techniques," J. Solid State Chem. 163 (2002) 412-420.

[61] C. Gleitzer, "Anhydrous Iron Phosphates and Oxyphosphates," Eur. J. Solid State Inorg. Chem. 28 (1991) 77-91.

[62] J.M. Rojo, J.L. Mesa, L Lezama, T. Rojo, "Magnetic Properties of the $Fe(PO_3)_3$ Metaphosphate," J. Solid State Chem. 145 (1999) 629-633.

[63] L.K. Elbouaanani, B. Malaman, R. Gérardin, "Structure Refinement and Magnetic Properties of C-$Fe(PO_3)_3$ Studied by Neutron Diffraction and Mössbauer Techniques," J. Solid State Chem. 148 (1999) 455-463.

[64] M.Bouchdoug, A. Courtois, R. Gerardin, K. Steinmetz, C. Gleitzer, "Preparation et Etude d`un Oxyphosphate $Fe_4(PO_4)_2O$," J. Solid State Chem. 42 (1982) 149-157.

[65] J.S. Swinnea, H. Steinfink, "Crystal Structure of $Fe_2P_2O_7$," J. Solid State Chem. 47 (1983) 278-283.

[66] M.M. Gadgil, S.K. Kulshreshtha, "Study of $FePO_4$ Catalyst," J. Solid State Chem. 111 (1994) 357-364.

[67] C. Gleitzer, A. Modaressi, R. J. D. Tilley, "Intergrowth Phases in the Fe_9PO_{12}–Fe_7SiO_{10} System," J. Solid State Chem., 59(3) (1985) 362-370.

[68] A. Modaressi, A. Courtois, R. Gerardin, B. Malaman, C. Gleitzer, "Fe_2PO_5, un phosphate de fer de valence mixte. Préparation et études structurale, Mössbauer et magnétique," J. Solid State Chem.,40(3) (1981) 301-311.

[69] M. Ijjaali, G. Venturini, R. Gerardin, B. Malaman, C. Gleitzer, "Synthesis, Structure and Physical Properties of a Mixed-valence Iron Diphosphate $Fe_3(P_2O_7)_2$: First Example of Trigonal Prismatic Fe(2+) with O(2-)-Ligands". Eur. J. Solid State Inorg. Chem. 28, (1991) 983-998.

[70] B. Malaman, M. Ijjaali, R. Gerardin, G. Venturini, C. Gleitzer, "$Fe_7(P_2O_7)_4$, a Mixed-valence Iron Diphosphate, the Missing Link between $Fe_2P_2O_7$ and $Fe_3(P_2O_7)_2$," Eur. J. Solid State Inorg. Chem. 29 (1992) 1269-1284.

[71] Y.M. Moustafa, "Characterization of Iron Oxychloride Potassium Phosphate Glasses," J. Phys. D: Appl. Phys. 32 (1999) 2278-2286.

[72] B.C. Bunker, G.W. Arnold, "Corrosion of Phosphorus Oxynitride Glasses in Water and Humid Air," J. Am. Ceram. Soc. 70[6] (1987) 425-430.

[73] N.H. Ray, Inorganic Polymers, Academic Press, New York, 1978.

[74] F.J.M. Almeida, J.R. Martinelli, C.S.M. Partiti, "Characterization of Iron Phosphate Glasses Prepared by Microwave Heating," J. Non-Cryst. Solids, 353 (2007) 4783-4791.

[75] M. Karabulut, E. Metwalli, D. E. Day, R. K. Brow, "Mössbauer and IR Investigations of Iron Ultraphosphate Glasses," J. Non-Cryst. Solids, 328 (2003) 199-206.

[76] U. Hoppe, M. Karabulut, E. Metwalli, R. K. Brow, P. Jovari, "The Fe-O Coordination in Iron Phosphate Glasses by X-Ray Diffraction with High-Energy Photons," J. Phys. Cond. Matter 15 (2003) 6143-6153.

[77] K. Tanaka, N. Soga, R. Ota, K. Hirao, "ESR and Mössbauer Studies of Crystallization Process of Iron Phosphate Glass," Bull. Chem. Soc. Jpn., 59 (1986) 1079-1085.

[78] C.S. Ray, X. Fang, M. Karabulut, G.K. Marasinghe, D.E. Day, "Effect of Melting Temperature and Time on Iron Valence and Crystallization of Iron Phosphate Glasses," J. Non-Cryst. Solids, 249 (1999) 1-16.

[79] G.K. Marasinghe, M. Karabulut, C. S. Ray, D. E. Day, M. G. Shumsky, W. B. Yelon, C. H.Booth, P. G. Allen, D. K. Shuh, “Structural Features of Iron Phosphate Glasses,” J. Non-Cryst. Solids, 222 (1997) 144-152.

PAPER

1. PHASE EQUILIBRIA IN THE Fe_2O_3- P_2O_5 SYSTEM

Liying Zhang[*], Mark. E. Schlesinger[†], and Richard K. Brow*

Department of Materials Science & Engineering, Missouri University of Science & Technology, Rolla, MO 65409

ABSTRACT

Four ferric phosphate compounds were identified in the Fe_2O_3-P_2O_5 system and the liquidus surfaces in the sub-systems Fe_3PO_7-$FePO_4$, $FePO_4$-$Fe_4(P_2O_7)_3$, and $Fe_4(P_2O_7)_3$-$Fe(PO_3)_3$, were determined. The results are significantly different from those presented by Wentrup in 1935. Fe_3PO_7 is the stable ferric oxo-phosphate compound, not $Fe_4P_2O_{11}$, and Fe_3PO_7 decomposes in air at 1090°C. The congruent melting point of $FePO_4$ (1208°C) is similar to what was reported, but $Fe_4(P_2O_7)_3$ melts congruently at 945°C, about 300°C lower than claimed by Wentrup. $Fe(PO_3)_3$, for which the melting temperature has not been previously reported, melts congruently at 1205°C. Eutectic points exist at 58.0 mole% Fe_2O_3 (1070°C), 42.7% Fe_2O_3 (925°C), and 37.0% Fe_2O_3 (907°C). The latter two eutectic points bracket the conventional glass-forming range for iron phosphate melts under consideration as alternative hosts for nuclear wastes.

---

[*] Member of the American Ceramic Society

[†] Corresponding author, mes@mst.edu

1.1. INTRODUCTION

Chemically durable iron phosphate glasses are compatible with a wide variety of other oxides and so have drawn much attention as alternative hosts for radioactive wastes.[1-5] Knowledge of phase equilibria in the iron phosphate system is of interest for understanding the effects of composition and temperature on glass formation, and for predicting crystallization behavior of iron phosphate melts and glasses.[6] In addition, iron phosphate compounds are finding increasing applications for use as electrode materials for Li-batteries,[7-8] and the availability of accurate phase equilibrium information would be useful for the preparation and characterization of these materials.

Wentrup determined the original ferric-phosphate phase diagram for the subsystems between Fe_2O_3, $Fe_4P_2O_{11}$, $FePO_4$ and $Fe_4(P_2O_7)_3$ by recording heating and cooling curves of appropriate mixtures of Fe_2O_3, $FePO_4$ and $Fe_4(P_2O_7)_3$.[9] One particularly controversial compound in the original Wentrup diagram is $Fe_4P_2O_{11}$. Wentrup reported the formation of a crystalline phase with this nominal composition, but did not characterize it. Korinth and Royen used X-ray diffraction (XRD) to study mixtures of Fe_2O_3 and $FePO_4$ heated at 800-900°C and determined that the stoichiometry of the lowest phosphate compound was in fact Fe_3PO_7 instead of $Fe_4P_2O_{11}$.[10] Gleitzer and co-workers studied the solid state equilibria and formation of ferric phosphate compounds at 900°C and confirmed that Fe_3PO_7, not $Fe_4P_2O_{11}$, is the stable oxo-phosphate compound.[11,12]

Another controversy associated with the Wentrup phase diagram concerns the $FePO_4$–$Fe_4(P_2O_7)_3$ system. The original phase diagram shows a melting temperature for ferric pyrophosphate, $Fe_4(P_2O_7)_3$, above 1200°C. However, research on glass-formation

in this system indicates that the melting temperature of the pyrophosphate must be below 950°–1150°C.[13-17] Many iron phosphate glass–forming compositions reported in the literature are centered on the $Fe_4(P_2O_7)_3$–$Fe(PO_3)_2$ system;[13,18,19] however, no investigation of the liquidus surface of this system has been reported.

Some information about the phase transition temperatures of the ferric phosphate compounds has been reported. $FePO_4$ was reported by Wentrup[9] to melt between 1230°C and 1240°C, and Shafer obtained a melting point of 1230°C using rapid heating in a strip furnace.[22] Caglioti mentioned the possible decomposition of Fe_3PO_7 to Fe_2O_3 and $FePO_4$ above 1100°C,[20] and Korinth and Ryan later confirmed that Fe_3PO_7 decomposes at 1200°C.[10] Three overlapping endothermic DTA peaks between 1000°C and 1150°C were reported for Fe_3PO_7, but were not explained, and the melting temperature of Fe_3PO_7 was estimated from DTA to be 1375°C.[21] Fe(III) in ferric phosphate systems often undergoes an endothermic reduction to Fe(II) when heated to the corresponding liquidus or decomposition temperatures, and P_2O_5 can volatilize at high temperatures (generally above 1000°C) from melts, particularly from phosphate rich compositions. These processes can make the interpretation of complex thermal curves more difficult, and may have contributed to the apparent errors in the Wentrup diagram.

Glasses with Fe_2O_3 contents between 33 and 59 mole% form from melts held at 1300°C,[18] and glasses with Fe_2O_3 contents between 50 and 63 mole% can form from melts at temperatures from 1150 – 1250°C.[23] Such studies provide some information about the liquidus surface of this system, although it is complicated by the reduction of some ferric ions to ferrous ions under typical melting conditions. No exact melting

temperature for crystalline $Fe(PO_3)_3$ has been reported, although glasses based on this composition have been prepared from melts quenched from 1250°C.[19]

In this paper, the existence of four ferric phosphate compounds is confirmed and the liquidus surface of the ferric phosphate system was determined between the compounds $Fe(PO_3)_3$ and Fe_3PO_7. This information is then related to other reported studies of iron phosphate glass formation and compound formation.

1.2. EXPERIMENTAL PROCEDURES

1.2.1. Compound Preparation. The ferric phosphate compounds were prepared by solid state reactions between stoichiometric mixtures of $FePO_4$ and Fe_2O_3 or $NH_4H_2PO_4$ at different temperatures, as summarized in Table I. $FePO_4 \cdot xH_2O$ (100%, Alfa Aesar), Fe_2O_3 (Alfa Aesar, ≤45 μm, ≥99%) and $NH_4H_2PO_4$ (Alfa Aesar, 98%) were used as raw materials. Samples obtained from these experiments were pulverized to <53 μm and characterized by X-ray diffraction (XRD Scintag XDS 2000) with a slow scanning rate (one degree every 1~2 minutes). Search and match of XRD patterns was achieved manually using DMSNT 1.37, which is based on a Hanawalt search method.

1.2.2. Phase Equilibria Studies.

1.2.2.1 Fe_3PO_7–$FePO_4$ system: Samples (<53 μm) weighing 100–200 mg placed in an open alumina crucible for differential thermal analysis and thermogravimetric analysis (DTA-TGA, Netzsch STA 409C/CD). DTA-TGA was run at 10°C/min under flowing air. The data obtained were analyzed by the Netzsch Proteus software, version 4.3. The accuracy of the characteristic temperatures was determined to be ±5°C by

calibration and multiple runs. DTA-TGA was used to determine the phase transition and decomposition temperatures of crystalline Fe_3PO_7 and $FePO_4$.

To study the decomposition of Fe_3PO_7, samples were heated in air for 10-12 hours at temperatures between 1000°C and 1350°C, and then quenched in water. These samples were dried, then either pulverized to <53 μm and analyzed by XRD, or mounted and coated with carbon for analytical scanning electron microscopy with energy dispersive spectrometry (SEM-EDS, FESEM S4700). Fe/P ratios were typically determined by EDS at low magnification (500X) using a calibration curve based on the EDS analyses of the four ferric phosphate compounds. In general, analyses were obtained from at least five different spots on each sample and the average compositions are reported. The compositions of the glassy regions of quenched samples obtained by EDS were used to determine the liquidus surface of the Fe_3PO_7-rich portion of this system, since these melts crystallize readily when quenched.[23] For the $FePO_4$–rich portion of this system, similar analyses were done on samples with the nominal composition (mole%) $51.4Fe_2O_3$–$48.6P_2O_5$ heated in air for twelve hours at different temperatures between 1150 and 1205°C. Experimental data for the liquidus surface were fit to an exponential function.

1.2.2.2 $FePO_4$–$Fe_4(P_2O_7)_3$ system: One to two grams of samples with nominal Fe_2O_3 contents of 44.5 and 47.5 mole% were prepared and analyzed by SEM-EDS to determine the compositions of the glassy phase of quenched samples that formed as a result of heat-treatments similar to those described above. $Fe_4(P_2O_7)_3$–rich compositions are good glass formers, so the liquidus surface was studied by characterizing samples quenched from temperatures that bracket the expected liquidus temperature. Samples about 0.6-1.0 g in size with Fe_2O_3-contents of from 40.0 to 43.0 mole%, were sealed

under air in silica ampoules to minimize Fe(III) reduction and P_2O_5 volatilization during subsequent thermal treatments. These sealed samples were heated for twelve hours to different temperatures that bracketed the expected liquidus temperature, followed by a water quench. The temperature intervals were set at 10°C. These quenched samples were analyzed by optical microscopy (OM) and powder XRD, and the liquidus surface was determined to be the midpoint between the highest temperature where crystals were observed and the lowest temperature where no crystals were observed.

1.2.2.3 $Fe_4(P_2O_7)_3$–$Fe(PO_3)_3$ system: P_2O_5–rich melts are good glass formers and so the P_2O_5–rich portion of the diagram was also studied by analyzing samples quenched from temperatures that bracket the expected liquidus temperatures. These samples (compositional intervals of ~1.5 mole% Fe_2O_3) were sealed in silica ampoules and heated in a similar way to what is described above for the $Fe_4(P_2O_7)_3$-rich samples. The quenched samples were studied by OM and micro-Raman spectroscopy (Horiba–Jobin Yvon LabRam-HR) using a He-Ne laser (632.8 nm). Raman spectra of crystalline $Fe_4(P_2O_7)_3$ and $Fe(PO_3)_3$ are more distinct than the respective XRD patterns, and so this technique was convenient for identifying isolated crystals in these quenched samples.

1.3. RESULTS AND DISCUSSION

1.3.1. Ferric Phosphate Compounds.

Single–phase samples of Fe_3PO_7, $FePO_4$, $Fe_4(P_2O_7)_3$ and $Fe(PO_3)_3$ were prepared according to the processes outlined in Table I and confirmed by XRD. The compound $Fe_4P_2O_{11}$ could not be obtained under the experimental conditions described in Table I. Instead, various mixtures of crystalline Fe_3PO_7 and $FePO_4$, or Fe_2O_3 and $FePO_4$, formed. The presence of Fe_3PO_7 instead of $Fe_4P_2O_{11}$ as the stable ‘iron-rich’ oxo-phosphate

compound in the ferric phosphate system is consistent with what was reported by Korinth.[10] but in disagreement with the conclusions of Wentrup.[9]

1.3.2. Phase Equilibria Studies.

1.3.2.1 Fe_3PO_7–$FePO_4$ system: Figure 1 shows the XRD patterns of Fe_3PO_7 quenched from 1000°C, 1150°C and 1200°C after being held in air for 12 hours. Crystalline Fe_2O_3, $FePO_4$ and $Fe_2P_2O_7$, as well as a small amount of glassy phase, are present in the samples heated at or above 1150°C. Reactions 1 and 2 summarize the possible decomposition reactions that account for the formation of these phases:

$$Fe_3PO_7 \rightarrow Fe_2O_3 + \text{Liquid } (FePO_4+Fe_2O_3) \quad (1)$$

$$2\ FePO_4 \rightarrow Fe_2P_2O_7 + \tfrac{1}{2}\ O_2 \quad (2)$$

Figure 2 shows DTA and TGA curves for Fe_3PO_7 and $FePO_4$ heated in air. For Fe_3PO_7, overlapping endothermic DTA peaks are present at temperatures around 1100°C, consistent with literature reports about the thermal behavior of Fe_3PO_7. [10,20,21] Several processes, including the decomposition and melting of Fe_3PO_7 (reaction 1) and the reduction of Fe(III) (reaction 2), may account for these endothermic events. The reduction of Fe(III) to Fe(II) accounts for the TGA weight loss. EDS analyses indicate that the overall Fe/P ratio in an Fe_3PO_7 sample heat-treated at 1200°C for twelve hours was 3.00±0.16, consistent with the initial stoichiometry of the sample, and indicating that no significant loss of P_2O_5 occurred from these iron-rich melts. Based on the results shown in Figs. 1 and 2, the decomposition temperature of Fe_3PO_7 is estimated to be 1090±8°C.

The DTA data for Fe_3PO_7 in Fig. 2 reveals a solid–state phase transition at 850°C. Wentrup reported a solid–state phase transition temperature of 869°C for his oxo-phosphate phase ($Fe_4P_2O_{11}$).[9] The DTA data for $FePO_4$ in Fig. 2 indicates that there are two solid–state phase transitions, at 710°C (α→β) and at 880°C (β→γ). These transition temperatures are similar to those previously reported (707°C and 889°C, respectively).[9,22]

Figure 3 shows backscattered electron (BSE) images of an Fe_3PO_7 sample quenched from 1200°C after being held there for twelve hours. EDS analyses reveal that the bright sphere-like areas are regions of Fe_2O_3. EDS and XRD indicate that the small crystals (<2 μm) formed around the spherical particles include $FePO_4$, $Fe_2P_2O_7$ and Fe_2O_3, the phases expected to precipitate from the liquid phase that forms at this temperature (reactions 1 and 2). The average composition of the regions around the large Fe_2O_3 particles was determined by EDS and used as the composition of the liquid phase at the respective heat treatment temperatures. Similar analyses were done on other compositions in this system, and these experimental data are used for the liquidus surface for the Fe_3PO_7–$FePO_4$ system that is plotted in Fig. 4; error bars indicate uncertainties in the quantitative EDS analyses. By extrapolating the line fitting these experimental points, the temperatures at which Fe_3PO_7 and Fe_2O_3 are predicted to fully melt are estimated to be 1380°C and 1600°C, respectively. These temperatures are similar to those reported in the literature (1375°C for Fe_3PO_7 [21] and 1565°C for Fe_2O_3[24]).

The $FePO_4$–Fe_3PO_7 system has a eutectic point at 58.0±1.2 mole% Fe_2O_3, and the eutectic reaction occurs at 1070±5°C. The eutectic composition and temperature of the $FePO_4$–$Fe_4P_2O_{11}$ system reported by Wentrup were 58.0 mole% Fe_2O_3 and 968°C.[9] Wentrup appears to have misidentified Fe_3PO_7 as $Fe_4P_2O_{11}$, and may have misinterpreted

endothermic evidence of Fe(III) reduction for eutectic melting. The eutectic temperature reported here was confirmed by observing the melting behavior of the eutectic composition. Glasses can be formed from melts with compositions around this eutectic point using rapid quench techniques, as reported elsewhere.[23]

1.3.2.2 $FePO_4$–$Fe_4(P_2O_7)_3$ system: The same sample preparation and characterization methods described above were used to determine the liquidus surface of the $FePO_4$–rich portion of the $FePO_4$–$Fe_4(P_2O_7)_3$ system. For the $Fe_4(P_2O_7)_3$–rich part of this system, samples were sealed in silica ampoules to minimize the effects of phosphorus volatility at high temperatures. EDS analyses of a sample of $Fe_4(P_2O_7)_3$ heated at 950°C for ~12 hours in air and in a sealed ampoule indicate Fe/P ratios of 0.75±0.05 and 0.70±0.02, respectively, compared to an expected ratio of 0.67. These analyses indicate that the ampoules do reduce phosphate volatilization. Figure 5 shows the XRD patterns collected from several compositions quenched from temperatures below their respective liquidus temperatures. These results were used to determine the liquidus temperatures and the eutectic point of the $FePO_4$–$Fe_4(P_2O_7)_3$ system.

Figure 6 shows the liquidus curves obtained by fitting the points obtained from the analyses described above. The $FePO_4$–$Fe_4(P_2O_7)_3$ system has a eutectic point at 42.7±0.4 mole% Fe_2O_3 and 925±8°C. In contrast, Wentrup reported a liquidus point at 46.5 mole% Fe_2O_3 and 954°C.[9]

1.3.2.3 $Fe_4(P_2O_7)_3$–$Fe(PO_3)_3$ system: EDS analyses of a sample of $Fe(PO_3)_3$ heated in a silica ampoule to 1250°C for four hours showed an Fe/P ratio of 0.37±0.07, compared to an expected ratio of 0.33. The silica content in this sample was <2.0 mole%, as measured at a distance of 1 mm from the ampoule wall on a sample that was 11 mm in

diameter. This analysis indicates that the nominal composition of this P_2O_5-rich sample was retained when melted in an ampoule.

Figure 7 shows the Raman spectra collected from samples in the $Fe_4(P_2O_7)_3$–$Fe(PO_3)_3$ system quenched from temperatures below their respective liquidus temperatures. By comparing the Raman spectra of these samples to those collected from crystalline $Fe(PO_3)_3$ and $Fe_4(P_2O_7)_3$, the equilibrium crystal phases at the quenching temperatures could be determined. A detailed discussion of the Raman spectra from iron phosphate compounds and glasses is reported elsewhere.[25]

Figure 8 shows the liquidus surface for the $Fe_4(P_2O_7)_3$–$Fe(PO_3)_3$ system obtained from the OM-Raman and EDS analyses. The eutectic point is 37.0±0.3 mole% Fe_2O_3 with a eutectic temperature of 907±8°C. This appears to be the first report of the liquidus surface and eutectic composition in this subsystem.

1.3.3. Discussion of the Liquidus Surface Determination. Figure 9 summarizes the liquidus surface of the ferric phosphate system between 25 and 75 mole% Fe_2O_3, and Table II summarizes the characteristic temperatures determined for this system. Four ferric phosphate compounds appear in this liquidus surface phase diagram; Fe_3PO_7 decomposes during heating, and the others melt congruently. Eutectic points exist in each subsystem, and these will be useful for studies of glass formation and for developing ceramic processes like sintering temperature control. Below the corresponding liquidus surface, neighboring solid compounds in the diagram are expected to co-exist at equilibrium, although the details of the solid phase equilibria were not studied in this work.

This work confirms the reports of Korinth[10] and Gleitzer[11,12] that Fe_3PO_7 ($3Fe_2O_3 \cdot P_2O_5$) is the only ferric oxo-phosphate phase with an iron-content between $FePO_4$ and Fe_2O_3. The solid-state phase transition temperature, decomposition temperature, and liquidus temperature determined in the present work are in good agreement with the respective temperatures reported in these earlier studies. The ferric oxo-phosphate phase reported in the Wentrup phase diagram,[9] $Fe_4P_2O_{11}$ ($2Fe_2O_3 \cdot P_2O_5$), could not be produced. This finding has implications for the development of ferric oxo-phosphate electrode materials. For example, the formation of Fe_3PO_7 as an electrode material for Li batteries was accomplished by heating stoichiometric mixtures of Fe_2O_3 and $FePO_4$ at 1050ºC for 12 hours.[7] This temperature is just below the eutectic temperature (1070ºC) of the Fe_3PO_7–$FePO_4$ system determined in this study (Fig. 4).

Glass-formation around the eutectic composition in the $FePO_4$-Fe_3PO_7 system has been evaluated and is described elsewhere.[23] The viscosities of those ferric phosphate melts near their respective liquidus temperatures were relatively low, necessitating the use of rapid quenching techniques (>10^3 ºC/sec) to form glasses. These quench rates were much faster than those needed to form glasses with compositions in the $Fe(PO_3)_3$-$Fe_4(P_2O_7)_3$ system. As shown in Fig. 9, the liquidus temperatures in the compositional range of approximately 36 to 43 mole% Fe_2O_3 are below 950ºC. This is the compositional range of greatest interest for vitrifying nuclear wastes[15-17] and the relatively low liquidus temperatures determined in this study are consistent with the glass forming tendencies reported in the literature.

To the best of our knowledge, this is the first report of liquidus temperature information for ferric-phosphate melts in the $Fe_4(P_2O_7)_3$–$Fe(PO_3)_3$ system. Part of the

difficulty in obtaining accurate information about these materials is avoiding the vaporization of P_2O_5, particularly at the higher temperatures required as compositions approach $Fe(PO_3)_3$. Glass formation from phosphate-rich melts has been reported,[19] but those glasses appear to have lost some phosphate and were subject to some iron reduction during the melting process.

Efforts were made in this study to minimize the effects of phosphate volatility and the reduction of ferric phases, but the compositional uncertainties associated with both processes may affect these final results. The compositional dependence of the liquidus temperatures of the ferric phosphate melts shown in Fig. 9 can be used for guidance in understanding the behavior of iron phosphate melts. However, these melts will reduce in air at typical melting temperatures (1000-1300ºC), to produce glasses with about 20% ferrous ions.[13] Information about the liquidus temperatures of iron phosphate glass forming melts is limited, but DTA studies of crystallization behavior of iron phosphate glasses reveal crystal melting temperatures near 900ºC,[6,17,26] consistent with the liquidus temperature for the ferric phosphate compositions summarized in Fig. 9.

1.4. CONCLUSIONS

The liquidus surface of the Fe_3PO_7–$Fe(PO_3)_3$ system was re-determined using sample preparation techniques that minimize the effects of sample volatilization and reduction. Significant differences are found when this work is compared to earlier reports. In particular, Fe_3PO_7 is the only ferric oxo-phosphate compound that forms and it decomposes in air at 1090°C. The liquidus temperature information in the $FePO_4$-Fe_3PO_7 sub-system is consistent with literature reports on processing materials of interest

for electrodes in lithium electrochemical devices. $Fe_4(P_2O_7)_3$ was found to melt congruently at 945°C, about 300°C lower than in earlier claims. For the first time, the liquidus surface of the $Fe(PO_3)_3$-$Fe_4(P_2O_7)_3$ subsystem has been reported. $Fe(PO_3)_3$ melts congruently at 1205°C and a eutectic point exists at 37.0% Fe_2O_3 (907°C). The liquidus temperatures of this sub-system are consistent with glass formation and crystallization behavior of compositions being developed for waste vitrification applications.

ACKNOWLEDGEMENTS

The authors are grateful to Dr. Eric W. Bohannan, Clarissa Wisner and Jong Wook Lim, Missouri University of Science and Technology, for their assistance with the XRD, SEM-EDS and Raman analyses, respectively. Fruitful discussions with Dr. Luciana Ghussn and Prof. Edgar Zanotto (São Carlos University, São Carlos, Brazil) on the crystallization behavior of iron phosphate melts are greatly appreciated. This work was supported by the National Science Foundation, grants DMR-0305202 and DMR-0502463.

REFERENCES

[1]M. G. Mesko and D. E. Day, "Immobilization of Spent Nuclear Fuel in Iron Phosphate Glass," *J. Nucl. Mater*. **273** 27-36 (1999).

[2]X. Yu, G. J. Long, R. K. Brow and D. E. Day, "Properties and Structure of Sodium–Iron Phosphate Glasses," *J. Non-Cryst. Solids* **215** 21-31 (1997).

[3]W. Huang, D. E. Day, C. S. Ray and C. W. Kim, "High Temperature Properties of an Iron Phosphate Melt Containing High Chrome Nuclear Waste," *J. Nucl. Mater*. **346** 298-305 (2005).

[4]C. W. Kim, C. S. Ray, D. Zhu, D. E. Day, D. Gombert, A. Aloy, A. Moguš-Milanković and M. Karabulut, "Chemically Durable Iron Phosphate Glasses for Vitrifying Sodium Bearing Waste (SBW) Using Conventional and Cold Crucible Induction Melting (CCIM) Techniques," *J. Nucl. Mater*. **322** 152-164 (2003).

[5]M. Karabulut, G. K. Marasinghe, C. S. Ray, D. E. Day, G. D. Waddill, C. H. Booth, P. G. Allen, J. J. Bucher, D. L. Caulder and D. K. Shuh, "An Investigation of the Local Iron Environment in Iron Phosphate Glasses Having Different Fe(II) Concentrations," *J. Non-Cryst. Solids* **306** 182-192 (2002).

[6]A. Moguš-Milanković, M. Rajić, A. Drašner, R. Trojko and D. E. Day, "Crystallization of Iron Phosphate Glasses," *Phys. Chem. Glasses* **39** 70-75 (1998).

[7]Y-S, Hong, Y.J. Park, K.S. Ryu and S.H Chang, "Crystalline Fe_3PO_7 as an Electrode Material for Lithium Secondary Batteries," *Solid State Ionics* **156** 27-33 (2003).

[8]C. M. Burba, J. M. Palmer and B. S. Holinsworth, "Laser-Induced Phase Changes in Olivine $FePO_4$: a Warning on Characterizing $LiFePO_4$-based Cathodes with Raman Spectroscopy," *J. Raman Spectrosc.* **40** 225-228 (2009).

[9] H. Wentrup. "Contribution on the System Iron-Phosphorus-Oxygen," *Arch. Eisenhüt.* **9** 57-60 (1935).

[10]J. Korinth and P. Royen. "Reaction in the System $Fe_2O_3/FePO_4$," *Z. Anorg. Allg. Chem*. **313** 121-37 (1961).

[11]J.C. Kaell, F. Jeannot and C. Gleitzer, "Study of the Progressive Reduction of $Fe_3(PO_4)_2$ and $Fe_9(PO_4)O_8$," *Ann. Chim*. **9** 169-80 (1984).

[12]A. Modaressi, J. C. Kaell, B. Malaman, R. Gérardin and C. Gleitzer. "Study of the System Fe-P-O (for Fe/P $\geq$1) and Its Compounds: the Oxyphosphates of Iron," *Mater. Res. Bull*. **18** 101-109 (1983).

[13]X. Fang, C. S. Ray, A. Mogus-Milankovic and D. E. Day. "Iron Redox Equilibrium, Structure and Properties of Iron Phosphate Glasses," *J. Non-Cryst. Solids* **283** 162-172 (2001).

[14]S. T. Reis, M. Karabulut and D. E. Day, "Structural Features and Properties of Lead–Iron–Phosphate Nuclear Wasteforms," *J. Nucl. Mater.* **304** 87-95 (2002).

[15]D. E. Day, Z. Wu, C. S. Ray and P. Hrma, "Chemically Durable Iron Phosphate Glass Wasteforms," *J. Non-Cryst. Solids* **241** 1-12 (1998).

[16]C. W. Kim and D. E. Day, "Immobilization of Hanford LAW in Iron Phosphate Glasses," *J. Non-Cryst. Solids* **331** 20-31 (2003).

[17] P.A. Bingham R. J. Hand, S. D. Forder, A. Lavaysierre, S. H. Kilcoyne and I. Yasin, "Preliminary Studies of Sulphate Solubility and Redox in $60P_2O_5$–$40Fe_2O_3$ Glasses," *Mater. Let.* **60** 844–847 (2006).

[18]G. K. Marasinghe, M. Karabulut, C. S. Ray, D. E. Day, M. G. Shumsky, W. B. Yelon, C. H. Booth, P. G. Allen and D. K. Shuh, "Structural Features of Iron Phosphate Glasses," *J. Non-Cryst. Solids* **222** 144-152 (1997).

[19]B. Pivac, A. Moguš-Milanković and D. E. Day, "Iron Valence and Coordination in Phosphate Glasses as Studied by Optical Spectroscopy," *J. Non-Cryst. Solids,* **226** 41-46 (1998).

[20]V. Caglioti, "The Structure of Ferric Phosphate," *Atti accad.Naz. Lincei Class Sci., Mat. Nat.* **22** 146-149 (1935).

[21]M. R. De Guire, T. R. S. Prasanna, G. Kalonji and R. C. O'Handley., "Phase Equilibria in the Iron Oxide–Cobalt Oxide–Phosphorus Oxide System," *J. Am. Ceram. Soc*. **70** 831-37 (1987).

[22]E. C. Shafer, M. W. Shafer and R. Roy, "Studies of Silica Structure Phases: II. Data on $FePO_4$, $FeAsO_4$, $MnPO_4$, BPO_4, $AIVO_4$, and Others," *Z. Krist.*, **108** 263-275 (1956).

[23]L. Zhang, R. K. Brow, M. E. Schlesinger, L. Ghussn and E. D. Zanotto, "Glass Formation from Iron-Rich Phosphate Melts," *J. Non-Cryst. Solid* **356** 252-257 (2010).

[24]D. L. Perry and S. L. Phillips, *Handbook of Inorganic Compounds*, CRC Press, Boca Raton (1995).

[25]L. Zhang, R. K. Brow and M. E. Schlesinger, "A Raman Study of Iron-Phosphate Compounds and Glasses," submitted to *J. Am. Ceram. Soc.,* Jun. 2010.

[26]L. Zhang, L. Ghussn, M.L. Schmitt, E.D. Zanotto, R.K. Brow and M.E. Schlesinger, "Thermal Stability of Glasses from the $Fe_4(P_2O_7)_3$-$Fe(PO_3)_3$ System," *J. Non-Cryst. Solids,* accepted 2010.

Table I. Preparation methods for ferric phosphate compounds.

Compound	**Raw materials**	**Preparation conditions**
Fe_3PO_7	$FePO_4 + Fe_2O_3$	12h at 950°C, then 72 hr at 1050°C
$Fe_4P_2O_{11}$	$FePO_4 + Fe_2O_3$, or $Fe_3PO_7 + FePO_4$	12-48h holds at 800, 900, 1000 and 1050ºC- all unsuccessful
$FePO_4$	$FePO_4 \cdot xH_2O$	12h at 880°C
$Fe_4(P_2O_7)_3$	$FePO_4 + Fe(PO_3)_3$	12h at 800°C, then 72h at 940°C
$Fe(PO_3)_3$	$Fe_2O_3 + NH_4H_2PO_4$	Ammonia burn-off from thoroughly mixed batch at 500°C overnight, followed by 12h hold at 800°C

Table II. Summary of the characteristic temperatures in the Fe_3PO_7–$Fe(PO_3)_3$ system.

Mole% Fe_2O_3	Temperature (ºC)	Description
75.0	1090±8	Decomposition of Fe_3PO_7
58.0±1.2	1070±5	Eutectic melting ($FePO_4$ - Fe_3PO_7)
50.0	1208±8	Congruent melting of $FePO_4$
42.7±0.4	925±8	Eutectic melting ($Fe_4(P_2O_7)_3$ - $FePO_4$)
40.0	945±8	Congruent melting of $Fe_4(P_2O_7)_3$
37.0±0.3	907±8	Eutectic melting ($Fe(PO_3)_3$ - $Fe_4(P_2O_7)_3$)
33.3	1205±8	Congruent melting of $Fe(PO_3)_3$

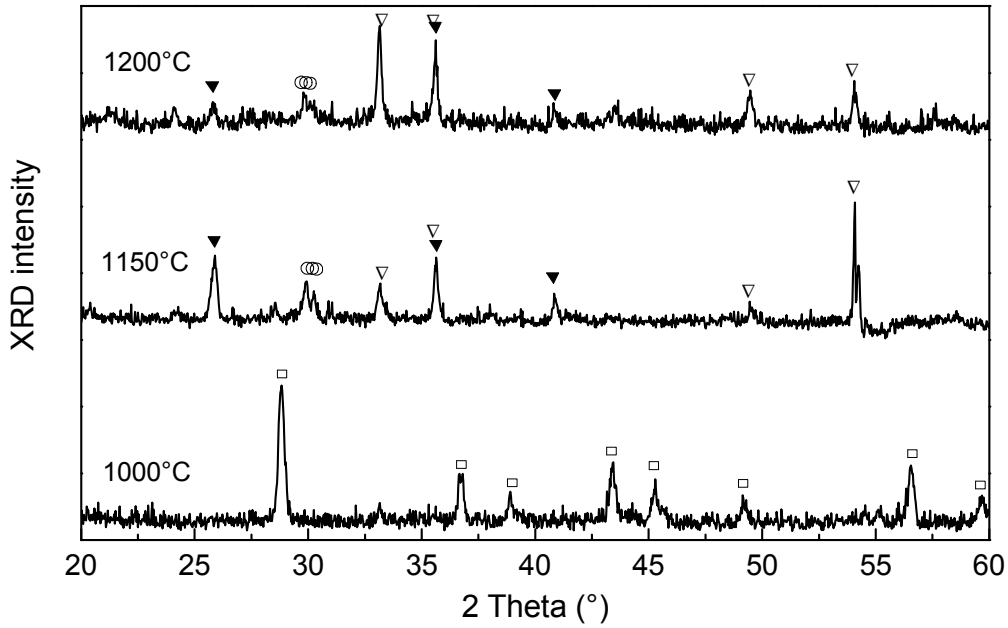

Figure 1: XRD patterns of Fe_3PO_7 quenched after 12 hours from (a) 1000°C, (b) 1150°C, and (c) 1200°C. □- Fe_3PO_7 (JCPD: 37-0061), ▼- $FePO_4$ (JCPD: 84-0875) , ∇ - Fe_2O_3 (JCPD:33-0664) and ○-$Fe_2P_2O_7$ (JCPD: 72-1516).

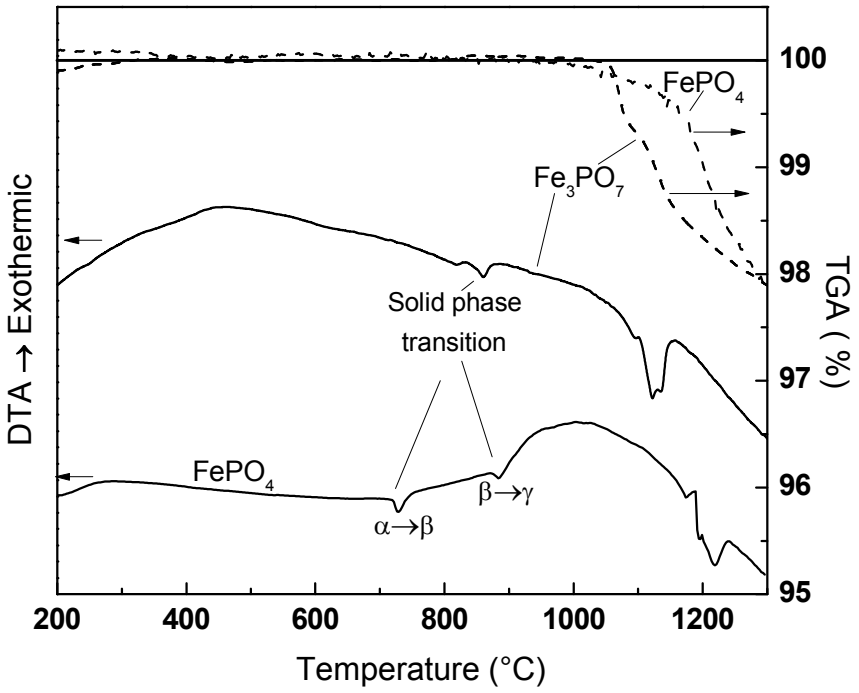

Figure 2: DTA and TGA patterns for Fe_3PO_7 and $FePO_4$.

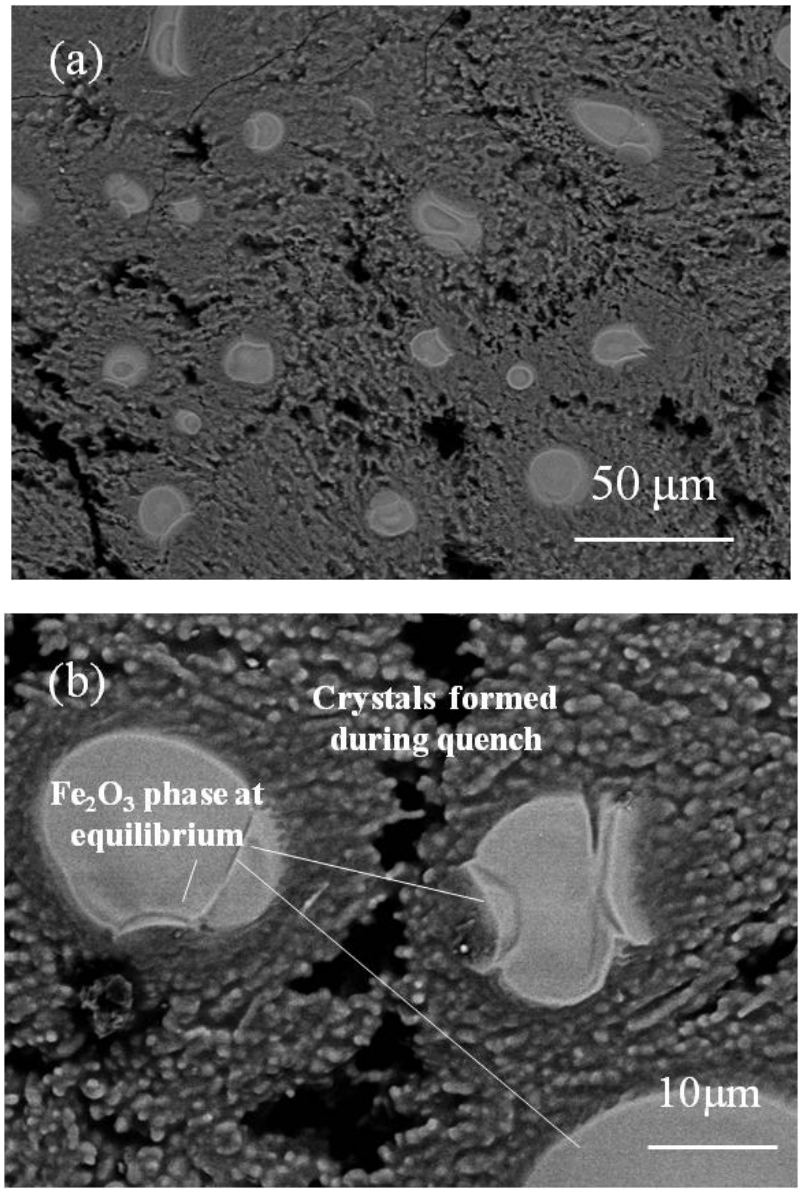

Figure 3: Backscattered electron images of Fe_3PO_7 quenched after dwelling for twelve hours at 1200°C.

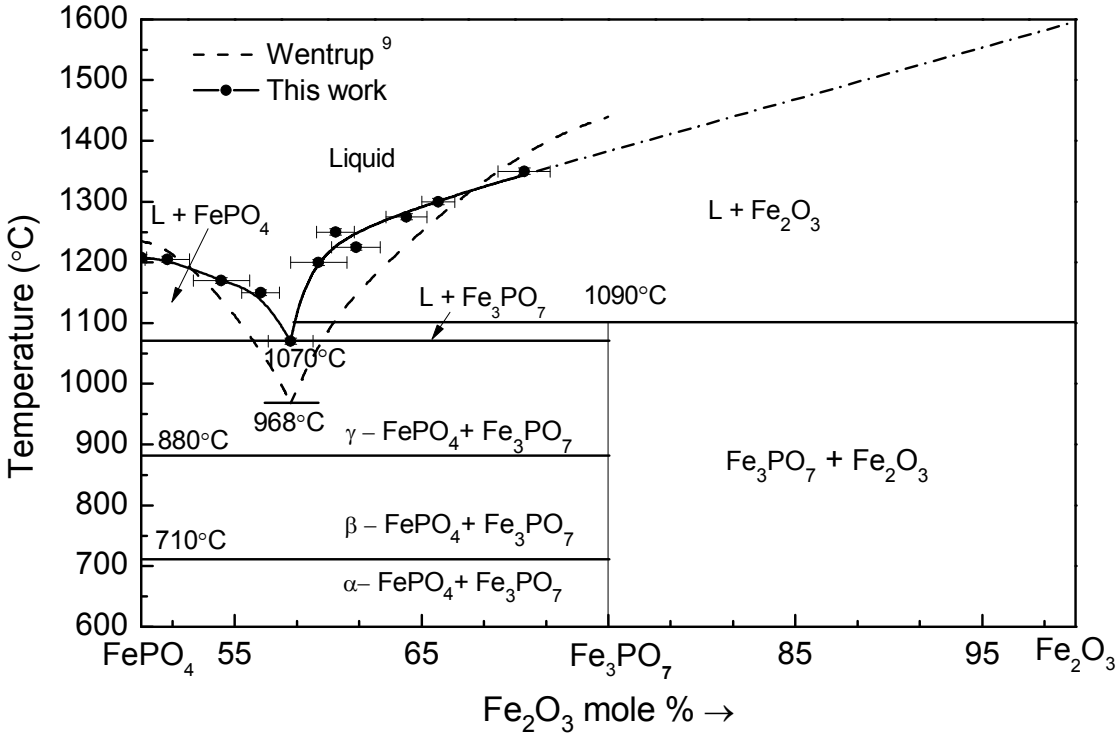

Figure 4: Phase diagram of the $FePO_4$–Fe_3PO_7 system. Dashed-dotted line is an extrapolation of the curve used to fit the experimental liquidus points.

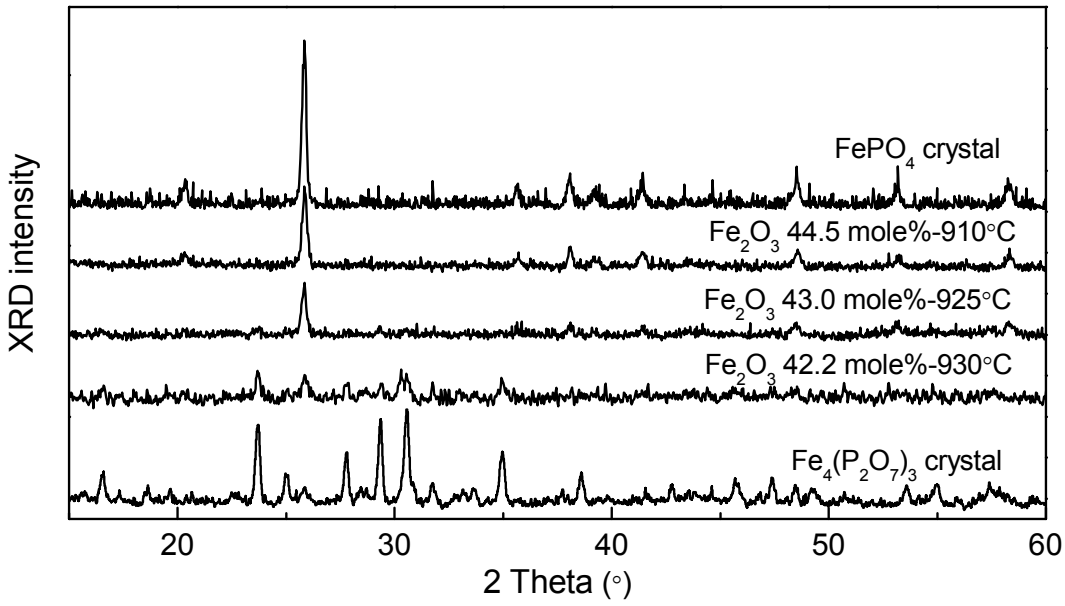

Figure 5: XRD patterns of some compositions quenched from the temperature below their liquidus temperature, compared with crystalline $FePO_4$ and $Fe_4(P_2O_7)_3$.

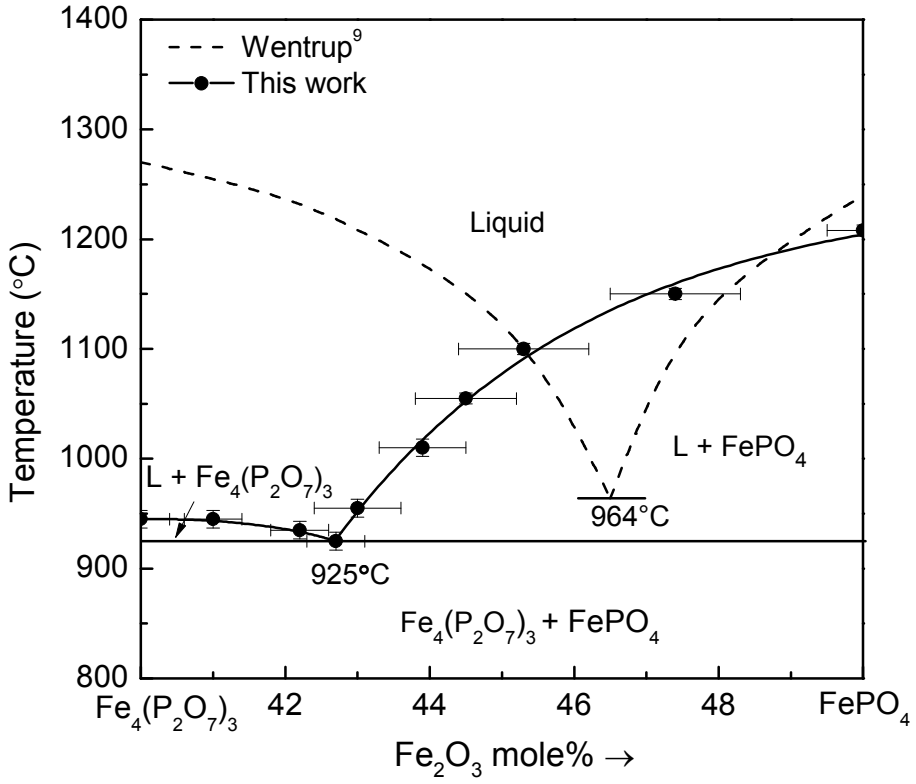

Figure 6: Liquidus surface of the $FePO_4$–$Fe_4(P_2O_7)_3$ system.

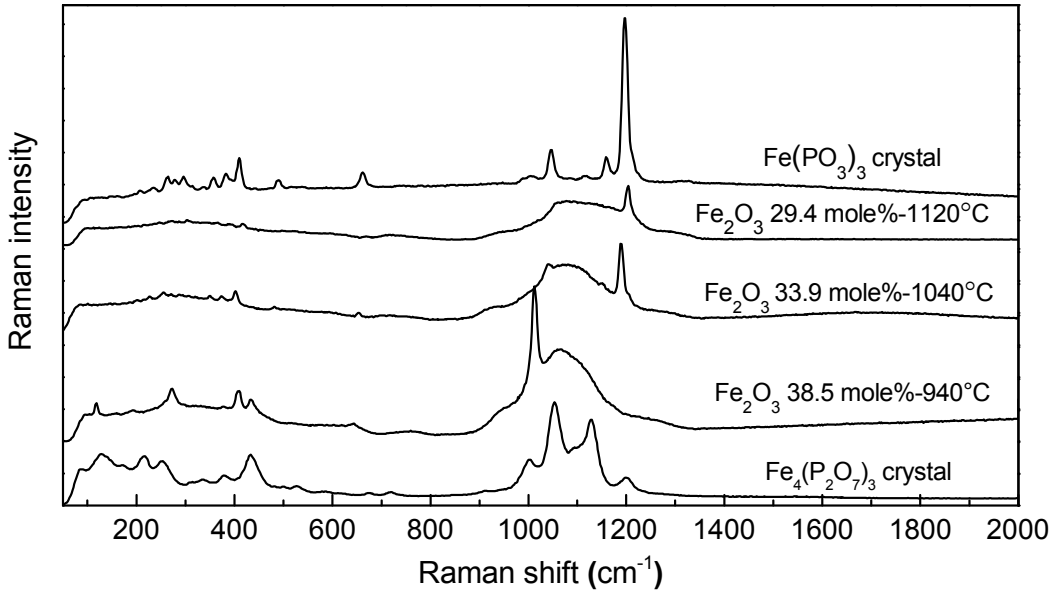

Figure 7: Raman spectra of several partially-crystallized samples quenched from the indicated temperatures and from crystalline $Fe(PO_3)_3$ and $Fe_4(P_2O_7)_3$.

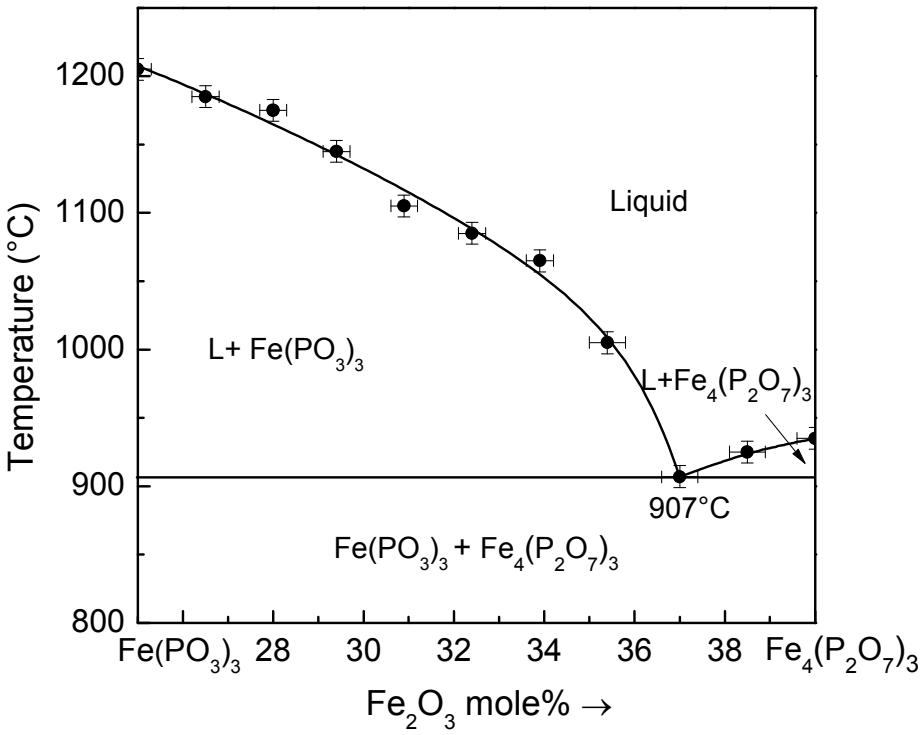

Figure 8: Liquidus surface of the $Fe_4(P_2O_7)_3$–$Fe(PO_3)_3$ system.

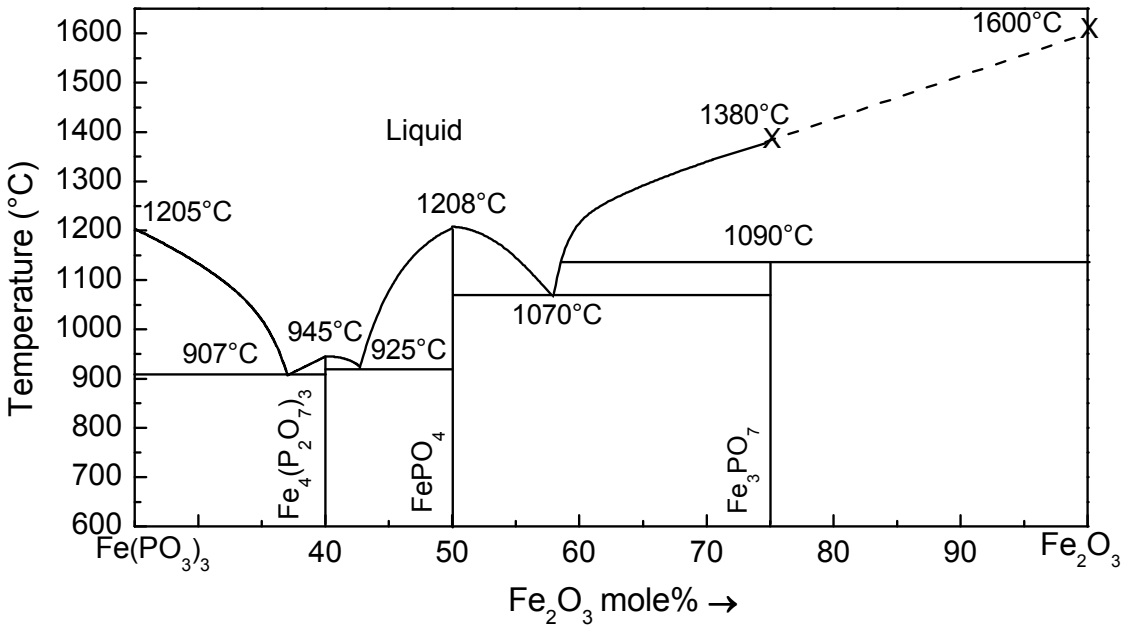

Figure 9: Summary of the liquidus surface of the ferric phosphate system.

2. GLASS FORMATION FROM IRON-RICH PHOSPHATE MELTS

L. Zhang[a], R.K. Brow[a,*], M.E. Schesinger[a], L. Ghussn[b], E.D. Zanotto[b]

[a] *Missouri University of Science and Technology, Department of Materials Science and Engineering, 1400 N. Bishop Ave., Rolla, MO 65409-0340 U.S.A.*

[b] *Universidade Federal de São Carlos, Vitreous Materials Laboratory, LaMaV, Rod. Washington Luis, Km. 235, 13.565-905 São Carlos, Brazil*

ABSTRACT

Iron-rich phosphate glasses with nominal Fe/P ratios between 1.0 and 1.6 were prepared by a roller-quenching technique. The critical cooling rates (CCR) for glass formation were estimated by differential thermal analysis and found to be in the range 10^3-10^4 ºC/sec for the iron-rich melts, compared to 1-10ºC/sec for conventional iron phosphate melts with nominal Fe/P ratios near 0.50. The $Fe(II)/Fe_{total}$ fraction in the quenched glasses increases with melt time and temperature, and ranges between 0.30 and 0.55 for the glasses studied. Raman spectroscopy indicates that the structures of the iron-rich phosphate glasses are based on isolated orthophosphate tetrahedra, similar to what are found in α-$FePO_4$.

Keywords: Iron phosphate glasses, iron-rich phosphate, glass formation, glass structure

---

*Corresponding author. Tel.: +01 573 341 6812; fax: +01 573 341 2071.

E-mail address:Brow@mst.edu.

2.1. INTRODUCTION

Iron phosphate glasses have been developed as alternative materials for high-level nuclear waste encapsulation [1–8]. The glasses can dissolve large quantities of a variety of waste components while retaining outstanding chemical durability. Iron phosphate glasses also exhibit interesting electrical and magnetic properties that depend on the iron coordination number and redox state [9,10].

Iron phosphate compositions with nominal Fe/P atom ratios between 0.33 and 0.67 have good glass forming ability (GFA) and have been widely studied [1–8]. Phosphate-rich ferrous ultraphosphate glasses (FeO/P_2O_5<1:1) were made in sealed silica tubes under vacuum and their structures and properties characterized [11,12]. Glasses with Fe/P ratios as high as 1.83 have been prepared by quenching microwave- or joule-heated melts between pre-cooled copper plates [13], but the structure and properties of these iron-rich glasses were not investigated. Glasses with Fe/P ratios between 1.0 and 2.3 were made by twin-roller quenching [14], and the magnetic properties of one glass (Fe/P =2.3) were reported. However, little is known about the structure and thermal stability of iron-rich (Fe/P>1) phosphate glasses.

The structures of iron phosphate glasses with Fe/P ratios between 0.33 and 0.67 are reported to be similar to the short range structure of crystalline $Fe_3(P_2O_7)_2$ [7]. Ferrous and ferric ions in distorted octahedral sites are assumed to link neighboring pyrophosphate anions to constitute the glass structure. The fraction of ferrous ions, Fe^{2+}/Fe_{total}, in the quenched glasses increases with melting temperature and with iron content. For conventional iron phosphate glasses, Fe^{2+}/Fe_{total} is below 0.4 and melts with

$Fe^{2+}/Fe_{total} \geq 0.4$ crystallize more rapidly while quenched in air by pouring into steel molds [7].

It is well-known that GFA is enhanced for melt compositions near deep eutectics [15-17]. GFA can be characterized using critical cooling rate (CCR) experiments to determine the conditions required to avoid crystallization upon quenching. Turnbull proposed that GFA was related to the ratio between the glass transition temperature (T_g) and the liquidus temperature (T_L); the greater T_g/T_L, the better the GFA [18]. Other common glass stability (GS) parameters are listed in Table 1. These GS parameters were evaluated by Nascimento, et al. [23] using thermal analytical information and related to GFA for eight different glass forming systems. The three GS parameters listed in Table 1 correlate well with experimental measurements of GFA, and their respective critical cooling rate relationships are also given in Table 1.

The liquidus surface of the Fe_3PO_7–$FePO_4$ system was reported by Wentrup [24] to have a eutectic point at Fe/P = 1.38 (molar). This system has been re-investigated as part of a larger study of the Fe_2O_3–P_2O_5 liquidus surface that is to be published elsewhere [25]; a similar eutectic composition was found, but at a greater eutectic temperature (1070°C vs 968°C) than reported by Wentrup.

In the present study, the glass forming tendencies of iron phosphate melts with initial molar compositions around the reported eutectic point of the Fe_3PO_7–$FePO_4$ system ($1.00 \geq Fe/P \geq 1.60$) were investigated. The melts studied here have significantly greater iron contents than typical iron phosphate glasses, and Raman spectroscopy indicates that these glasses possess “invert” structures [26] based on isolated

orthophosphate tetrahedra linked through iron polyhedra. The glass forming ability of these melts was studied using DTA characterization and the GS parameters in Table 1.

2.2. EXPERIMENTAL PROCEDURES

Compositions near the eutectic point between $FePO_4$ and Fe_3PO_7, with nominal Fe/P atom ratios between 1.0 and 1.6, were investigated, along with compositions of conventional iron phosphate glass (Fe/P = 0.5, 0.67 and 0.82). A total of two grams of reagent grade Fe_2O_3 (Alfa Aesar, ≤45 μm, ≥99%) and $FePO_4$, obtained by dehydrating $FePO_4 \cdot xH_2O$ (>99%, Alfa Aesar), were used to prepare the iron–rich (Fe/P ≥ 1.0) phosphate glasses. Mixtures of $NH_4H_2PO_4$ (Alfa Aesar, 98%) and Fe_2O_3 were used to prepare 10-30 grams of the conventional (Fe/P<1.0) iron phosphate glasses. For all glasses, the raw materials were thoroughly mixed and then heated in alumina crucibles for the times and temperatures indicated in Table 2. Melts were quenched either by cooling thick (2–4 mm) patties in air, by pressing thin (~1 mm) samples between steel plates, or by preparing very thin (<100 μm) ribbons with a twin-roller quencher. The distance between the two rollers and the rotation rate could be adjusted to modify the ribbon thickness, and thus the quench rate.

The quenched samples were pulverized to <53 μm and analyzed by x-ray diffraction (XRD Scintag XDS 2000) and differential thermal analysis (Perkin-Elmer DTA7). The DTA runs were performed in air at a heating rate of 10°C/min. Characteristic temperatures from the DTA experiments were used to calculate CCRs based on the equations reported by Nascimento, et al. [23] and summarized in Table 1.

The melting times and temperatures were varied for some samples to study processing effects on the Fe^{+2}/Fe_{total} ratio. The Fe^{2+}/Fe_{total} ratios in the glasses were determined by a titration method [27] with 2 mM $KMnO_4$. Raman spectra (Horiba-Jobin Yvon LabRam-HR) in the range of 50-2000 cm^{-1} were collected using a He-Ne laser (632.8 nm) on glass powders and on powders of crystalline α-$FePO_4$ and $Fe_3(P_2O_7)_2$. Powders from roller-quenched iron-rich ($Fe/P \geq 1$) glasses were analyzed, along with powders from plate-quenched conventional ($Fe/P < 1$) glasses. α-$FePO_4$ was prepared by dehydrating $FePO_4 \cdot xH_2O$ at 880°C for ~24 hours. $Fe_3(P_2O_7)_2$ was prepared by heating stoichiometric mixtures of $Fe_4(P_2O_7)_3$ and $Fe_2P_2O_7$ in sealed silica tubes for twelve hours at 900°C. $Fe_4(P_2O_7)_3$ was initially prepared using methods reported in [28], and $Fe_2P_2O_7$ was prepared by reducing $FePO_4$ in forming gas (10% H_2 and 90% Ar) at 560°C.

2.3. RESULTS

2.3.1. Glass Forming Tendency. Figure 1 shows the XRD patterns of glasses from (a) a roller-quenched Fe/P = 1.30 melt and (b) the same melt after quenching between steel plates. The broad diffuse peak in the pattern for the roller quenched glass indicates the amorphous state of the sample. The crystalline phases detected in this partially crystallized, plate-quenched sample are $FePO_4$, $Fe_3(P_2O_7)_2$ and $Fe_7(PO_4)_6$.

Table 3 summarizes the XRD analyses of glasses prepared from melts with different nominal compositions and quenched by different means. Every sample prepared from the iron-rich melts ($Fe/P \geq 1.0$) exhibited evidence of crystallization when cooled in air or between steel plates. However, the roller-quenched melts yielded glasses with no detectable crystallinity. The cooling rates that each method can achieve depend on the

melt temperature, sample size and other experimental conditions. From reports in the literature, cooling in air from temperatures below 1300°C and pressing from 1300°C between steel plates can achieve cooling rates in the range 10-10^3 °C/sec [23,29]. Twin-roller quenching can achieve cooling rates as high as 10^6 °C/sec [30].

2.3.2. The Dependence of Fe(II) Content on Melt Conditions. Figure 2 shows that the relative Fe(II) content of roller-quenched, iron-rich glasses increases with melt time, reaching a constant value after about one hour. Figure 3 shows that the Fe(II) content increases with melt temperature, and that glasses with greater Fe/P ratios have greater Fe(II) contents when quenched from melts held at the same temperature. A model to predict the effects of melt composition, atmosphere and temperature on the equilibrium Fe^{2+}/Fe_{total} ratio has been developed and will be reported elsewhere [31].

2.3.3. Thermal Characteristics. Figure 4 shows DTA patterns collected in air for several glasses (melting time: two hours) investigated in this work. In general, for glasses melted under similar conditions, T_g increases and the peak temperature for crystallization (T_X^p) decreases with increasing Fe/P ratio, as summarized in Fig. 5. (Note that the characteristic temperatures for the iron-rich glasses were obtained from roller-quenched samples, whereas plate-quenched samples of the conventional iron phosphate glasses were evaluated.) The estimated uncertainty of these temperatures is ±5°C based on the multiple DTA runs. Also shown in Fig. 5 are the liquidus temperatures (T_L) for the respective melts, as reported elsewhere [25]. The values of (T_X^p -T_g) for the iron-rich (Fe/P ≥ 1.0) glasses are much smaller (35-67°C) than that (~300°C) of the conventional iron phosphate glass (Fe/P = 0.50). This is consistent with the much better glass forming tendency of the latter composition, as indicated by the XRD results summarized in

Table 3. Moguš-Milanković, et al. [32] report a similar decrease in (T_X^p -T_g) with increasing Fe/P content for a much smaller range of iron phosphate glass compositions.

2.3.4. Glass Structure. Raman spectra collected from plate-quenched glasses with nominal Fe/P ratios less than 1.0 are compared with that collected from crystalline $Fe_3(P_2O_7)_2$ in Fig. 6. For $Fe_3(P_2O_7)_2$, peaks in the range 1000-1200 cm^{-1} can be assigned to symmetric and asymmetric stretching modes of P-O bonds in the pyrophosphate anions [33]. The low intensity peak near 760 cm^{-1} is assigned to a P-O-P stretching mode, the peak near 670 cm^{-1} is assigned to a P-O bending mode, and the series of peaks below 400 cm^{-1} are assigned to various Fe-O and P-O modes. The Raman spectra from the iron phosphate glasses have a broad peak centered near 1030-1050 cm^{-1}, several low intensity peaks below 600 cm^{-1}, and, for the glasses with Fe/P = 0.50 and 0.67, a less intense peak between 690-800 cm^{-1}. The broad peak centered near 1030-1050 cm^{-1} has been assigned to the symmetric and asymmetric stretching modes of non-bridging oxygens associated with different phosphate tetrahedra; for example, non-bridging oxygens on tetrahedra with one bridging oxygen (Q^1 tetrahedra) account for peaks near 1030-1050 cm^{-1} and those on tetrahedra with two bridging oxygens (Q^2) account for shoulders near 1200 cm^{-1} [34,35]. The peak between 600-800 cm^{-1} is assigned to the symmetric stretching mode of bridging oxygens, $(P\text{-}O\text{-}P)_{sym}$, in the glass structure [36]. The similarity in the spectra from these glasses with that from crystalline $Fe_4(P_2O_7)_2$ is consistent with the proposal that these glasses possess short-range structures that are similar to the short range structure of crystalline $Fe_4(P_2O_7)_2$ [7]. In particular, these glasses possess pyrophosphate anions that are linked by ferrous and ferric polyhedra.

Raman spectra collected from roller-quenched iron-rich glasses (Fe/P ≥ 1.00) are shown in Fig. 7, and are compared with that collected from crystalline α-$FePO_4$. The Raman spectra from the iron-rich glasses are distinctly different from those of the conventional iron phosphate glasses, shown in Fig. 6. The spectra from the iron-rich glasses are dominated by an intense peak centered near 1002 cm^{-1}, as well as a number of lower intensity peaks in the range between 100 and 500 cm^{-1}. The peak centered near 1002 cm^{-1} is assigned to $P\text{-}O^-$ stretching modes of non-bridging oxygens on Q^0 tetrahedra, consistent with the spectrum from α–$FePO_4$, where this peak is found at 1009 cm^{-1}. This peak is broader (full width at half-maximum = 30-50 cm^{-1}) in the spectra from the glasses than that obtained from α–$FePO_4$ (FWHM = 10 cm^{-1}), consistent with a greater degree of disorder associated with these roller-quenched glasses. (The glass with Fe/P = 1.6 fluoresced substantially when the Raman spectra were collected. This might contribute to the relative broadening of the 1000 cm^{-1} peak noted for this sample in Fig. 7.) The broadening and decrease in frequency of this peak for the glasses, compared to α-$FePO_4$, is consistent with what was reported by Burba, et al. [37] in their recent study of crystalline and disordered α-$FePO_4$. There is no distinct evidence for nonbridging oxygen modes at greater wave numbers in the Raman spectra of the iron-rich glasses, nor for the $(P\text{-}O\text{-}P)_{sym}$ stretching mode near 700 cm^{-1}. The peaks between 400-500cm^{-1} arise from the O-P-O bending modes of Q^0 units [32,38]. The peaks at ~260 cm^{-1} are likely related to the bending Q^0 with Fe as modifier [38]. The peaks below 200 cm^{-1} have been assigned to both P-O and Fe-O modes [39,40]. The similarity in the spectra from the iron-rich glasses with the spectrum from α–$FePO_4$ in Fig. 7 indicates that similar P- and Fe-tetrahedra likely exist in the glasses.

2.4. DISCUSSION

2.4.1. Glass Formation and Structure. Figure 8 compares the glass-forming range (region 'a') for conventional iron phosphate glasses based on the reported data [6,7,9], with the glass-forming range for the new iron-rich phosphate glasses studied in this work (region 'b'). Here, the open symbols represent the compositions of the glass batches and the 'x' symbols within region 'b' indicate the compositions of the iron-rich, x-ray amorphous glasses prepared by roller quenching. The reduction of Fe^{3+} to Fe^{2+} during melting decreases the O/P ratios of these quenched glasses from their nominal values. The heavy line in Fig. 8 indicates compositions with an O/P ratio of 4.0; compositions below this line have O/P > 4.0. The new glass-forming range (region 'b') for iron-rich compositions is bounded by the crystalline phases $FePO_4$, $Fe_2P_2O_7$, $Fe_3(P_2O_7)_2$, Fe_3PO_7 and $Fe_7(PO_4)_6$, each of which has been identified by XRD in various partially crystallized samples (Table 3).

It is worth emphasizing that the reported glass-forming range for the conventional iron phosphate glasses (region 'a' in Fig. 8) represent lower quenching rates (as cast or plate quench) than are obtained by the roller quench techniques used to produce the iron-rich glasses (region 'b'). It is expected that roller-quenching would increase substantially the glass-forming range of meta- and polyphosphate compositions ($3 \leq O/P \leq 4$) beyond that indicated in 'region a'. In the present work, only roller-quenched melts near the orthophosphate ($O/P \geq 4$) composition were studied.

If the acidic phosphate units accept oxygens from the more basic iron oxide, then at O/P = 4, only nonbridging oxygens will be associated with the phosphate anions, forming isolated orthophosphate (Q^0) units that must be linked to neighboring iron

polyhedra through the nonbridging oxygens. For glasses with O/P > 4, the additional oxygens must be incorporated into the structure in the form of Fe-O-Fe bonds, with little effect on the nature of the orthophosphate anions. (Similar 'invert' structures have been reported for titanium-rich phosphate glasses [41].) The Raman spectra of the iron-rich glasses (Fig. 7) are dominated by a narrow peak at 1002 cm^{-1} that indicates the presence of the expected orthophosphate units, and this peak does not change with increasing Fe/P (and O/P) ratio. In contrast, the broad Raman peak centered near 1050 cm^{-1} in the spectrum of the Fe/P glass (Fig. 6) shifts to lower wavenumbers with increasing Fe/P ratio, consistent with the replacement of Q^2-tetrahedra by Q^1-tetrahedra as the overall O/P ratio increases. The Raman spectra indicate that the phosphate-rich compositions have larger phosphate anions that include Q^2 (middle units) and Q^1 (chain terminators) tetrahedra, whereas the iron-rich glassses possess only isolated (Q^0) tetrahedra. The relative complexity of the conventional glasses is reflected in the broader Raman peak associated with the P-O stretching modes (Fig. 6), compared to the respective peaks from the iron rich glasses. A detailed description of the Raman spectra of iron phosphate compounds and glasses will be presented elsewhere [42].

2.4.2. Critical Cooling Rate Estimation. Figure 9 shows the calculated critical cooling rates (CCRs) for the iron phosphate melts based on the characteristic temperatures shown in Fig. 5 and the equations listed in Table 1. The CCRs for the iron-rich (Fe/P $\geq$ 1.0) phosphate melts are in the 10^3-10^4 ºC/sec range, compared to CCRs of 1-10ºC/sec for conventional Fe-phosphate melts. The calculated CCRs indicate the difficulties of making iron-rich phosphate glass by quenching in air or pressing between

metal plates. The tendency of CCR to increase with increasing Fe/P ratio is consistent with the glass forming experiments summarized in Table 3.

In general, phosphate glasses with longer phosphate chains (smaller O/P ratios) are more stable against devitrification. For example, Wange, et al. [43] report that crystallization tendency of a complex Ca-phosphate glass increases with increasing O/P ratio as smaller phosphate anions are available to constitute the glass structure. (Crystallization tendency also depends on the nature of oxides used to modify the glass; oxides that strengthen the glass network, like Al_2O_3 and TiO_2, increase viscosity and reduce crystallization tendency compared to oxides like CaO and Na_2O.) The addition of various oxides to an iron phosphate base glass tends to reduce the temperature difference between T_g and T_x, indicating an increase in crystallization tendency with increasing O/P ratio [8], although the extent of the temperature difference also depends on the nature of the oxide added. The enhanced crystallization behavior may be related to the changes in the rheological properties of phosphate glasses with shorter average phosphate chain-lengths. The rheological characteristics and the tendency of a phosphate melt to crystallize when sheared also depend on the type of phosphate anions that are present in the melt [44]. Smaller anions are often associated with faster crystallization.

The high CCR for glass formation from the iron-rich phosphate melts will limit the use of these glasses, particularly for applications like waste fixation that require the formation of relatively large samples with minimal crystallization. However, the expanded range of glass formation to the orthophosphate 'invert' structures raises the likelihood that other compositions with similar structures can be developed, including those with a lower CCR. For example, the structures of the 'NASICON' (sodium super-

ionic conductors) family of glasses are based on orthophosphate ions and include ferric phosphate versions [45]. More recently, lithium-doped iron orthophosphate glasses have been produced in studies to develop cathode materials for Li-ion batteries [46]. The crystallization tendency of these glasses, determined by the difference in T_g and T_x obtained by DTA measurements, decreases with the addition of Li_2O.

2.5. CONCLUSIONS

Studies of glass formation and structure in the iron phosphate system have been extended to iron-rich compositions, with nominal Fe/P ratios in the range 1.0-1.6. Critical cooling rates estimated from characteristic temperatures obtained by differential thermal analyses are at least 10^3 times greater for the new iron-rich compositions than for the conventional iron phosphate melts. The fraction of Fe(II) increases with increasing melt time and temperature. These new glasses have structures based on isolated phosphate tetrahedra (Q^0) and on Fe(II) and Fe(III) polyhedra.

ACKNOWLEDGMENTS

The authors gratefully acknowledge Melodie L. Schmitt and Jong Wook Lim for their kind assistance and helpful discussion. This work is supported by the National Science Foundation (U.S.A.) under Grant DMR-0502463, CNPq (Brazil) Grant no. 492565/04-0 and FAPESP (Brazil) Grant 07/08179-9.

REFERENCES

[1] B. C. Sales, L. A. Boatner, Science, 226 (1984) 45.

[2] M. G. Mesko, D. E. Day, J. Nucl. Mater., 273 (1999) 27.

[3] S. T. Reis, M. Karabulut, D. E. Day, J. Nucl Mater., 304 (2002) 87.

[4] W. Huang, C. W. Kim, C. S. Ray, D. E. Day, Ceram. Trans., 143 (2003) 347.

[5] W. Huang, D. E. Day, C. S. Ray, C. W. Kim, A. Mogus-Milankovic, J. Non-Cryst. Solids, 327 (2004) 46.

[6] X. Fang, C. S. Ray, A. Mogus-Milankovic, D. E. Day, J. Non-Cryst. Solids, 283 (2001) 162.

[7] G.K. Marasinghe, M. Karabulut, C. S. Ray, D. E. Day, M. G. Shumsky, W. B. Yelon, C. H. Booth, P. G. Allen, D. K. Shuh, J. Non-Cryst. Solids, 222 (1997) 144.

[8] P. A. Bingham, R. J. Hand, O. M. Hannant, S. D. Forder, S. H. Kilcoyne, J. Non-Cryst. Solids, 355 (2009) 1526.

[9] Y. M. Moustafa, K. El-Egili, H. Doweidar, I. Abbas, Phys., 353 (2004) 82.

[10] J. L. Shaw, A. C. Wright, R. N. Sinclair, G. K. Marasinghe, D. Holland, M. R. Lees, C. R. Scales, J. Non-Cryst. Solids, 345&346 (2004) 245.

[11] U. Hoppe, M. Karabulut, E. Metwalli, R. K. Brow, P. Jovari, J. Phys Cond. Matter, 15 (2003) 6143.

[12] M. Karabulut, E. Metwalli, D. E. Day, R. K. Brow, J. Non-Cryst. Solids, 328 (2003) 199.

[13] F. J. M. Almeida, J. R. Martinelli, C. S. M. Partiti, J. Non-Cryst. Solids, 353 (2007) 4783.

[14] K. Tanaka, N. Soga, R. Ota, K. Hirao, Bull. Chem. Soc. Jpn., 59 (1986) 1079.

[15] D. R. Uhlmann, J. Am. Ceram. Soc., 66 (1983) 95.

[16] W. Vogel, Glass Chemistry, 2nd ed., Springer, Berlin (1985).

[17] H. Bürger, K. Kneipp, H. Hobert, W. Vogel, V. Kozhukharov, S. Neov, J. Non-Cryst. Solids, 151 (1992) 134.

[18] D. Turnbull, Contemp. Phys., 10 (1969) 473-488.

[19] Z. P. Lu, C. T. Liu, Acta. Mater., 50 (2002) 3501.

[20] Z. P. Lu, C. T. Liu, Phys. Rev. Lett., 91 (2003) 115505.

[21] M. C. Weinberg, Phys. Chem. Glasses, 35 (1994) 119.

[22] A. Hruby, Czech J. Phys. B, 22 (1972) 1187.

[23] M. L. F. Nascimento, L. A. Souza, E. B. Ferreira, E. D. Zanotto, J. Non-Cryst. Solids, 351 (2005) 3296.

[24] H. Wentrup, Arch. Eisenhüt., 9 (1935) 57.

[25] L. Zhang, M. E. Schlesinger, R. K. Brow, "Phase Equilibria in the Iron Phosphate System," to be published.

[26] H. J. L Trapp, J. M. Stevels, Phys. Chem. Glasses., 1 (1960) 107.

[27] S. I. Grishin, J. M. Bigham, O. H. Tuovinen, Appl. Environ. Microbiol., 54 (1988) 3101.

[28] L.K. Elbouaanai, B. Malaman, R. Gérardin, M. Ijjaali, J. Solid State Chem. 163 (2002) 412.

[29] M. Milanova, R. Iordanova, Y. Dimitriev, K. Kostov, S. Vassilev, J. Mater. Sci., 42 (2007) 3349.

[30] K. B. R. Varma, Bull. Mater. Sci., 9 (1987) 1.

[31] M. L. Schmitt, R. K. Brow, M. E. Schlesinger, "Predicting the Iron Redox Ratio in Iron Phosphate Melts: A Thermodynamic Model," to be submitted.

[32] A. Moguš-Milanković, M. Rajić, A. Drašner, R. Trojko, D. E. Day, Phys. Chem. Glasses, 39 (1998) 70.

[33] E. J. Baran, R. C. Mercader, A. Massaferro, E. Kremer, Spectrochim. Acta Part A, 60 (2004) 1001.

[34] A. Mogus-Milankovic, B. Pivac, K. Furic, D. E. Day, Phys. Chem. Glasses, 38 (1997) 74.

[35] C. Nelson, D. R. Tallant, Phys. Chem. Glasses, 26 (1985) 119.

[36] A. M. Efimov, J. Non-Cryst. Solids, 209 (1997) 209.

[37] C. M. Burba, J. M. Palmer, B. S. Holinsworth, J. Raman Spectrosc., 40 (2009) 225.

[38] A. Moguš-Milanković, A. Šantić, S. T. Reis, K. Furić, D. E. Day, J. Non-Cryst. Solids, 342 (2004) 97.

[39] S. Okada, T. Yamamoto, Y. Okazaki, J. Yamaki, M. Tokunaga, T. Nishida, J. Power Sources, 146 (2005) 570.

[40] C. Murli, S. M. Sharma, S. K. Kulshreshtha, S. K. Sikka, Pramana, 49 (1997) 285.

[41] R. K. Brow, D. R. Tallant, W. L. Warren, A. McIntyre, D. E. Day, Phys. Chem. Glasses, 38 (1997) 300.

[42] L. Zhang, R. K. Brow, M. E. Schlesinger, "A Raman Study of Iron Phospahte Compounds and Glasses," to be submitted.

[43] P. Wange, J. Vogel, S. Knoche, and C. Russel, Glass Sci. Technol.,77[4] 172 (2004)

[44] J. U. Otaigbe, G. H. Beall, Trends in Polymer Science, 5[11] (1997) 369.

[45] T. Banu, K. K. Rao, M. Vithal, Phys. Chem. Glasses – Eur. J. Glass Sci. Tech. B, 44 (2003) 30.

[46] P. Jozwiak, J. E. Garbarczyk, M. Wasiucionek, I. Gorzkowska, F. Gendron, A. Mauger, C. M. Julien, Solid State Ionics, 179 (2008) 46.

Table 1: GS parameters and calculation equation.

GS parameter	Reference	Equation for Critical Cooling Rate (°C/sec), from ref. [23]
$K_T = \frac{T_g}{T_L}$	[18]	--
$K_L = \frac{T_X^p}{T_g + T_L}$	[19,20]	CCR = 16.7-33.1 K_L
$K_W = \frac{T_X^p - T_g}{T_L}$	[21]	CCR = 4.0-20.5 K_W
$K_H = \frac{T_X^p - T_g}{T_L - T_X^o}$	[22]	CCR = 3.0-2.44 K_H

Table 2: Glass compositions and the melting conditions.

Initial Fe/P ratio	Melting temperature (°C)	Melting Time (hrs)
1.60	1250	2
1.50	1200	2
1.38	1150	0.5, 1.0, 2.0, 6.0
1.38	1200	0.5, 2
1.30	1200	2
1.00	1250	2
1.00	1300	0.5, 1.0, 2.0, 6.0
0.82	1200	2
0.67	1200	2
0.50	1200	2

Table 3: Major crystalline phases detected by XRD from Fe_2O_3-P_2O_5 melts quenched by different methods; all melting time was 2 hrs.

Nominal (Fe/P ratio)	Air quench	steel quench	Roller quench
0.50	None detected	None detected	None detected
0.67	None detected	None detected	None detected
0.82	$FePO_4$, $Fe_3(P_2O_7)_2$	None detected	None detected
1.00	$FePO_4$, $Fe_2P_2O_7$	$FePO_4$, $Fe_2P_2O_7$	None detected
1.30	$Fe_7(PO_4)_6$, $Fe_3(P_2O_7)_2$, $FePO_4$	$Fe_7(PO_4)_6$, $Fe_3(P_2O_7)_2$, $FePO_4$	None detected
1.38	$FePO_4$, $Fe_3(P_2O_7)_2$	$FePO_4$, $Fe_3(P_2O_7)_2$	None detected
1.50	$FePO_4$, $Fe_7(PO_4)_6$	$FePO_4$, $Fe_7(PO_4)_6$	None detected
1.60	$FePO_4$, $Fe_7(PO_4)_6$, Fe_3PO_7	$FePO_4$, $Fe_7(PO_4)_6$, Fe_3PO_7	None detected

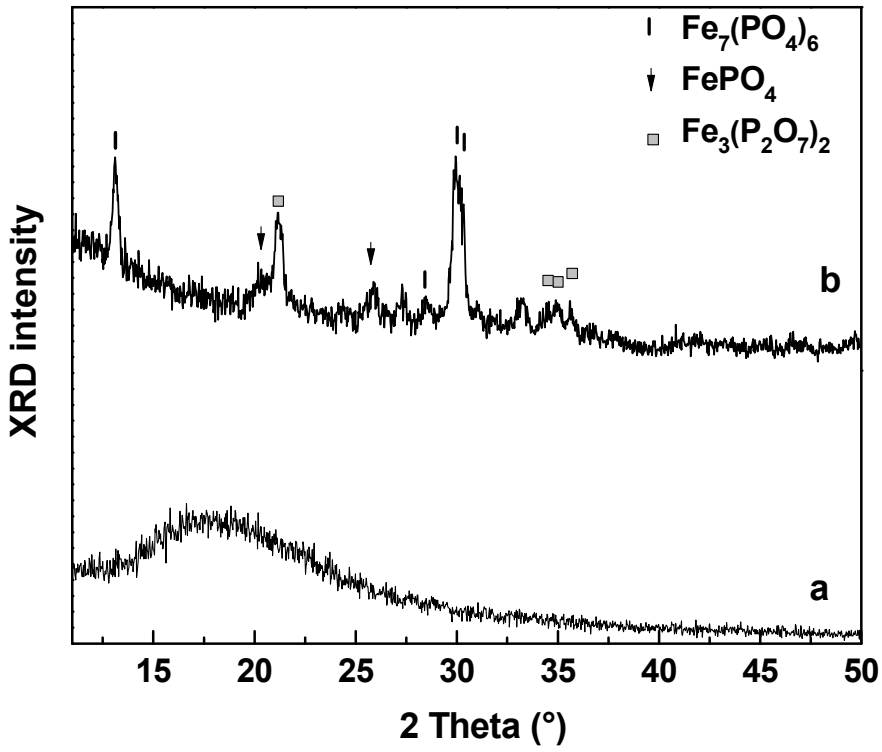

Figure 1: XRD patterns from samples quenched from melts with a nominal Fe/P = 1.30, held for two hours at 1200°C, then a) roller quenched, or b) quenched between steel plates.

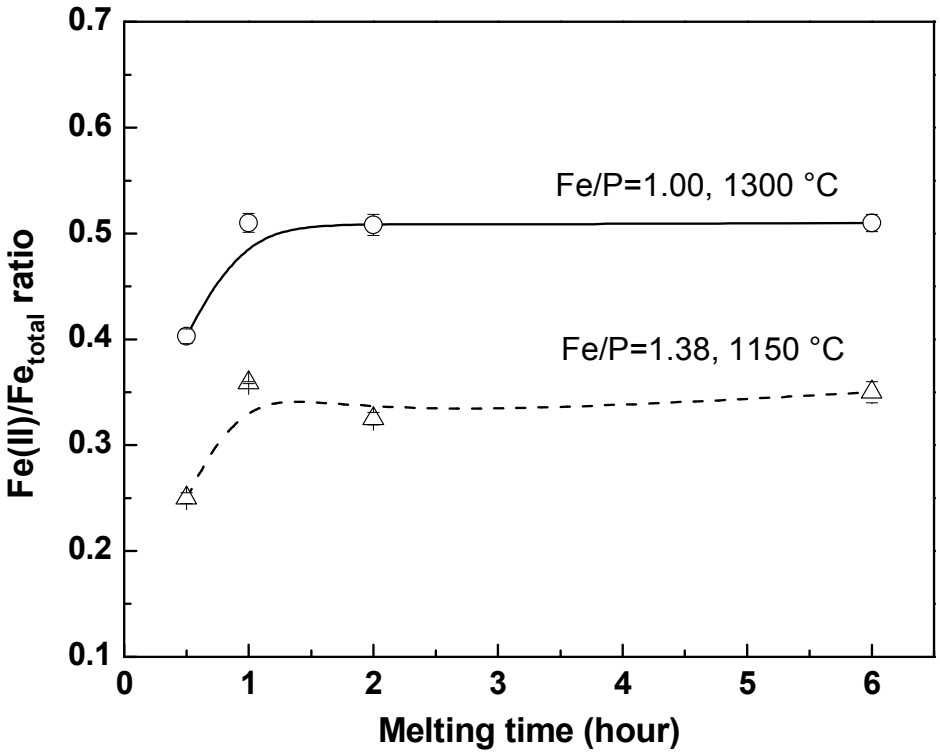

Figure 2: Fe(II)/Fetotal ratios for two sets of roller-quenched glasses prepared from melts held at different temperatures for up to six hours. Lines are added as guides for the eye.

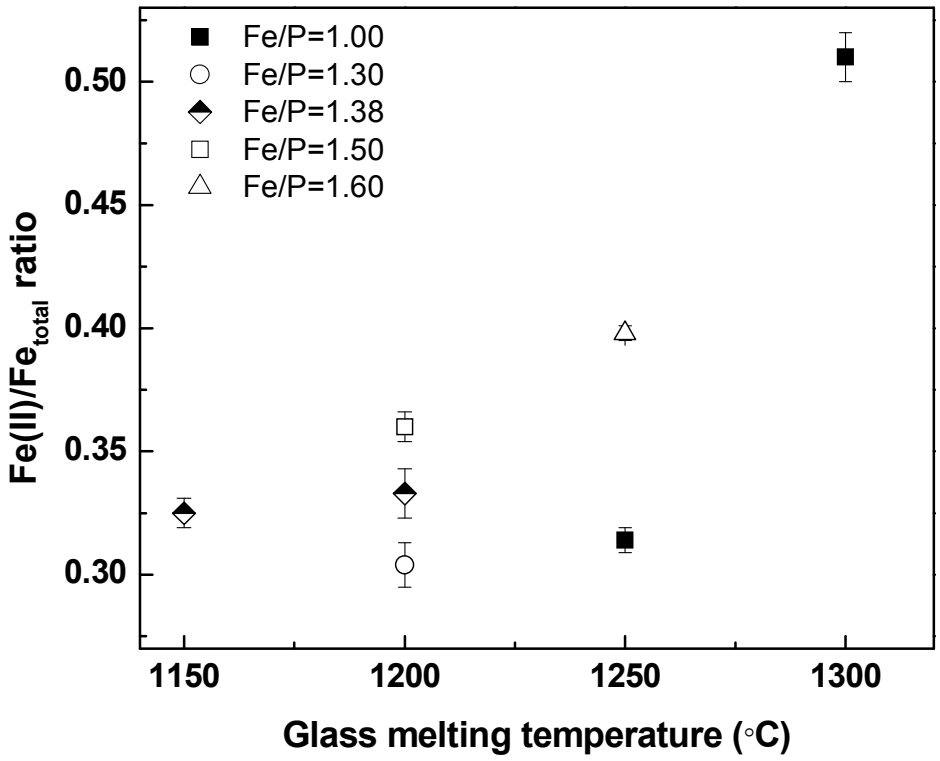

Figure 3: Summary of the Fe(II)/Fetotal ratios of roller-quenched glasses from melts held for two hours at different temperatures.

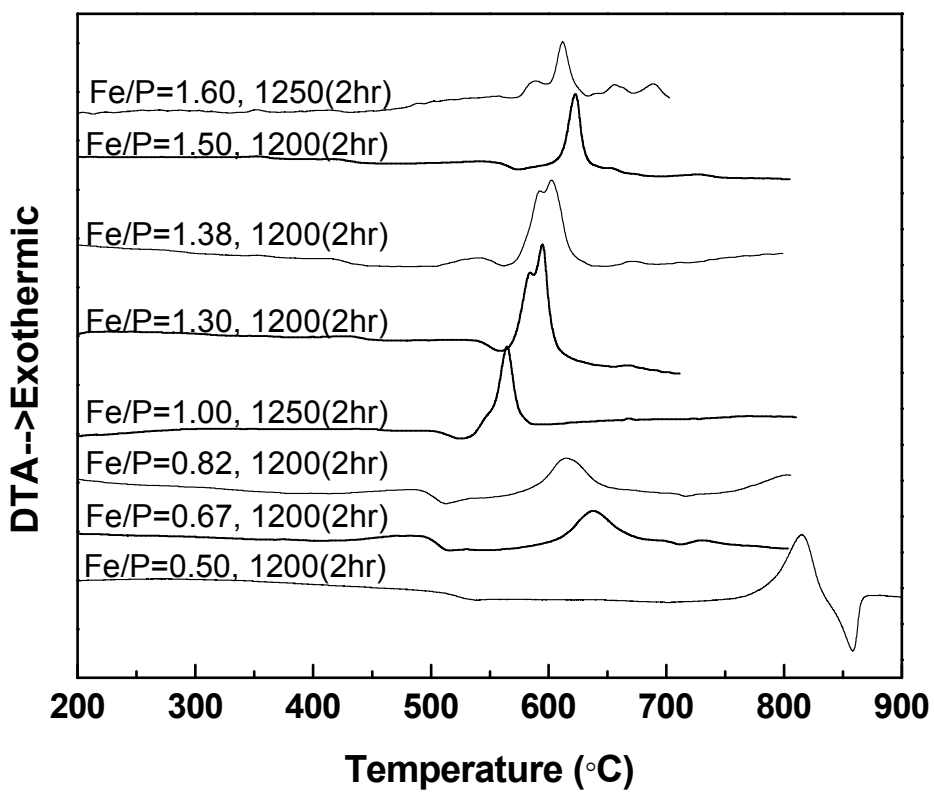

Figure 4: DTA patterns of iron-rich phosphate glasses; the data were collected in air at 10°C/min.

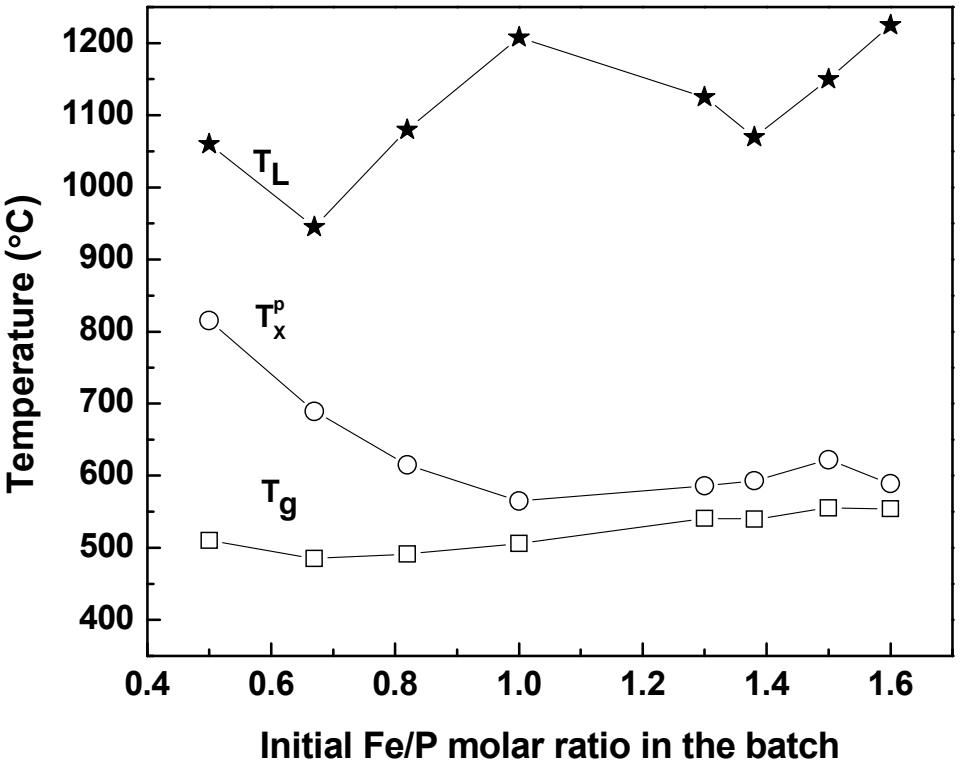

Figure 5: Characteristic temperatures of the glasses investigated in this work, determined by DTA. Liquidus temperatures are from ref. [25]. Lines are added as guides for the eye.

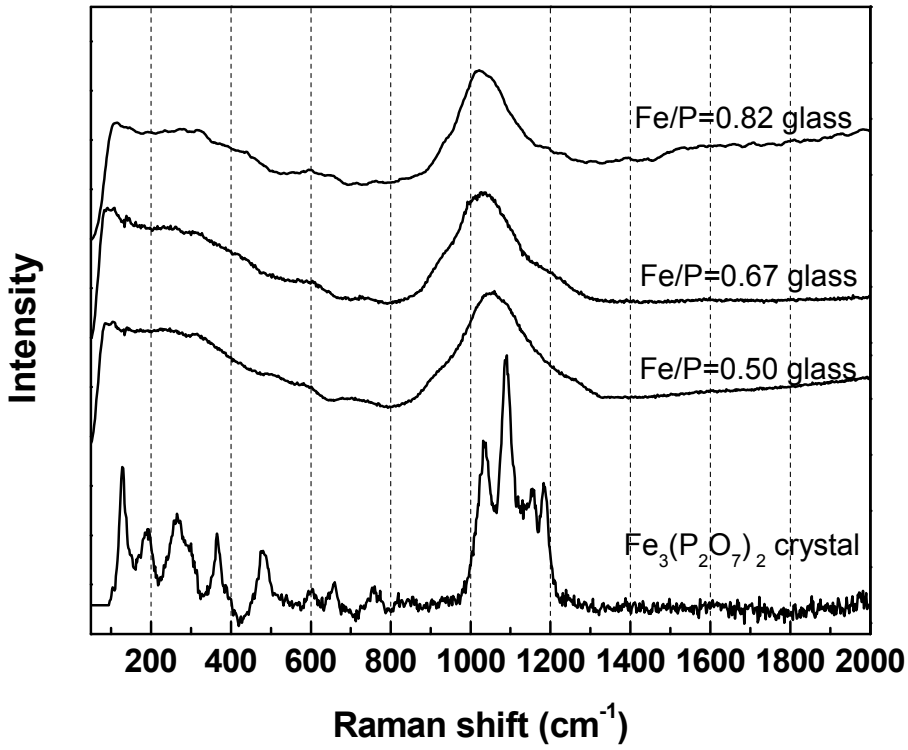

Figure 6: Raman spectra of the glasses with Fe/P<1.00 compared to crystalline $Fe_3(P_2O_7)_2$.

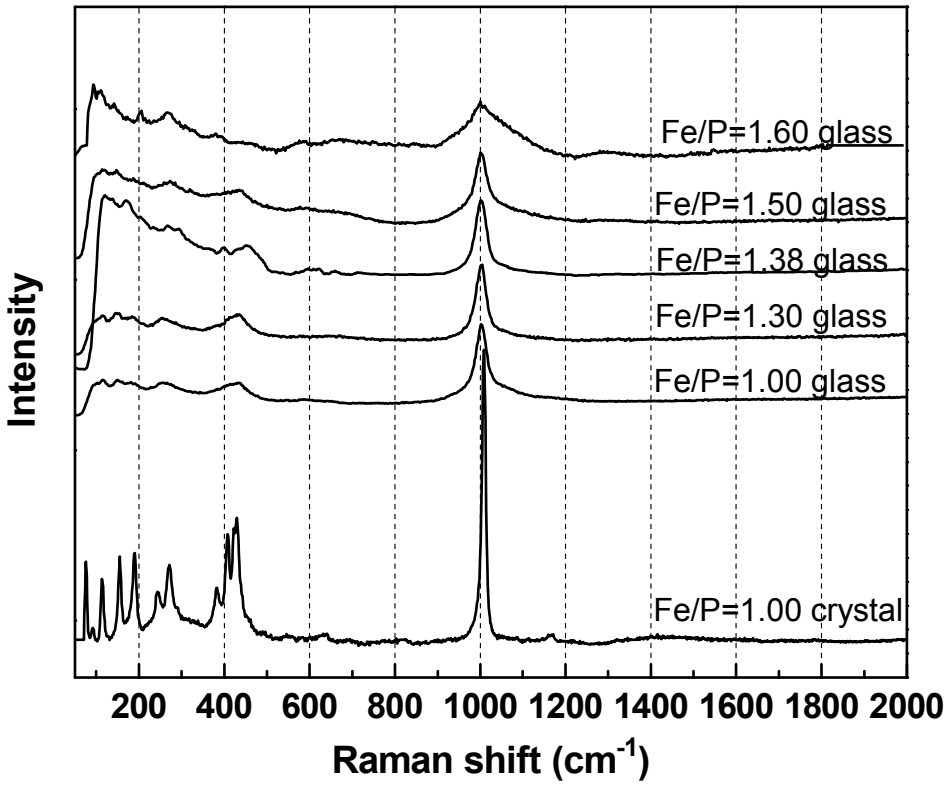

Figure 7: Raman spectra of iron-rich glasses compared to crystalline $FePO_4$.

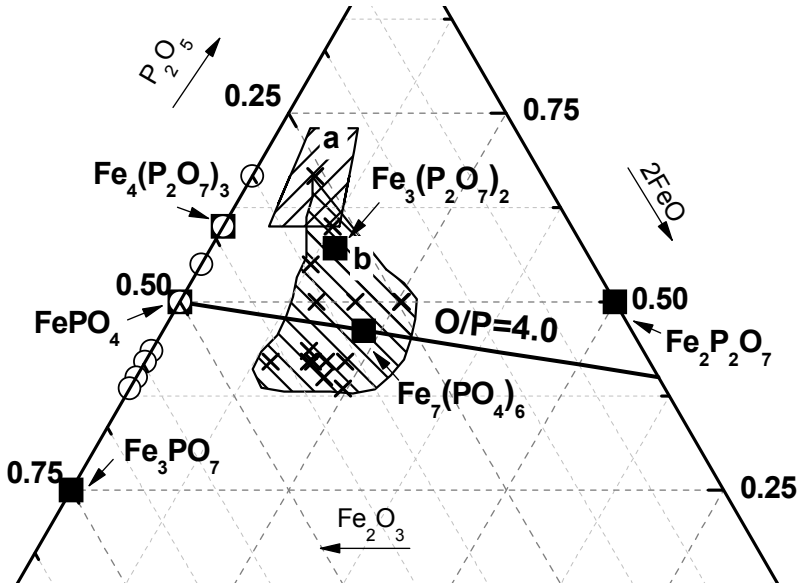

Figure 8: Compositions of iron-rich glasses prepared in this study. ○ - nominal composition of the batch; ×- analyzed glass composition after roller-quenching (Table 2); ■ - crystalline phases identified in partially-crystallized samples (Table 3). Region 'a' is the glass-forming region for typical iron phosphate glasses [6,7] and region 'b' includes the iron-rich compositions identified in the present study.

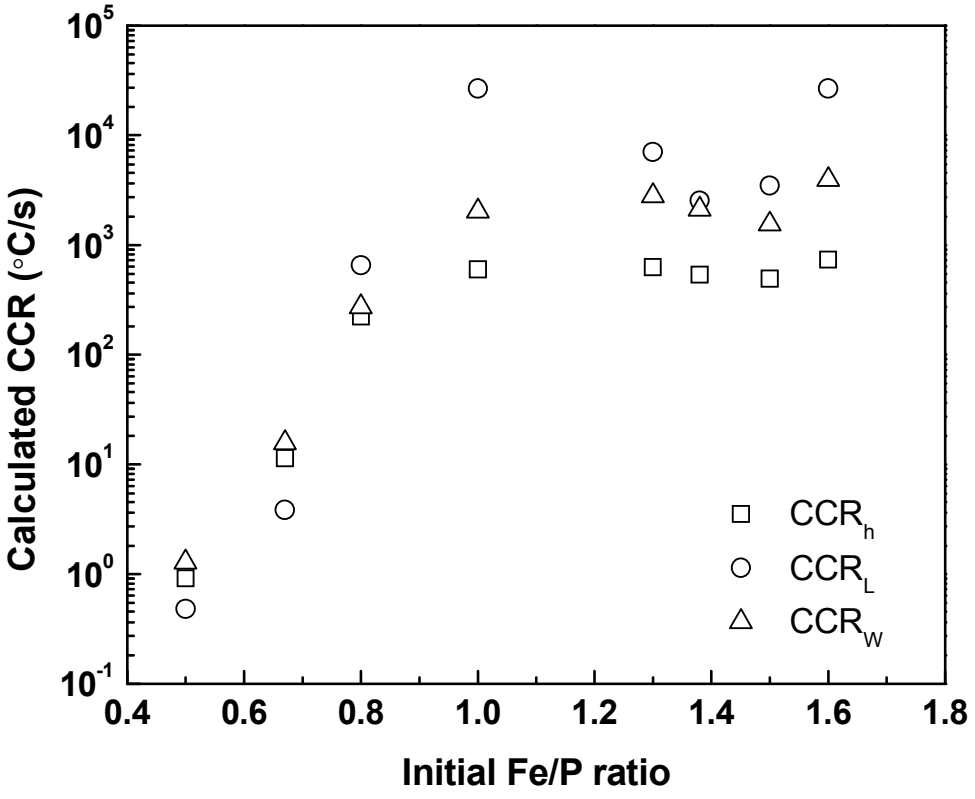

Figure 9: Estimated CCRs for iron phosphate melts using characteristic temperatures from DTA experiments and the relationships in Table 1.

3. THERMAL STABILITY OF GLASSES FROM THE $Fe_4(P_2O_7)_3 – Fe(PO_3)_3$ SYSTEM

Zhang, Liying[1]; Ghussn, Luciana[2]; Schmitt, Melodie L.[1]; Zanotto, Edgar D.[2]; Brow, Richard K.[1*]; Schlesinger, Mark E.[1]

[1] Department of Materials Science and Engineering, Missouri University of Science and Technology, Rolla, MO, USA

[2] Department of Materials Engineering, Federal University of São Carlos, São Carlos, Brazil

ABSTRACT

Iron phosphate glasses with nominal Fe/P compositions between 0.50 and 0.67 were prepared and characterized. The effects of melt conditions and the initial composition on the Fe(II) –content are reported. Characteristic temperatures, including the glass transition temperature and crystallization temperature, were measured by differential scanning calorimetry (DSC). The stability of melts against crystallization, described by the Angel and Weinberg parameters, generally decreases with increasing O/P and Fe/P ratios.

Key words: Iron phosphate glass; Ferric pyrophosphate; Ferric metaphosphate; Glass stability

---

[*] Corresponding author. Tel.: +01 573 341 6812; fax: +01 573 341 2071. Email address: brow@mst.edu.

3.1. INTRODUCTION

Iron phosphate glasses and crystals have interesting chemical, thermal and electrical properties. Crystalline iron phosphate compounds have been developed for several applications, including catalysts, optical materials and electrodes [1-5]. Chemically durable iron phosphate glasses have been studied as alternative materials for vitrifying high-level nuclear waste [6-10]. Other iron phosphate glasses have been developed for corrosion-resistant, reinforcing fibers for composite materials [11-12].

The liquidus behavior of a melt can provide information useful for making glasses. Wentrup (1935) reported a portion of the phase diagram for the Fe_2O_3-$Fe_4(P_2O_7)_3$ system [13], but did not cover the conventional glass-forming range for iron phosphate compositions, where the nominal Fe_2O_3/P_2O_5 molar ratio is between 1/3 and 2/3 [2-4,14-16]. More recently, we have reported the ferric-phosphate liquidus surface between $Fe(PO_3)_3$ and Fe_3PO_7 [17], updating and expanding Wentrup's analysis. In that study, we report the presence of a eutectic point between $Fe(PO_3)_3$ and $Fe_4(P_2O_7)_3$ at 37.2 mol% Fe_2O_3 and 907°C. This point is near the baseline compositions of glasses developed for vitrifying nuclear wastes.

Angell and other researchers suggested that the difference between the glass transition temperature (T_g) and the crystallization peak temperature (T_p) from a DTA experiment, $K_A = (T_p - T_g)$, is a measure of the stability of a supercooled glass melt against crystallization: the greater the value of K_A, the more stable the melt is against crystallization [18,19]. Weinberg used the parameter $(T_p - T_g)/T_m$, where T_m the melting temperature, to describe the stability of supercooled melts that crystallize congruently [20]. As reported by Nascimento et al. [21], a modified forms of the Weinberg

parameter, $K_W = (T_X - T_g)/T_L$, where T_X is the crystallization onset temperature and T_L is the liquidus temperature, can be used to describe the stability of melts against crystallization.

Information about the thermal stability of supercooled iron phosphate glasses against crystallization is quite useful for the consideration of these glasses as hosts for nuclear wastes and for other applications, such as processing glass fibers which should not devitrify on the cooling path during fabrication. In the present work, the modified Weinberg parameter (K_W) and the Angell parameter ($K_A = T_X - T_g$) are used to describe the stability against crystallization of iron phosphate melts.

3.2. EXPERIMENTAL PROCEDURES

From 60 to 100 grams of glass with nominal compositions between 33 and 40 mol% Fe_2O_3 were melted in alumina crucibles in air for two hours either at 1100°C or 1200°C. Fe_2O_3 and $NH_4H_2PO_4$ were used as the raw materials. Prior to melting, batches were calcined at 500°C for four hours to remove ammonia and water. Melts were quenched on steel plates to form glasses. Powders (≤ 53 μm) were obtained by grinding the quenched glass in a mortar with a pestle. These powders were analyzed by differential scanning calorimetry (Netzsch 404), using alumina sample pans in air at a heating rate of 10°C/min. Samples were analyzed by X-ray diffraction (Scintag XDS 2000) and Raman spectrometry (Horiba–Jobin Yvon LabRam-HR); the latter used a He-Ne laser (632.8 nm) as the excitation source. The Fe(II) content of the glasses was determined by titration using a 2 mM $KMnO_4$ solution [22].

Glass powders were crystallized by heating at temperatures between 600 and 850°C for twelve hours and the detected phases were prepared and studied by DTA/TGA (Netzsch STA 409C) to help interpret the DSC data obtained from the glasses. $FePO_4$ was prepared by dehydrating $FePO_4 \cdot xH_2O$ (100%, Alfa Aesar). $Fe(PO_3)_3$ was prepared by heating a stoichiometric mixture of $FePO_4$ and $NH_4H_2PO_4$ (98%, Alfa Aesar), first for six hours at 500°C for calcination, then for 12 hours at 800°C. $Fe_4(P_2O_7)_3$ was made by the solid state reaction of $FePO_4$ and $Fe(PO_3)_3$ at 800°C for 12 hours and then at 940°C for 12 hours [23]. $Fe_3(P_2O_7)_3$ was prepared by heating a stoichiometric mixture of $Fe(PO_3)_3$ and Fe_2PO_5 in a sealed ampule at 900°C for 12 hours. Fe_2PO_5 was prepared according to the method described by Modaressi, *et al.* [24]. The purity of these crystallized samples was confirmed by X-ray diffraction.

3.3. RESULTS

3.3.1. Redox Ratio and Raman Spectra. Figure 1 shows the measured Fe(II) content and the calculated O/P ratios of glasses with different nominal Fe/P ratios, quenched from melts held in air for two hours at different temperatures. Glasses with the same nominal Fe/P ratio quenched from melts held at 1200ºC have greater Fe(II) contents than glasses melted at 1100ºC, and the loss of oxygen associated with the reduction of Fe(III) to Fe(II) reduces the nominal O/P ratio. In addition, glasses with greater nominal Fe/P ratios have greater fractions of Fe(II), when melted under the same conditions. These results are similar to those reported for the effects of melt history on the composition and structure of 40.0 mol% Fe_2O_3 glasses [25]. The redox behavior of iron phosphate melts will be described in another publication [26]. The uncertainty in the

Fe(II)-contents shown in Fig. 1 represents the standard deviations from three titrations for each sample.

Based on the analyzed Fe(II) contents, the glass compositions can be relocated in the ternary ferrous-ferric phosphate compositional diagram (Fig. 2), where it is seen that these glasses have compositions that fall between the metaphosphate and pyrophosphate stoichiometries (dashed lines). The region outlined by the solid lines represents the glass compositions reported in the literature [25,26], and the glasses studied here generally fall in the same region.

Raman spectra of the glasses melted at 1100ºC are shown in Fig. 3. Broad peaks or shoulders in the 1000-1200 cm^{-1} range are assigned to the symmetric and asymmetric stretching modes of nonbridging oxygens on Q^1 and Q^2 tetrahedra [27,28]. (The superscript 'x' in the Q^x notation refers to the number of bridging oxygens per P-tetrahedron.) The broad peaks between 600 and 800 cm^{-1} are assigned to the symmetric stretching modes of P-O-P bonds that link neighboring P-tetrahedra [29]. For glasses with increasing nominal iron content, the relative fraction of Q^1 units is expected to increase, consistent with the shift in the P-O stretching mode from 1069 to 1037 cm^{-1} as the O/P ratio increases from 3.22 to 3.44. The relative intensity of the peak due to the P-O-P stretching mode (near 700 cm^{-1}) also decreases with increasing O/P ratio. The spectral trends for the glasses melted at 1200°C (not shown) are similar.

3.3.2. Crystallization Behavior. Figure 4 shows DSC patterns collected in air for the glasses melted at 1100°C and 1200°C. At least two exothermic peaks are detected when each sample is heated. For glasses with increasing iron contents melted at a constant temperature, T_g decreases slightly and T_X is largely changed.

Marasinghe reported similar DTA patterns for the glasses with batch compositions near 40.0 mol% Fe_2O_3, and reported that the first exothermic peak ~640°C is due to the crystallization of $Fe_3(P_2O_7)_3$, which mostly (90%) transforms to $Fe_4(P_2O_7)_3$ at ~800°C [30]. In this work, three crystalline phases, $FePO_4$, $Fe_3(P_2O_7)_2$ and $Fe_4(P_2O_7)_3$, were detected in the heat-treated samples. The thermal behavior of the crystalline phases formed in the glasses can help explain the endothermic events around 900°C in the patterns in Fig. 4 as shown below.

Figure 5 shows DTA/TGA data collected in air from crystalline $FePO_4$ and $Fe_4(P_2O_7)_3$ powders. $FePO_4$ is stable below 1000°C, exhibiting two endotherms related to solid phase transitions [13,31]. In contrast, $Fe_4(P_2O_7)_3$ loses some weight above 800°C because of the reduction of Fe(III) to Fe(II). The slope of the DTA baseline changes around 900°C because of the change in heat capacity when the solid melts. $Fe_3(P_2O_7)_2$ decomposes around 925°C [32]. The reported thermal behavior of the compounds indicate that the endothermic events around 900°C in the DSC patterns of the glass (Fig. 4) are related to the melting and decomposition of $Fe_4(P_2O_7)_3$ and $Fe_3(P_2O_7)_2$.

Table 1 lists the values of T_g and the onset temperature of the first crystallization peak, T_X, obtained from the DSC scans for each glass. The uncertainty in T_g and T_X was estimated to be ± 5°C, based on multiple runs for the glasses studied in this work. Also listed are the estimated ranges of liquidus temperatures (from [17]), and the values for K_A and K_W for the two series of glasses.

3.4. DISCUSSION

The glass transition temperature decreases with increasing nominal Fe_2O_3 content (Table 1). There are two structural effects caused by iron oxide additions: a decrease in the relative fraction of oxygens that bridge neighboring P-tetrahedra and an increase in the number of oxygens that link neighboring Fe-polyhedra with the P-tetrahedra. The increase in the O/P ratios for the glasses with increasing Fe_2O_3-content (Table 1) indicates that the number of P-O-Fe bonds increases relative to the number of P-O-P bonds.

Glass stability is evaluated using the characteristic temperatures collected by DTA and other techniques [17], using the Angell parameter K_A and Weinberg parameter K_W. Figure 6 shows the dependence of the glass stability parameters on glass composition. The trends in K_A and K_W both indicate that supercooled melts with lower O/P and lower Fe/P ratios have greater stability against crystallization. These results indicate that glasses with longer P-O-P chains are more difficult to crystallize, which is also consistent with laboratory experience. There is little discernible effect of Fe(II) content on glass thermal stabilities.

3.5. SUMMARY

Glasses melted from compositions in the $Fe_4(P_2O_7)_3$-$Fe(PO_3)_3$ system were studied using thermal characteristic temperatures. Results show that decreasing the Fe/P and O/P ratios produces supercooled melts that are more stable against crystallization. This information is useful for the design of good glass forming compositions.

ACKNOWLEDGEMENTS

The authors gratefully acknowledge Jong Wook Lim for his kind assistance in the collection of the Raman spectra. This work is supported by the National Science Foundation (U.S.A.) under Grant DMR-0502463, by CNPq (Brazil) Grant no. 492565/04-0 and by FAPESP (Brazil) Grant 07/08179-9.

REFERENCES

[1] R. C. Haushalter, L. A. Mundi, Chem. Mater. 4 (1992) 31.

[2] A. Clearfield, Chem. Rev. 88, 125 (1988).

[3] K. Zaghib, C.M. Julien, J. Power Sources 142 (2005) 279.

[4] M. Ai, K. Ohdan, Appl. Catal. A 180 (1999), p. 47.

[5] N. Aliouane, T. Badechet, Y. Gagou, E. Nigrelli, P. Saint-Gregoire, Ferroelectrics 241 (2000) 255.

[6] X. Yu, D.E. Day, G.J. Long, R.K. Brow, J. Non-Cryst. Solids 215 (1997) 21.

[7] D.E. Day, Z. Wu, C.S. Ray, P. Hrma, J. Non-Cryst. Solids 241 (1998) 1.

[8] X. Fang, C.S. Ray, G.K. Marasinghe, D.E. Day, J. Non-Cryst. Solids 263&264 (2000) 293.

[9] L. Kahl, D. Clark, W. White, Adv. Ceram. 20 (1986) 141.

[10] B. Samuneva, P. Tzvetkova, I. Gugov, V. Dimitrov, J. Mater. Sci. Lett. 15 (1996) 2180.

[11] V.Simon, S.G. Chiuzbăian, M. Neumann, D. Eniu, E. Indrea, A. Tőrők-kiss, S. Simon, Mod. Phys. Lett. B 14 (2000) 767.

[12] S.T. Lin, S.L Krebs, S. Kadiyala, K.W. Leong, W.C. LaCourse, B. Kumar, Biomaterials 15 1057 (1994).

[13] H. Wentrup, Arch. Eisenhüt. 9[7] (1935) 57.

[14] Y.M. Moustafa, K. El-Egili, H. Doweidar, I. Abbas, Phys. B 353 (2004) 82.

[15] M. Karabulut, M. Yuksek, G.K. Marasinghe, D.E. Day, J. Non-Cryst. Solids 355 (2009) 1571.

[16] D.E. Day, Z. Wu, C.S. Ray, P. Hrma, J. Non-Cryst. Solids 241 (1998) 1.

[17] L. Zhang, M.E Schlesinger, R.K. Brow, J. Am. Ceram. Soc. submitted.

[18] E.I. Cooper, C.A. Angell, J. Non-Cryst. Solids 56 (1983) 75.

[19] M.G. Drexhage, O.H. El-Bayoumi, H. Lipson, S.T. Moynihan, A.J. Bruce, J. Lucas, G. Fonteneau, J. Non-Cryst. Solids 56 (1983) 51.

[20] M.C. Weinberg, Phys. Chem. Glasses, 35 (1994) 119.

[21] M.L.F. Nascimento, L.A. Souza, E.B. Ferreira, E.D. Zanotto, J. Non-Cryst. Solids 351 (2005) 3296.

[22] S.I. Grishin, J.M. Bigham, O.H. Tuovinen, Appl. Environ. Microbiol., 54 (1988) 3101.

[23] C. Gleitzer. Eur. J. Solid State Inorg. Chem. 28 77-91 (1991).

[24] A. Modaressi, A. Courtois, R. Gerardin, B. Malaman, C. Gleitzer, J. Solid State Chem. 40(1981) 301.

[25] X. Fang, C.S. Ray, A. Mogus-Milankovic, D.E. Day, J. Non-Cryst. Solids 283 (2001) 162.

[26] M.L. Schmitt, R.K. Brow, M.E. Schlesinger, "Predicting the Iron Redox Ratio in Iron Phosphate Melts: A Thermodynamic Model," to be submitted.

[27] A. Mogus-Milankovic, B. Pivac, K. Furic, D.E. Day, Phys. Chem. Glasses, 38 (1997) 74.

[28] C. Nelson, D.R. Tallant, Phys. Chem. Glasses, 26 (1985) 119.

[29] A.M. Efimov, J. Non-Cryst. Solids, 209 (1997) 209.

[30] G.K. Marasinghe, M. Karabulut, C.S. Ray, D.E. Day, M.G. Shumsky, W.B. Yelon, C.H. Booth, P.G. Allen, D.K. Shuh, J. Non-Cryst. Solids 222 (1997) 144.

[31] E.C. Shafer, M.W. Shafer, R. Roy, Z. Krist. 108 (1956) 263.

[32] L. Zhang, M.E. Schlesinger, R.K. Brow, "Preparation and characterization of iron phosphate compounds," to be submitted.

[33] L. Popović, D. de Waal, J.C.A. Boeyens, J. Raman Spectrosc. 36 (2005) 2.

Table 1: The summary of T_L and DTA/DSC characteristic parameters.

Nominal Fe_2O_3 mol%	1100°C series						1200°C series					
	O/P	T_L range [a]	T_g (°C)	T_X (°C)	K_A (°C)	K_W[b]	O/P	T_L range [a]	T_g (°C)	T_X (°C)	K_A (°C)	K_W[b]
33.3	3.22	1030-1060	500	728	228	0.171-0.175	3.20	1025-1065	506	785	279	0.209-0.215
35.4	3.27	990-1010	485	646	161	0.125-0.127	3.24	985-1015	493	767	274	0.213-0.218
37.2	3.34	880-910	482	616	134	0.113-0.116	3.30	875-915	493	671	178	0.150-0.155
40	3.44	920-950	476	606	130	0.106-0.109	3.40	915-955	484	597	113	0.092-0.095

[a] *Liquidus* temperatures are given as a range, based on reported data in [17] and laboratory experience.
[b] Errors are from the *liquidus* temperature range.

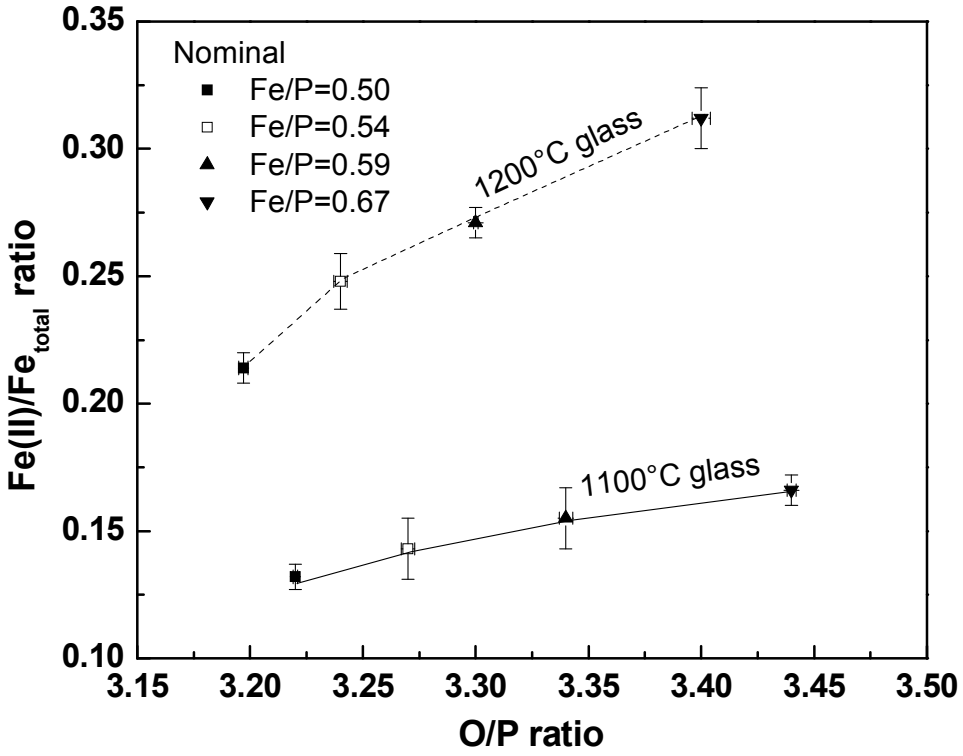

Figure 1: Redox ratio and O/P ratio of glasses with different nominal Fe/P ratios melted in air for two hours at different temperatures. The lines are guides for the eye.

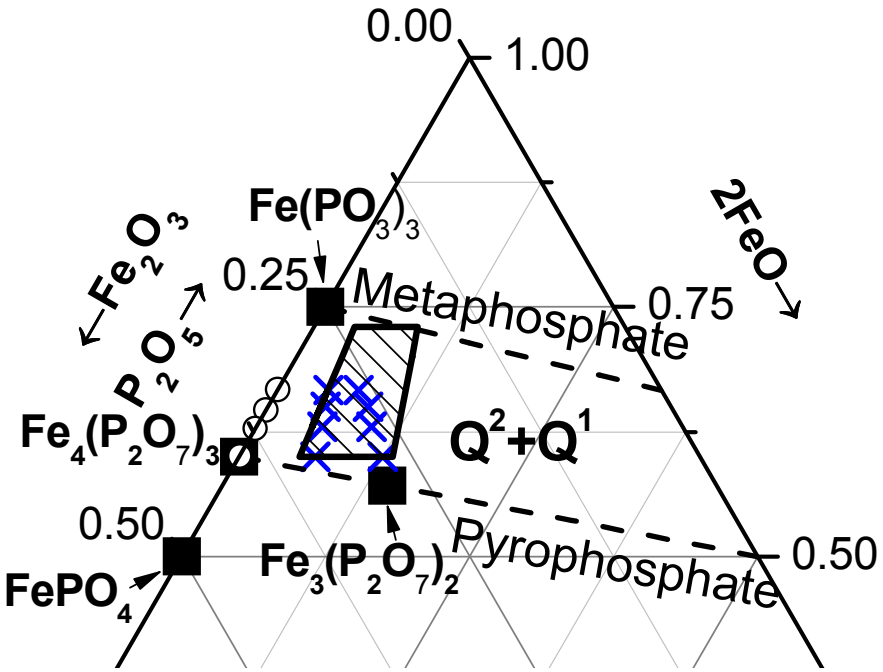

Figure 2: Compositions of glasses prepared in this study. ○ - nominal composition of the batch; ×- analyzed glass compositions; ■- crystalline phases identified in partially-crystallized samples.

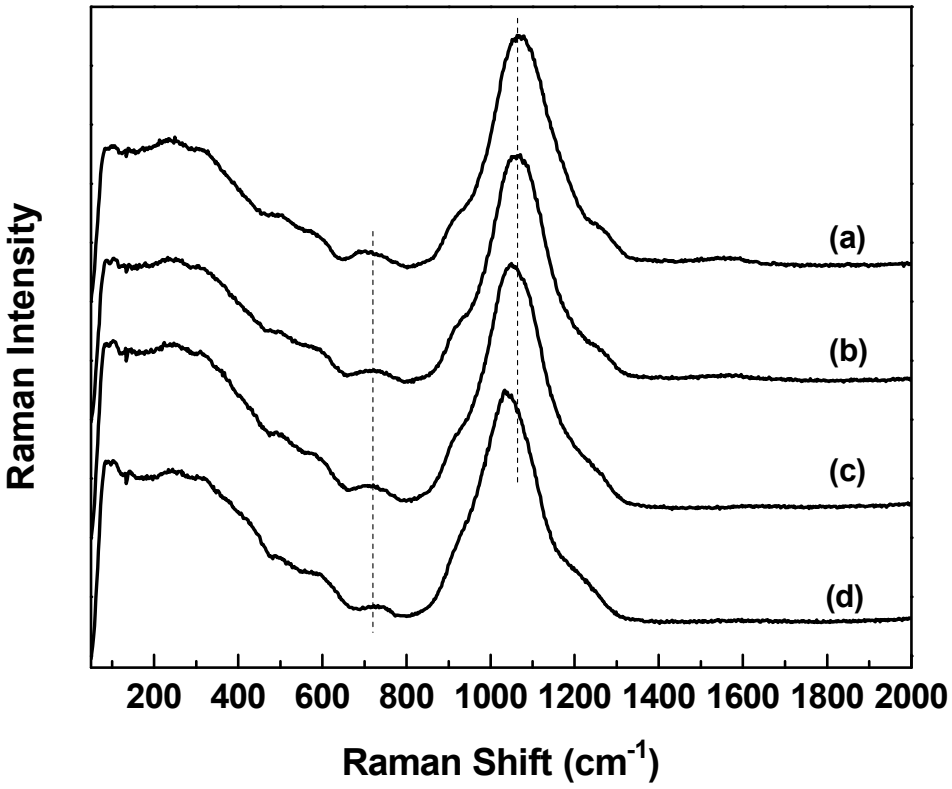

Figure 3: Raman spectra of glasses melted at 1100ºC with a nominal Fe_2O_3 content of (a) 33.3 mol%; (b) 35.4 mol%; (c) 37.2 mol%; and (d) 40.0 mol%.

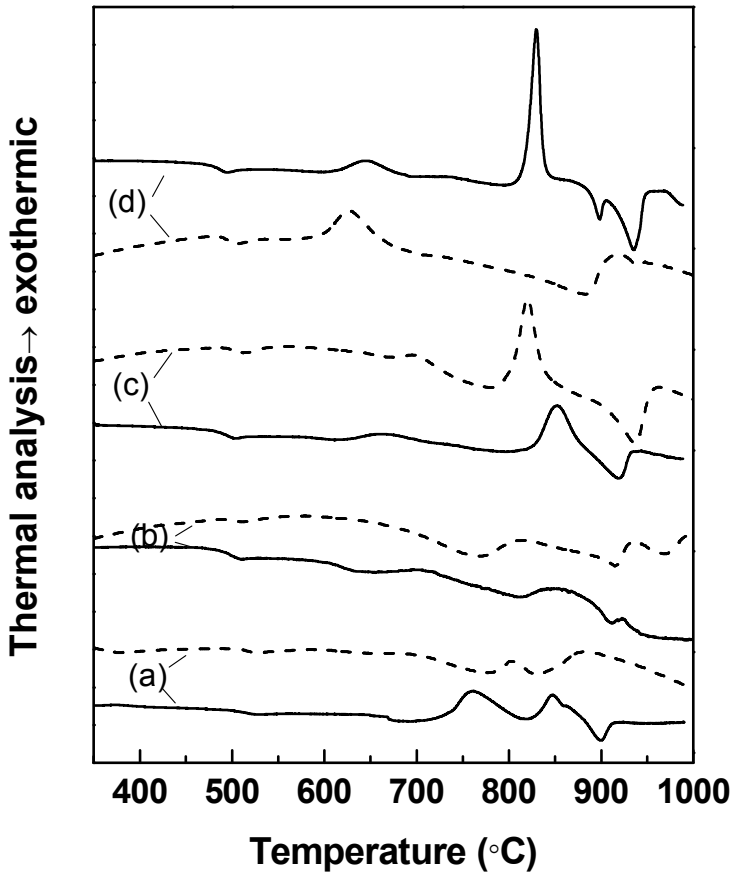

Figure 4: DSC patterns for 1100 and 1200°C series of glasses as solid and dashed lines, respectively, with nominal Fe_2O_3 of (a) 33.3 mol%; (b) 35.4 mol%; (c) 37.2 mol%; and (d) 40.0 mol%.

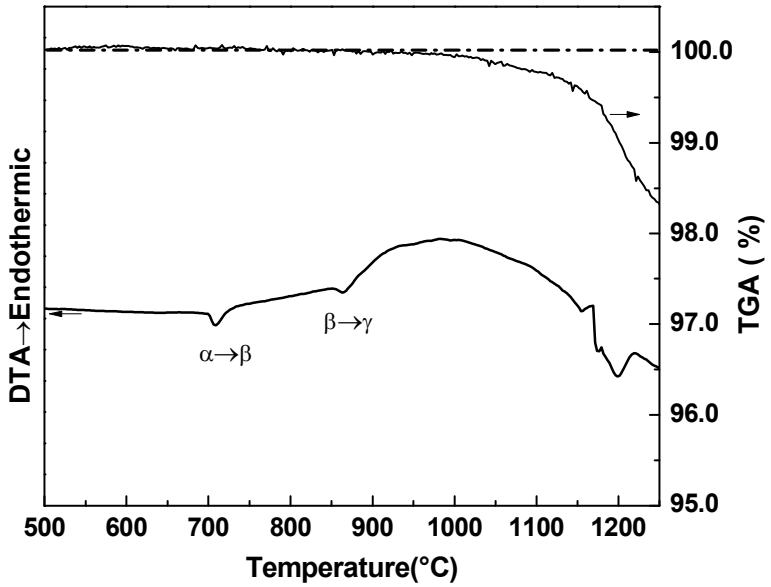

(a)

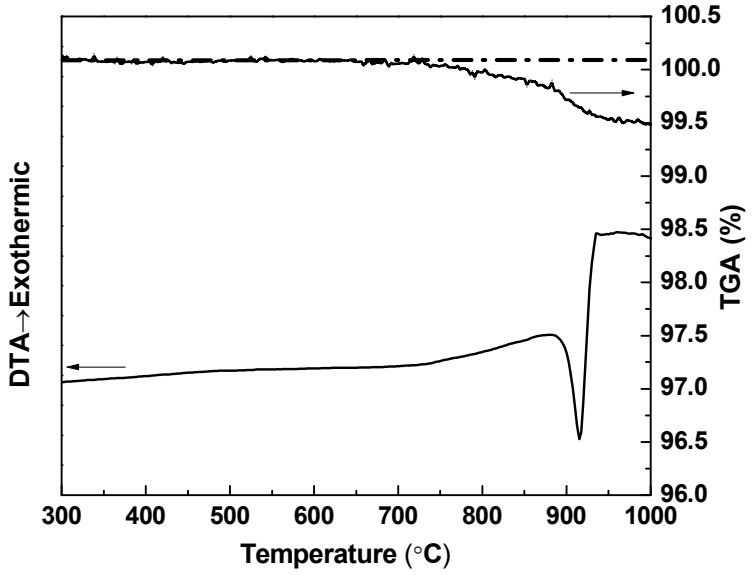

(b)

Figure 5: DTA/TGA patterns of (a) $FePO_4$ and (b) $Fe_4(P_2O_7)_3$ crystals heated in air.

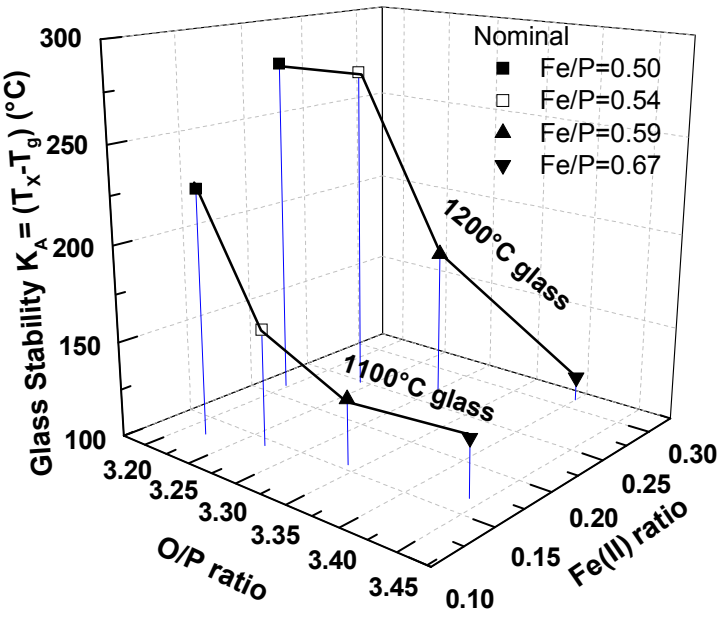

(a)

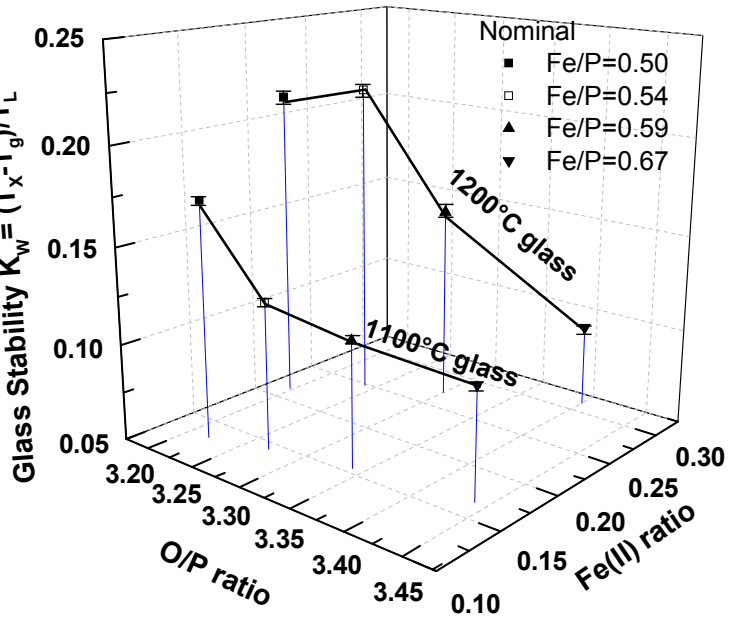

(b)

Figure 6: Glass stability parameters (a) K_A and (b) K_W for iron phosphate glasses as functions of the O/P, Fe/P and Fe(II) content. The lines are guides for the eye.

4. A RAMAN STUDY OF IRON-PHOSPHATE COMPOUNDS AND GLASSES

Liying Zhang, Richard K. Brow, Mark E. Schlesinger

Department of Materials Science and Engineering, Missouri University of Science and Technology, Rolla, MO, USA

ABSTRACT

Ferrous and ferric phosphate crystalline compounds and glasses were studied using Raman spectroscopy. A comparison of the spectra from crystalline and glassy ortho-, pyro-, and metaphosphates indicate that similar phosphate anions constitute the structures of the respective materials, and some information about the compositional dependence of the phosphate-site distributions in the glasses can be gleaned from relative peak intensities. A correlation exists between the average P-O bond distance and the Raman peak frequencies in the crystalline compounds, and this correlation is used to provide information about the structures of the iron phosphate glasses. For example, the average P-O bond distance decreases from about 1.57 Å for iron metaphosphate glasses (O/P~3.0) to 1.54 Å for iron orthophosphate glasses (O/P~4.0) These bond distances are in good agreement with those reported from diffraction studies of similar glasses.

4.1. INTRODUCTION

Crystalline and amorphous iron phosphate materials are being developed for a variety of technological applications. For example, amorphous and crystalline $FePO_4$ and similar compounds have been developed as catalysts,[1] and the catalytic performance is

affected by reduction to $Fe_2P_2O_7$.[2] $LiFePO_4$ has been proposed as a cathode material for rechargeable Li-ion batteries[3,4] and the dilithiation process can form disordered products that are sometimes difficult to characterize by conventional diffraction techniques. Fe_3PO_7 has also been characterized as a potential electrode material.[5]

Iron phosphate glasses are of interest for a variety of applications, including as corrosion resistant hosts for radioactive wastes.[6,7] Typical iron phosphate glasses for waste applications are based on a ferric pyrophosphate ($40Fe_2O_3$-$60P_2O_5$ molar) stoichiometry in which some fraction of ferric ions reduce to ferrous ions, to yield a structure based on ferric and ferrous polyhedra that link various phosphate anions.[8,9] The properties of these glasses are sensitive to changes in iron valence and the Fe/P ratio, both of which affect the overall O/P ratio which determines the distribution of phosphate anions. Glasses with O/P~3 are classified as metaphosphates and possess relatively long chains of P-tetrahedra that link neighboring tetrahedra through two nonbridging oxygens; these tetrahedra are sometimes classified as Q^2-tetrahedra.[10] The chains are terminated by phosphate units with a single bridging oxygen (Q^1 units). A pyrophosphate composition (O/P~3.5) could have a structure based only on Q^1 tetrahedra that form $P_2O_7^{4-}$ anions.

Raman spectroscopy has been widely used to provide information about the anions that constitute the structures of phosphate glasses and crystals.[11-16] The frequency of the P-O stretching vibrations changes systematically with the number of bridging oxygens (Q^x) on a tetrahedron, and so Raman peaks associated with the different P-O vibrational modes can be used to identify different structural elements. Rulmont[15] compared the Raman and IR spectra of crystalline and glassy pyro- and meta-phosphates and showed that crystalline and glassy phosphates with similar compositions have similar

structures. In addition, more quantitative information about structure, including estimates of P-O bond lengths and P-O-P bond angles, can be obtained from Raman peak positions.[16,17]

There have been several Raman studies of iron phosphate glasses.[10, 17,18] The compositions studied were generally limited to those near the pyrophosphate stoichiometry of interest for waste vitrification applications. Qualitative changes in peak shapes and positions have been related to glass compositions, but little detailed information has been reported. In the present study, the Raman spectra of ten crystalline ferric, ferrous, and mixed ferric-ferrous phosphate compounds, including ortho- (O/P=4.0, Q^0), pyro- (O/P=3.5, Q^1) and metaphosphates (O/P=3.0, Q^2), are analyzed, and those results are used to interpret the Raman spectra of iron phosphate glasses with similar O/P and Fe/P ratios. These studies then provide information about tetrahedral distributions and estimates of P-O bond lengths for a much broader range of iron phosphate glass compositions than have been previously reported.

4.2. EXPERIMENTAL PROCEDURES

Iron phosphate crystalline compounds were prepared following the procedures listed in Table I. X-ray diffraction (Scintag XDS 2000) was used to confirm that the desired phases were formed.

Glasses were prepared by melting and quenching the different crystalline iron phosphate compounds. The melt conditions are summarized in Table II. Some melts were done in sealed silica ampoules to minimize P_2O_5-volatilization and the reduction of ferric ions to ferrous ions. In general the sample sizes were 0.6~2.5 grams for glasses

melted in sealed silica ampoules and 3-5 grams for orthophosphate glass series prepared by the roller quenching method.[19] Every glass was pulverized to ~53 μm and characterized by XRD to confirm the vitreous state. Samples of glass powders were coated by carbon and their Fe/P ratios were determined using the energy dispersive x-ray spectrometry (EDS) associated with the Hitachi S4700 scanning electron microscope. These analyses were based on an Fe/P calibration curve determined by analyzing the corresponding crystalline compounds. At least five measurements were done on each sample, and the average Fe/P ratio, with one standard deviation, is reported. The Fe^{2+}/Fe_{tot} contents of the glasses were determined by a titration technique using $KMnO_4$ (~2 mM), [20] with an absolute uncertainty of 2%. The Fe/P and Fe^{2+}/Fe_{tot} ratios were used to calculate the O/P ratio for every glass.

An Horiba-Jobin Yvon LabRam-HR spectrometer was used to collect Raman spectra with a He-Ne laser (632.8 nm) as the excitation source. In general, spectra were collected through a 10X microscope objective from the surfaces of crystalline powders (53 micron particle size) and from the surfaces of quenched glass samples.

4.3. RESULTS

Table III lists the crystallographic parameters reported in the literature for the iron phosphate compounds prepared in this study. The average P-O bond distances for nonbridging ($P\text{-}O_{nb}$) and bridging ($P\text{-}O_{br}$) oxygens are indicated. Nonbridging oxygens are those that are linked to one P-tetrahedron, and bridging oxygens are linked two P-tetrahedra. Also listed are the average P-O-P bond angles for the pyro- and metaphosphate compounds.

Table IV summarizes the compositions of the glasses prepared by melting the different iron phosphate compounds. The O/P ratios were calculated from the measured Fe^{2+}/Fe_{total} ratios, obtained by titration, and the Fe/P ratios obtained by EDS. In general, the O/P ratios differ from their nominal values principally because of a change in the average Fe-redox state after melting.

Figure 1 shows the Raman spectra collected from the crystalline iron orthophosphate (O/P=4) compounds and from two orthophosphate glasses. The major band near ~1009 cm^{-1} in the spectra from $FePO_4$ and $Fe_7(PO_4)_6$ is assigned to the symmetric PO_4 stretching mode associated with the Q^0 PO_4^{3-} tetrahedral. [21, 22] For $Fe_3(PO_4)_2$-A and -B, the intense bands between 900 and 980 cm^{-1} are also assigned to the symmetric PO_4 stretching modes. The less intense bands between 900 and 1100 cm^{-1} in the spectra from $Fe_7(PO_4)_6$, $Fe_3(PO_4)_2$-A and $Fe_3(PO_4)_2$-B are assigned to the asymmetric PO_4 modes associated with the reduced symmetry of these PO_4^{3-} units.[23] The peaks below 600 cm^{-1} are related to different P-O and Fe-O stretching and bending modes.[22, 24]

The Raman spectra from the O1 and O2 glasses are similar to that obtained from crystalline $FePO_4$. The spectra from the orthophosphate glasses are dominated by an intense peak centered near 1002 cm^{-1}, due to the PO_4 stretching modes; some lower intensity peaks are present in the range between 200 and 500 cm^{-1}. The broader full widths at half-maximum (FWHM = 30-40 cm^{-1}) and the lower frequencies of the peaks from the glasses compared to crystalline $FePO_4$ (FWHM= 10 cm^{-1}) are consistent with what was reported by Burba, et al.[22] for amorphous and crystalline $FePO_4$. The assignments for the low frequency peaks in the spectra from the O1 and O2 glasses are the same as those described above for the crystalline samples.

Figure 2 shows the Raman spectra collected from the iron pyrophosphate (O/P=3.5) crystalline compounds. The most intense peaks, between 1000 and 1100 cm^{-1}, in each spectrum correspond to the symmetric PO_3 vibrations of inequivalent nonbridging oxygens associated with the Q^1 $P_2O_7^{4-}$ anions.[25] The less intense peaks between 1000 and 1200 cm^{-1} are assigned to the asymmetric PO_3 modes associated with Q^1 tetrahedra. The centrosymmetric $Fe_2P_2O_7$ crystals do not have as many Raman active PO_3 stretching modes due to the symmetry of the compound.[25,26] Compared with $Fe_2P_2O_7$ and $Fe_7(P_2O_7)_4$, $Fe_3(P_2O_7)_2$ and $Fe_4(P_2O_7)_3$ have many more asymmetric PO_3 modes (Fig. 2), consistent with the lower symmetry of these phosphate units (Table IV).

The bands between 700 and 800 cm^{-1} in Fig. 2 are assigned to the symmetric P-O-P stretching mode associated with the bridging oxygen that links two Q^1 tetrahedra in a pyrophosphate anion. $Fe_2P_2O_7$ has a relatively intense P-O-P peak near ~731 cm^{-1}, which agrees with the spectrum reported in reference [25]. For the other iron pyrophosphate crystalline compounds, the intensities of the P-O-P peak are relatively weak. The peak near ~935 cm^{-1} in the spectrum of near $Fe_7(P_2O_7)_4$ is assigned to the asymmetric vibration of P-O-P bonds, as is the weak peak near ~1000 cm^{-1} in the spectrum of $Fe_4(P_2O_7)_3$.

Figure 3 shows the Raman spectra collected from several iron pyrophosphate glasses. In general, the broad peaks in the spectra from the glasses occur at similar frequencies as those from the crystalline pyrophosphates (Fig. 2), and similar assignments can be made for the peaks in the spectra from the glasses. The most intense peak in each spectrum, at frequencies from ~1060 cm^{-1} to ~1090 cm^{-1}, can be assigned to the PO_3 stretching modes associated with the nonbridging oxygens on Q^1 tetrahedra.[25] The higher frequency shoulders evident in each spectrum could be due to asymmetric

PO_3 modes associated with the Q^1 tetrahedra, but also could be due to symmetric PO_2 stretching modes associated with Q^2-tetrahedra. This latter assignment seems particularly true for the P4 glass which has a relatively low O/P ratio (Table IV) and so should have a greater fraction of Q^2 tetrahedra. Likewise, the shoulders near ~1000 cm^{-1} could be assigned to other PO_3 modes associated with the Q^1, or to PO_4 modes associated with Q^0 units in the glasses. The bands between 700 and 800 cm^{-1} are related to the symmetric P-O-P stretching modes associated with Q^1. It is interesting that the peak for P-O-P symmetric band (between 750 and 780 cm^{-1}) has a greater relative intensity for the ferrous P2 glass than for the other glasses. In addition, the peak position varies, from 720 cm^{-1} for the P4 glass to 765 cm^{-1} for the P2 glass.

Figure 4 shows the Raman spectra of the crystalline ferric and ferrous metaphosphate (O/P=3) compounds and several metaphosphate glasses. The $Fe(PO_3)_3$ and $Fe(PO_3)_2$ compounds have bands at similar frequencies, however, the relative intensities are quite different. The very strong peak near ~1196 cm^{-1} in the spectrum from the $Fe(PO_3)_3$ compound corresponds to the PO_2 stretching modes associated with Q^2-tetrahedra,[16,17,27] and the intense peaks at 1160 and 1205 cm^{-1} in the spectrum from the $Fe(PO_3)_2$ compound also correspond to these symmetric PO_2 stretching modes associated with inequivalent P-O_{nb} bonds.[28] The less intense bands between 1000 and 1250 cm^{-1} are likely related to the asymmetric PO_2 modes.[28,29] For the glasses, the major bands between 1150 and 1200 cm^{-1} are assigned to the PO_2 stretching modes associated with Q^2-tetrahedra. The spectra from glasses M1, M2 and M3 each has a broad peak centered near 1060-1070 cm^{-1}. These are most likely due to PO_3 stretching modes associated with Q^1-tetrahedra. The low intensity peak centered near 1300 cm^{-1} in each spectrum of the

metaphosphate glasses is assigned to asymmetric PO_2 stretching modes associated with Q^2-tetrahedra. The peak due to the P-O-P stretching modes is present in each spectrum from the metaphosphate glasses, between 683 cm^{-1} (M4) and 720 cm^{-1}. The relative intensity of this peak varies considerably with composition.

4.4. DISCUSSION

4.4.1. Peak Assignments and Phosphate Tetrahedral Distributions. Table V summarizes the Raman peak assignments for the various samples. The Raman frequencies for iron phosphate glasses fall into the similar ranges with the corresponding iron phosphate compounds, indicating some structural similarity between the glassy and corresponding crystalline phosphate compounds. In addition, the peak positions vary systematically with phosphate chemistry, with the frequency (wavenumbers) of the P-O stretching modes increasing in the order orthophosphate < pyrophosphate < metaphosphate.

It is obvious that the relative contributions of the various P-O stretching modes in the range of 900 and 1400 cm^{-1} change with glass composition. To quantify these changes, each spectrum was fit by four Gaussian curves centered near ~940-970 cm^{-1}, ~1040-1080cm^{-1}, ~1120-1200 cm^{-1} and ~1250-1300 cm^{-1}. The peak positions and full widths at half-maximum (FWHM) of these curves were allowed to vary until a best-fit solution was achieved. An example of one fit, for the P4 glass, is shown in Fig. 5.

The relative intensities (RI) of the four peaks are plotted as a function of the O/P ratio for each of the iron phosphate glasses in Fig. 6. The relative intensities of the peaks near 1180 and near 1300 cm^{-1} both decrease with increasing O/P ratio and the relative

intensity of the peak centered near 1070 cm^{-1} increases, reaching a maximum at O/P~3.5. The peak near 970 cm^{-1} remains low for O/P<3.3, but becomes the dominant peak for glasses with O/P>3.5.

Assignment of these four peaks to specific structural units in the glass is not unambiguous. It is likely, for example, that the Raman peak near 1180 cm^{-1} for glasses with O/P ratios between 3.0 and 3.5 will have overlapping contributions from symmetric PO_2 stretching modes associated with P-O_{nb} bonds on Q^2 tetrahedra, and asymmetric PO_3 stretching modes associated with P-O_{nb} bonds on Q^1 tetrahedra. Nevertheless, the trends in peak intensity in Fig. 6 can be interpreted using well-known phosphate structural chemistry models if the peaks near 1180 and 1300 cm^{-1} are assigned to the symmetric and asymmetric PO_2 stretching modes associated with P-O_{nb} bonds on Q^2 tetrahedra, respectively, the peak centered near 1070 cm^{-1} is assigned to PO_3 stretching modes associated with P-O_{nb} bonds on Q^1 tetrahedra, and the peak centered near 970 cm^{-1} is assigned to PO_4 stretching modes associated with P-O_{nb} bonds on Q^0 tetrahedra. The dashed lines in Fig. 6 show the compositional dependences of the distributions of Q^x-tetrahedra, assuming the simplest chemical model in which Q^2 tetrahedra convert to Q^1 tetrahedra, which then convert to Q^0 tetrahedra, with increasing O/P ratio.[11] In general, the relative intensities of the peaks centered at 1180, 1070 and 970 cm^{-1} change in the same qualitative way as the predicted fractions of Q^2, Q^1 and Q^0 tetrahedra, respectively. (The compositional dependence of the relative intensity of the peak near 1250 cm^{-1} parallels that of the 1180 cm^{-1} peak, supporting the assignment of the former to asymmetric vibrational modes on nonbridging oxygens on Q^2 tetrahedra.) Similar

spectral trends have been reported from Raman studies of other polyphosphate glasses, including Li-phosphates[30], Zn-phosphates[14,31] , Ca- and Mg-phosphates.[32]

The Raman spectra of the iron phosphate glasses are more complex than can be explained by the 'chemically simple' structural model, shown in Fig. 6. For example, the spectra collected from glasses like P1, P2 and P3 have peaks that indicate the concomitant presence of Q^0, Q^1, and Q^2 tetrahedra for pyrophosphate compositions that should possess mostly Q^1 tetrahedra. Similar features in the Raman spectra from Zn-polyphosphate[14] and Pb-polyphosphate[33] glasses were interpreted using the Van Wazer site distribution model[34] for the phosphate melts that rely on the following disproportionation reaction:

$$2Q^1 \leftrightarrow Q^2 + Q^0 \qquad (1)$$

It has been shown that increasing the field strength of metal cations in a polyphosphate melt shifts the site distribution reaction to the right, increasing the structural complexity of the resulting glasses.[35,36] Obtaining quantitative measurements of the site distributions from the Raman spectra is difficult, not least because of overlapping peaks due to the different symmetric and asymmetric stretching modes associated with the different tetrahedra. However, the comparison of the Raman peak intensities with the predicted Q^x-distributions in Fig. 6 is qualitatively consistent with the site disproportionation model for compositions around the pyrophosphate stoichiometry. It seems clear, then, that to understand the effects of composition on the properties of iron phosphate glasses, the role of a broad distribution of different phosphate anions must be considered.

The relative intensity of the P-O-P symmetric stretching peak between about 680 and 770 cm^{-1} also appears to depend on the average oxidation state of the iron in these iron phosphate glasses and crystalline compounds. For example, compare the intensity of this peak from the P2 glass (95% Fe^{2+}) to that from the P1 glass (16% Fe^{2+}) in Fig. 3. Both glasses have similar O/P ratios, but the former glass has a much more intense peak at 765 cm^{-1}. Similarly, the relative intensity of the P-O-P symmetric stretching peak at 683 cm^{-1} for the M4 glass (97% Fe^{2+}) is much greater than that for the M1 glass (5% Fe^{2+}) in Fig. 4. Figure 4 also shows that the relative intensity of the P-O-P symmetric stretching peak from crystalline $Fe(PO_3)_2$ is significantly greater than for crystalline $Fe(PO_3)_3$.

Figure 7 plots the ratio of the intensity of the Raman peak due to the P-O-P symmetric stretch, relative to the most intense peak due to the $P\text{-}O_{nb}$ stretching modes, as a function of the Fe^{2+}/Fe_{tot} ratio; the P-O-P peak intensity increases with an increasing fraction of ferrous ions, particularly when Fe^{2+}/Fe_{tot} exceeds ~0.6. Changes in Raman peak intensities in phosphate glasses have been related to the degree of covalency in the P-O bond associated with the relevant vibration,[13,37] but those studies involved the effects of cation interactions on the $P\text{-}O_{nb}$ stretching modes, not the P-O-P stretching modes, where the influence of neighboring ferrous or ferric ions is expected to be less. It is unclear why the presence of ferrous ions is associated with an increase in the relative intensity of this peak, although it is evident for pyrophosphate and metaphosphate glasses and crystals. An low intensity $(POP)_{sym}$ peak has been noted in the Raman spectrum of $SrFe_2(P_2O_7)_2$, but no explanation for this was offered.[38]

The frequency of the $(POP)_{sym}$ peak is lower for crystalline iron metaphosphates (e.g., 680 cm^{-1} for $Fe(PO_3)_2$, Fig. 4) than for the pyrophosphates (e.g., 731 cm^{-1} for $Fe_2P_2O_7$, Fig. 2). The inset to Fig. 7 shows that for the iron phosphate glasses, there is a systematic decrease in the frequency of this peak as the O/P ratio increases. These peaks are too broad (and in some cases, the intensities are too low) to distinguish separate peaks due to Q^1 and Q^2 linkages, as can be seen in the Raman spectra of Zn-[13] and Pb-polyphosphate glasses.[33] This systematic increase in frequency can be related to systematic changes in the nature of the P-O-P linkages, as is discussed below.

4.4.2. P-O Bond Distances. The systematic changes in the Raman peak positions can provide additional information about the structures of the iron phosphate glasses and compounds. Rouse et al.[12] indicated that the Raman frequency of the PO_2 symmetric stretching mode for a series of metaphosphate glasses depends on the bond force constant between the modifying metal cation and the nonbridging oxygens (greater force constant, higher Raman peak frequency), and on the size of the modifying metal cation, which affects the O-P-O intra-tetrahedral bond angles (increasing bond angle, lower Raman peak frequency). A similar effect can be seen in Fig. 4, where the PO_2 peak frequencies of the two metaphosphate glasses dominated by greater field strength ferric ions (M1, 1184 cm^{-1} and M2, 1205 cm^{-1}) exceed those of the two 'ferrous' metaphosphate glasses (M3, 1173 cm^{-1} and M4, 1170 cm^{-1}).

Popović[16] has related similar peak shifts to changes in P-O bond lengths, with shorter bonds corresponding to greater Raman frequencies. By comparing the Raman spectra from more than twenty inorganic crystalline phosphates, including ortho-, pyro-

and meta-phosphates, Popović developed an empirical relationship that correlates the position of the P-O stretching mode (ν in cm^{-1}) with the P-O bond lengths (R in Å):[17]

$$v = 6.3\times10^{3} - (3.43\times10^{3})R \qquad (2)$$

Equation (2) produces bond length predictions from Raman frequencies with uncertainties of ±0.01 Å for alkali and alkaline earth phosphates, and Popović indicated that similar predictions could be made for amorphous materials.

Equation (2) is plotted in Fig. 8, along with the corresponding *average* P-O bond lengths (Table III) and the average Raman peak positions for the iron phosphate crystalline compounds analyzed in this study. There is good agreement between the measured and predicted dependences of the Raman peak positions on the average P-O bond lengths for the P-O stretching modes associated with nonbridging oxygens on the Q^0, Q^1 and Q^2 tetrahedra. However, the Raman frequencies for the P-O-P stretching modes (except one point from $Fe_7(P_2O_7)_4$) falls about 30-240 cm^{-1} below those predicted for the reported average P-O-P bond lengths of the crystalline pyro- and metaphosphate compounds. This discrepancy may be due to the inability to detect and assign the peaks due to asymmetric P-O-P stretching modes, which should fall in the range of 900-1000 cm^{-1} and so should increase the average peak position to the range predicted by Popović.

Equation (2) was used to predict the average $P\text{-}O_{nb}$ and $P\text{-}O_{br}$ bond distances for the iron phosphate glasses, using the most intense peak in the range from 1000 to 1300 cm^{-1} for the former, and the peak due to the P-O-P symmetric stretch in the 600-800 cm^{-1} range for the latter. These bond distances are reported as a function of O/P ratio in Fig. 9. In general, it appears that the average $P\text{-}O_{nb}$ bonds become longer and the average $P\text{-}O_{br}$

bonds become shorter as the O/P ratio increases. Also plotted are the *overall average* P-O bond lengths, calculated from a weighted average of P-O_{nb} and P-O_{br} distances for each respective glass. The overall average P-O bond distance decreases slightly, from 1.57 Å to 1.54 Å, with increasing O/P ratio, as nonbridging oxygens replace bridging oxygens. The open symbols in Fig. 9 report the average P-O bond distances from x-ray and neutron diffraction studies of ferrous metaphosphate[39] and ferric polyphosphate glasses.[40,41] Overall, there is reasonable agreement between the P-O bond distances predicted from the Raman spectra and those reported from the diffraction studies, although the former are consistently ~0.02 Å longer than the latter. This difference is likely associated with the assumptions made in the use of the Popović relationship. It is worth noting that the positions of the Raman peaks associated with the P-O_{br} stretching modes from the iron phosphate crystals are 40-80 cm^{-1} lower than those for the related iron phosphate glasses (i.e., inset to Fig. 9). From equation (2), this corresponds to an average P-O-P bond distance that is 0.01-0.02Å shorter for the crystalline compounds.

4.5. SUMMARY

Raman spectra collected from ferrous, ferric and ferrous-ferric phosphate compounds and glasses provide information about the phosphate anions that constitute the structures of these materials. In general, the glasses have structures that are similar to crystals with similar stoichiometries, although the glass structures are complicated by the presence of broader distributions of phosphate anions, produced by disproportionation of pyrophosphate units to form orthophosphate and metaphosphate tetrahedra. Systematic changes in Raman peak positions with glass compositions can be related to changes in the

numbers of bridging and nonbridging oxygens, which lead to changes in the average P-O bond distances.

ACKNOWLEDGEMENTS

The authors are very grateful to Jong Wook Lim for his kind help with Raman spectra collection. This work was supported by the National Science Foundation under Grant No. DMR-0305202 and DMR-0502463.

REFERENCES

[1]J. E. Miller, M. M. Gonzales, L. Evans, A. G. Sault, C. Zhang, R. Rao, G. Whitwell, A. Maiti and D. King-Smith, "Oxidative Dehydrogenation of Ethane over Iron Phosphate Catalysts," *Appl. Catal A-Gen.*, **231**[1] 281-292 (2002)

[2]M. M. Gadgil and S. K. Kulshreshtha, "Study of $FePO_4$ Catalyst," *J. Solid State Chemistry*, **111**, 357-364 (1994).

[3]A. K. Padhi, K. S. Nanjundaswamy and J. B. Goodenough, "Phospho-olivines as Positive-Electrode Materials for Rechargeable Lithium Batteries," *J. Electrochem. Soc.*, **144** [4] 1188-1194 (1997).

[4]A. Yamada, S. C. Chung and K. Hinokuma, "Optimized $LiFePO_4$ for Lithium Battery Cathodes," *J. Electrochem. Soc.*, **148**, A224-A229 (2001).

[5]Y.-S. Hong, Y. J. Park, K. S. Ryu and S. H. Chang, "Crystalline Fe_3PO_7 as an Electrode Material for Lithium Secondary Batteries," *Solid State Ion.*, **156**[1-2] 27-33 (2003).

[6]M. G. Mesko and D. E. Day, "Immobilization of Spent Nuclear Fuel in Iron Phosphate Glass," *J. Nucl. Mater.*, **273,** 27-36 (1999).

[7]X. Yu, D. E. Day, G. J. Long and R. K. Brow, "Properties and Structure of Sodium–Iron Phosphate Glasses," *J. Non-Cryst. Solids*, **215**, 21-31 (1997).

[8]G. K. Marasinghe, M. Karabulut, C. S. Ray, D. E. Day, M. G. Shumsky, W. B. Yelon, C. E. Booth, P. G. Allen and D. K. Shuh, "Structural Features of Iron Phosphate Glasses," *J. Non-cryst. Solids*, **222**, 144-152 (1997).

[9]X. Fang, C. S. Ray, A. Moguš-Milanković and D. E. Day, "Iron Redox Equilibrium, Structure and properties of Iron Phosphate Glasses," *J. Non-Cryst. Solids*, **283**, 162-172 (2001).

[10]R. K. Brow, "Review: The Structure of Simple Phosphate Glasses," *J. Non-Cryst. Solids*, **263/264** 1-28 (2000).

[11]G. B. Rouse, P. J. Miller and W. M. Risen, "Mixed Alkali Glass Spectra and Structure**,**" *J. Non-Cryst. Solids*, **28**, 193-207 (1978).

[12]B. N. Nelson and G. J. Exarhos, "Vibrational Spectroscopy of Cation-site Interactions in Phosphate Glases," *J. Chem. Phys*., **71**[7] 2739-2747 (1979).

[13]R. K. Brow, D. R. Tallant, S. T. Myers and C. C. Phifer, "The Short Range Structure of Zinc Phosphate Glass," *J. Non-Cryst. Solids* **191**, 45-55 (1995).

[14]J. J. Hudgens, R. K. Brow, D. R. Tallant and S.W. Martin, "Raman Spectroscopy Study of the Structure of Lithium and Sodium Ultraphosphate Glasses," *J. Non. Cryst. Solids,* **223**[1,2] 21-31 (1998).

[15]A. Rulmont, R. Cahay, M. Liegeois-Duyckaerts and P. Tarte, "Vibrational Spectroscopy of Phosphates: some General Correlations between Structure and Spectra," *Eur. J.Solid State Inorg. Chem.*, **28**, 207-219 (1991).

[16]L. Popović, D. de Waal and J. C. A. Boeyens, "Correlation between Raman Wavenumbers and P-O Bond Lengths in Crystalline Inorganic Phosphates," *J. Raman Spectrosc.*, **36**, 2-11(2005).

[17]A. Mogus-Milankovic, B. Pivac, K. Furic and D. E. Day, "Structural study of iron phosphate glasses," *Phys. Chem. Glasses* **38**[2] 74-78 (1997).

[18]P. A. Bingham, R. J. Hand, O. M. Hannant, S. D. Forder, S. H. Kilcoyne, "Effects of Modifier Additions on the Thermal Properties, Chemical Durability, Oxidation State and Structure of Iron Phosphate Glasses," *J. Non-Cryst. Solids*, **355**[28-30] 1526-1538 (2009)

[19]L. Zhang, R. K. Brow, M. E. Schlesinger, L. Ghussn and E. D. Zanotto, "Glass Formation from Iron-Rich Phosphate Melts," *J. Non-Cryst. Solids,* **356**, 252-257 (2010).

[20]S. I. Grishin, J. M. Bigham and O. H. Tuovinen, "Characterization of Jarosite Formed upon Bacterial Oxidation of Ferrous Sulfate in a Packed Bed Reactor," *Appl. Environ. Microbiol.*, **54,** 3101-3106 (1988).

[21]C. M. Burba, J. M. Palmer and B. S. Holinsworth, "Laser-induced Phase Changes in Olivine $FePO_4$: a Warning on Characterizing $LiFePO_4$-based Cathodes with Raman Spectroscopy," *J. Raman Spectrosc.*, **40**, 225-228 (2009).

[22]M. P. Pasternak, G. Kh. Rozenberg, A. P. Milner, M. Amanowicz, T. Zhou, U. Schwarz, K. Syassen, R. Dean Miller, M. Hanfland, and K. Brister, "Pressure-induced Concurrent Transformation to an Amorphous and Crystalline Phase in Berlinite-type $FePO_4$," *Phys Rev Lett*, **79**[22] 4409-4412 (1997).

[23]W. H. Baur, "The Geometry of Polyhedral Distortions. Predictive Relationships for the Phosphate Group," *Acta Cryst.* B **30**, 1195-1215 (1974).

[24]R. L. Frost, T. Kloprogge, M. L. Weier, W. N. Wayde, Z. Ding and G. H. Edwards, "Raman Spectroscopy of Selected Arsenates – Implications for Soil Remediation," *Spectrochim. Acta, Part A*, **59,** 2241–2246 (2003).

[25]E. J. Baran, I. L. Botto and A. G. Nord, "The Vibrational Spectrum and the Conformation of the $P_2O_7^{4-}$ Anion in $Fe_2P_2O_7$," *J. Mol. Struct.*, **143**, 151-154 (1986).

[26]K. Nakamoto, *Infrared and Raman Spectra of Inorganic and Coordination Compounds*, John Wiley & Sons, Inc., New York (1997).

[27]S. H. Morgan, R. H. Magruder and E. Silberman, "Raman Spectra of Rare-Earth. Phosphate Glasses," *J. Am. Ceram. Soc.*, **70**, C378-C380 (1987).

[28] K. Viswanathan, V. U. Nayar and G. Aruldhas, "Infrared and Raman Spectra of Three Tetrametaphosphates $M_2P_4O_{12}$ (*M* = Fe, Ni, Zn)," *J. Chem. Sci.*, **95**[5-6] 463-469 (1985).

[29]W. Zhou, W. He, X. Zhang, J. Liu, Y. Du, S. Yan, X. Tian, X. Sun, X. Han and Y. Yue, "Simple and Rapid Synthesis of $Fe(PO_3)_3$ by Microwave Sintering," *J. Chem. Eng. Data*, **54**, 2073 -2076 (2009).

[30]M. Tatsumisago, Y. Kowada and T. Minami, "Raman Spectra of Rapidly Quenched Glasses and Melts Containing Large Amounts of Li_2O," *J. Non-Cryst. Solids*, **150**, (1992) 207-211.

[31]H. Takebe, Y. Baba, and M. Kuwabara, "Dissolution Behavior of ZnO-P_2O_5 Glasses in Water" *J. Non-Cryst. Solids*, **352**, 3088-3094 (2006).

[32]M.A. Karakassides, A. Saranti and I. Koutselas, "Preparation and Structural Study of Binary Phosphate Glasses with High Calcium and/or Magnesium Content," *J. Non-Cryst. Solids*, **347**[1-3] 69-79 (2004).

[33]G. LeSaout, P. Simon, F. Fayon, A. Blin and Y. Vaills, "Raman and Infrared Study of $(PbO)_x(P_2O_5)_{(1-x)}$ Glasses," *J. Raman Spectroscopy*, **33**, 740-746 (2002).

[34]J. R. Van Wazer, *Phosphorus and its compounds*, Interscience, New York, NY. 1958.

[35]T. R. Meadowcraft and F. D. Richardson, "Structural and Thermodynamic Aspects of Phosphate Glasses," *Trans. Faraday Soc*., **61**, 54-70 (1965).

[36]B. C. Sales and L. A. Boatner, "Physical and Chemical Characteristics of Lead-Iron Phosphate Nuclear Waste Glasses," *J. Non-Cryst. Solids*, **79**, 83-116 (1986).

[37]J. Koo, B-S Bae and H-K Na, "Raman Spectroscopy of Copper Phosphate Glasses," *J. Non-Cryst. Solids*, **212**, 173-179 (1997).

[38]E. J. Baran, R. C. Mercader, A. Massaferro and E. Kremer, "Vibrational and ^{57}Fe-Mössbauer Spectra of some Mixed Cation Diphosphates of the Type $M^{II}Fe_2^{III}(P_2O_7)_2$," *Acta Part A*, **60**, 1001-1005 (2004).

[39]U. Hoppe, M. Karabulut, E. Metwalli, R. K. Brow and P. Jóvári, "The Fe–O Coordination in Iron Phosphate Glasses by X-Ray Diffraction with High Energy Photons," *J. Phys.: Condens. Matter*., **15**, 6143-6153 (2003).

[40]M. Karabulut, G. K. Marasinghe, C. S. Ray, G. D. Waddill and D. E. Day "A High Energy X-ray and Neutron Scattering Study of Iron Phosphate Glasses Containing Uranium," *J. Applied Phys.*, **87**, 2185-2193 (2000).

[41]A. C. Wright, R. N. Sinclair, J. L. Shaw, R. Haworth, G. K. Marasinghe, and D. E. Day, "A Neutron Diffraction Study of the Structure of Iron Phosphate Glasses," *Phys Chem Glasses- Eur. J. Glass Sci. Technol. B*, 49[1] 1-7 (2008).

[42]A. Goiffon, J.C. Dumas and E. Philippot, "Alpha-quartz Type Phases: Structure of $FePO_4$ and ^{57}Fe Mossbauer Spectroscopy," *Rev. Chim. Miner.*, **23**, 99-110 (1986).

[43]J. K. Warner, A. K. Cheetham, A. G. Nord, R. B. Von Dreele and M. Yethiraj, "Magnetic Structure of Iron(II) Phosphate, Sarcopside, $Fe_3(PO_4)_2$," *J. Mater. Chem.* **2**, 191-196 (1992).

[44]J. K. Warner, A. K. Cheetham and D. E. Cox, "Determination of Cation Distribution in $NiFe_2(PO_4)_2$ using Resonant X-ray and neutron Powder Diffraction," *J. Appl. Cryst.*, **28**, 494-502 (1995).

[45]Y. A. Gorbunov, B. A. Maksimov, Y. K. Kabalov, A. N. Ivashchenko, O. K. Mel'nikov and N. V. BeloV, "Crystal Structure of $Fe^{2+}{}_3Fe^{3+}{}_4[PO_4]_6$," *Dokl. Akad. Nauk SSSR*, **254**, 873-877 (1980).

[46]L. K. Elbouaanani, B. Malaman, R. Gérardin and M. Ijjaali, "Crystal Structure Refinement and Magnetic Properties of $Fe_4(P_2O_7)_3$ Studied by Neutron Diffraction and Mössbauer Techniques," *J. Solid State Chem.*, **163**, 412-420 (2002).

[47]J. T. Hoggins, J. S. Swinnea and H. Steinfink, "Crystal Structure of $Fe_2P_2O_7$," *J. Solid State Chem.*, **47**, 278-283 (1983).

[48]M. Ijjali, G. Venturini, R. Gerardin, B. Malaman and C. Gleitzer, "Synthesis Structure and Physical Properties of a Mixed-valence Iron Diphosphate $Fe_3(P_2O_7)_2$: First Example of Trigonal Prismatic Fe^{2+} with O^2-Ligands," *Eur. J. Solid State Inorg. Chem.*, **28**, 983-998 (1991).

[49]B. Malaman, M. Ijjali, R. Gerardin, G. Venturini and C. Gleitzer, "$Fe_7(P_2O_7)_4$, a Mixed Valence Iron Diphosphate the Missing Link Between $Fe_2P_2O_7$ and $Fe_3(P_2O_7)_2$," *Eur. J. Solid State Inorg. Chem.*, **29**, 1269-1284 (1992).

[50]J. M. Rojo, J. L. Mesa, L. Lezama and T. Rojo, "Magnetic Properties of the $Fe(PO_3)_3$ Metaphosphate," *J. Solid State Chem.*, **145**, 629-633 (1999).

[51]E. A. Genkina, B. A. Maksimov and O. K. Melnikov, "Crystal Structure of Iron Tetrametaphosphate $Fe_2P_4O_{12}$ and its Comparison with the Structure of Other M_2^{2+} PO_4(M^{2+}=Ni, Mg, Cu, Co)," *Sov. Phys. Crystallogr.*, **30**, 885-889 (1985).

Table I. Preparation conditions for iron phosphate compounds.

Compound	Batch materials	Preparation conditions
$FePO_4$	$FePO_4 \cdot xH_2O$	880°C for 12 hours
$Fe_3(PO_4)_2$ A	$FePO_4$, Fe_2O_3	Reduced in forming gas[*1] at 680–690°C for 6 hours [*2]
$Fe_3(PO_4)_2$ B	$Fe_3(PO_4)_2$ A	1150°C for 12 hours in sealed ampoule
$Fe_7(PO_4)_6$	Fe_2O_3, FeP_2O_6	900°C for 12 hours in sealed ampoule
$Fe_4(P_2O_7)_3$	$FePO_4$, $Fe(PO_3)_3$	800°C for 12 hours, then 940°C for 24-48 hours
$Fe_2P_2O_7$	$FePO_4$	Reduced in forming gas[*1] at 560°C for 6 hours[*2]
$Fe_3(P_2O_7)_2$	$Fe(PO_3)_3$, Fe_2PO_5	900°C for 12 hours in sealed ampoule
$Fe_7(P_2O_7)_4$	$Fe_2P_2O_7$, $Fe_3(P_2O_7)_2$	900°C for 12 hours in sealed ampoule
$Fe(PO_3)_3$	Fe_2O_3, $NH_4H_2PO_4$	Ammonia burn-off at 500°C overnight, thoroughly milled and then cooked at 800°C for 12 hours
$Fe(PO_3)_2$	$FePO_4$, $NH_4H_2PO_4$	Ammonia burn-off at 500°C overnight, after thoroughly milled and then reduced in forming gas[*1] at 650 for 6 hours[*2]

*1: Forming gas is 10% H_2 and 90% Ar.

*2: Reducing time is related to the reducing gas flow and sample size.

Table II. Conditions used to prepare iron phosphate glasses.

Glass	Initial compound (mole fraction)	Atmosphere	Temp.(°C) / Time (H)	Quench method
O1	80% $FePO_4$ + 20% Fe_2O_3	In Air	1200/0.5hr	Roller quench[19]
O2	$FePO_4$	In Air	1300 /2hr	Roller quench[19]
P1	$Fe_4(P_2O_7)_3$	In Air	1100 /2hr	Steel plate quench
P2	$Fe_2P_2O_7$	Sealed* under vacuum	1200 /2hr	Water quench
P3	$Fe_7(P_2O_7)_4$	Sealed* under vacuum	1200 /3hr	Water quench
P4	21% $Fe_4(P_2O_7)_3$ + 79% $Fe(PO_3)_3$	Sealed in air*	1110 /12hr	Water quench
M1	9% $Fe_4(P_2O_7)_3$ + 91% $Fe(PO_3)_3$	Sealed in air*	1180 /12hr	Water quench
M2	$Fe(PO_3)_3$	Sealed in air*	1250 /4hr	Water quench
M3	$Fe(PO_3)_2$	Sealed* under vacuum	1200 /2hr	Water quench
M4	$Fe(PO_3)_2$	Sealed* under vacuum	1200 /0.5hr	Water quench

* Sealed in silica tubes (Inner diameter and outer diameter: 11 and 13mm).

Table III. Crystallographic parameters for the crystals prepared in this work.

Compound	Space group	Average $P\text{-}O_{nb}$[a] (Å)	Average $P\text{-}O_{br}$[a] (Å)	P-O-P bond angle	Reference
$FePO_4$	$P3_121$	1.530	-	-	42
$Fe_3(PO_4)_2$ A	$P2_1/c$	1.537	-	-	43
$Fe_3(PO_4)_2$B	$P2_1/c$	1.540	-	-	44
$Fe_7(PO_4)_6$	$P\bar{1}$	1.543	-	-	45
$Fe_4(P_2O_7)_3$	$P2_1/n$	1.514	1.575	155.7º	46
$Fe_2P_2O_7$	$C\bar{1}$	1.519	1.554	---[b]	47
$Fe_3(P_2O_7)_2$	Pnma	1.506	1.593	135.2º	48
$Fe_7(P_2O_7)_4$	$C222_1$	1.512	1.596	136.5º	49
$Fe(PO_3)_3$	Ic	1.484	1.577	143º [c]	50
$Fe(PO_3)_2$	C2/c	1.485	1.59	137.5º	51

[a] Non-bridging oxygen bond length and bridging oxygen bond length.

[b] No exact P-O-P angles reported.

[c] Estimated based on average of reported smallest (137°) and largest (149°) P-O-P angles.

Table IV. Glass compositions.

Glass	O1	O2	P1	P2	P3	P4	M1	M2	M3	M4
Fe/P ratio	1.80±0.10	0.98±0.12	0.68±0.07	0.92±0.13	0.65±0.11	0.45±0.02	0.34±0.03	0.37±0.07	0.51±0.06	0.51±0.07
Fe^{2+}/Fe_{total}	35±1%	51±3%	16±1%	95±4%	64±8%	7±3%	5±2%	17±4%	81±4%	97±1%
O/P ratio	4.89±0.10	3.72±0.16	3.47±0.12	3.45±0.16	3.27±0.15	3.16±0.04	3.03±0.04	3.02±0.10	3.06±0.07	3.02±0.07

Table V. Summary of Raman frequencies related to various phosphate groups in iron phosphate compounds and glasses.

Raman frequency range (cm^{-1})		Assignment
Compounds	Glasses	
200-600	200-600	Network Bending
660-680	680-720	P-O-P symmetric stretch (Q^2)
710-760	760-780	P-O-P symmetric stretch (Q^1)
960-1010	990-1040	PO_4 symmetric stretch (Q^0)
1040-1110	1030-1090	PO_3 symmetric stretch (Q^1)
1120-1200	~1200	PO_3 asymmetric stretch (Q^1)
1150-1210	1060-1220	PO_2 symmetric stretch (Q^2)
1260-1300	1250-1310	PO_2 asymmetric stretch (Q^2)

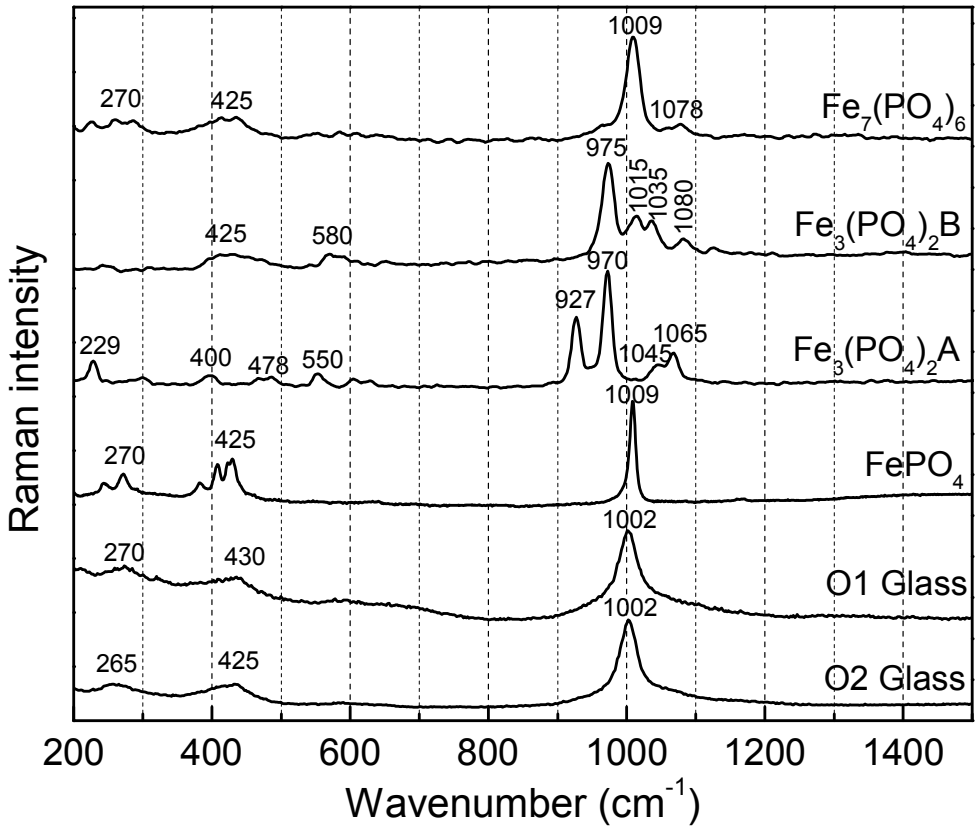

Figure 1: Raman spectra of iron orthophosphate crystals and glass.

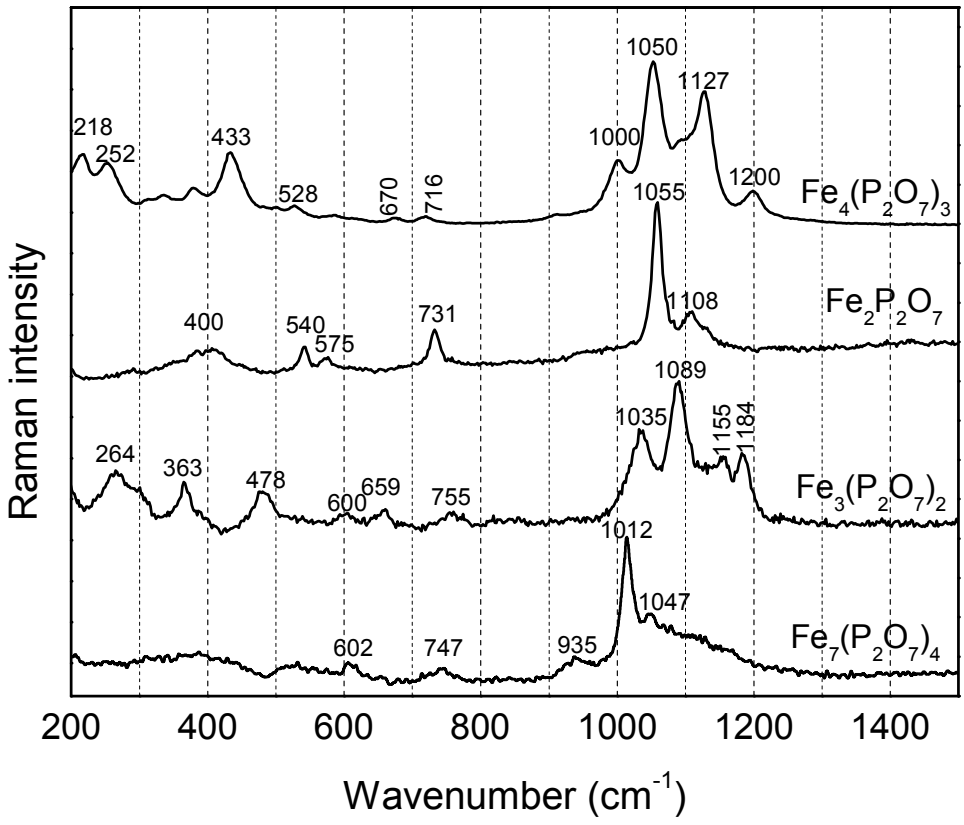

Figure 2: Raman spectra of crystalline iron pyro-phosphate compounds.

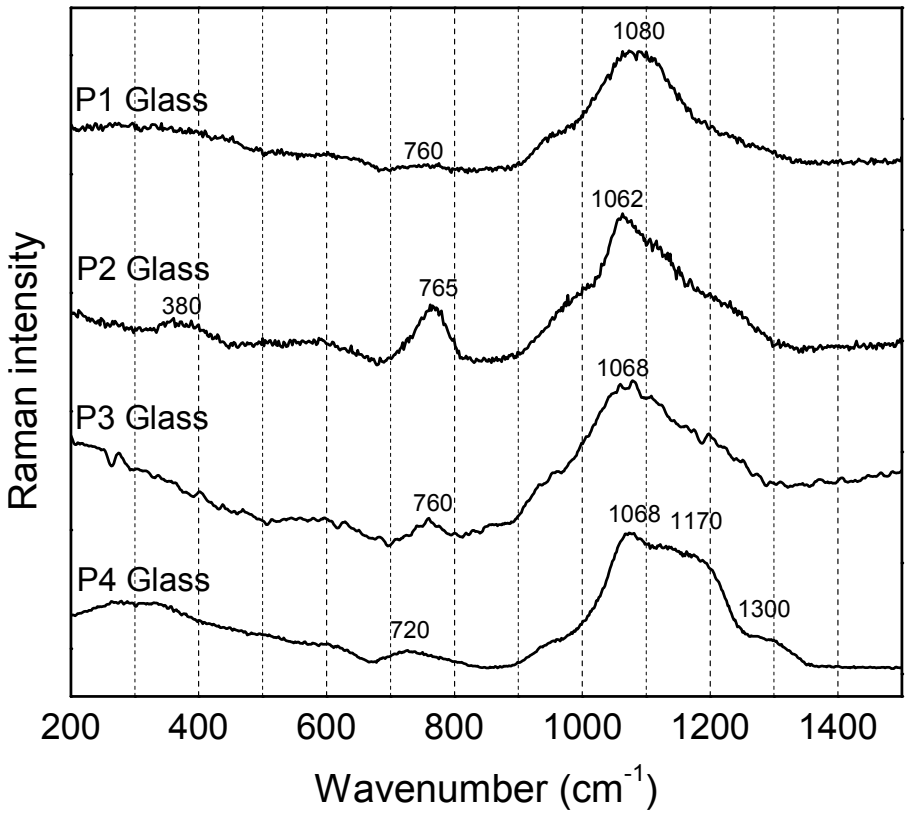

Figure 3: Raman spectra of glasses melted from pyro-phosphates.

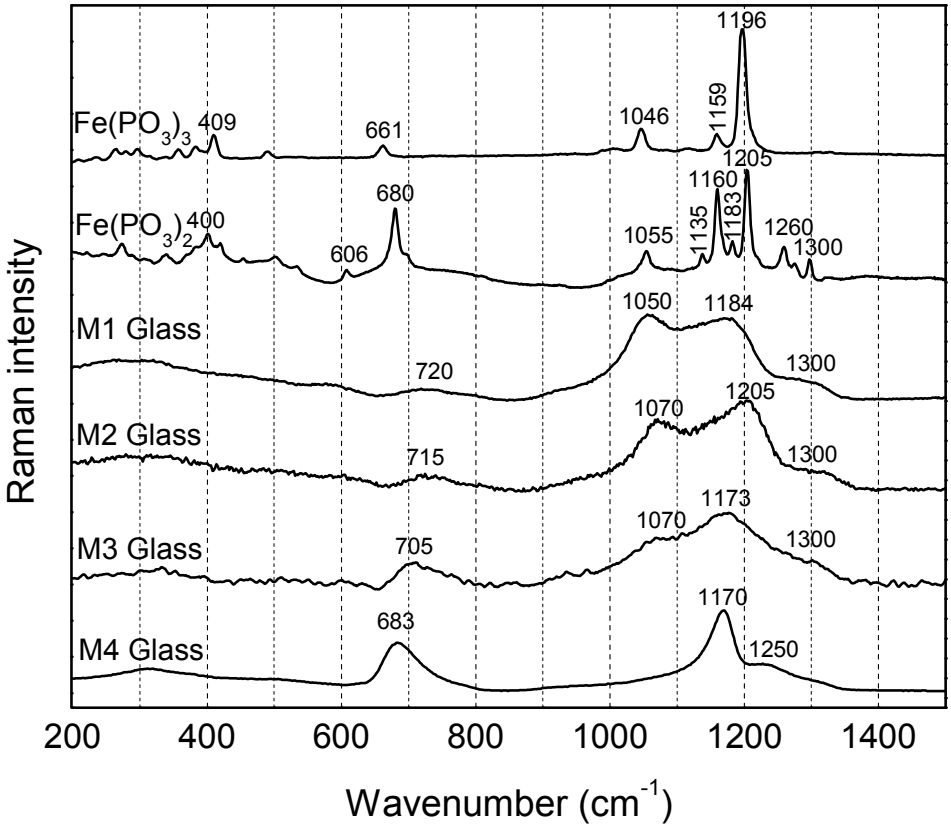

Figure 4: Raman spectra of iron metaphosphate crystal and glasses.

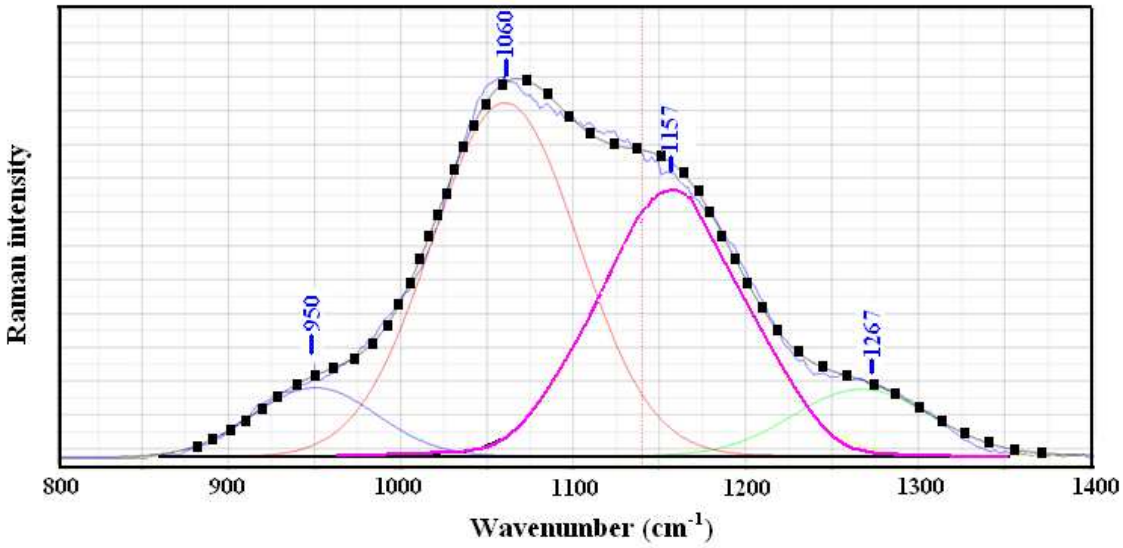

Figure 5: Decomposition of the Raman spectrum (blue line) for the P4 glass into four Gaussian peaks, the sum of which is indicated by the dotted line.

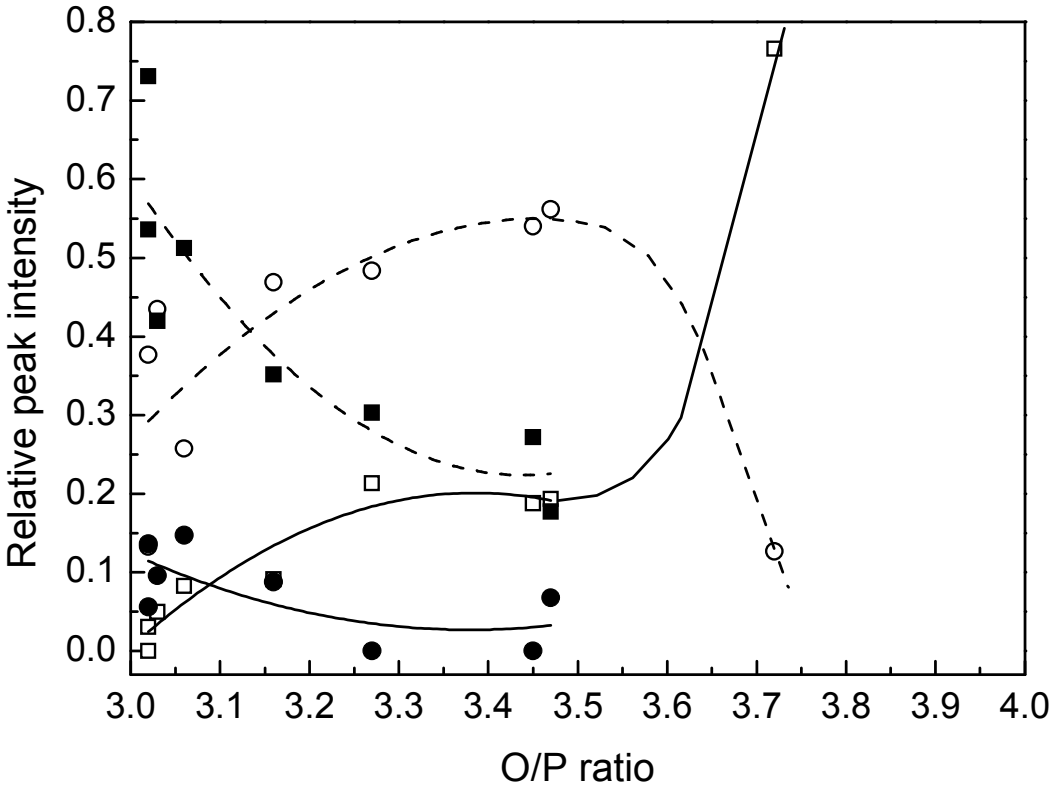

Figure 6: Relative intensities of the four Gaussian peaks used to fit the Raman spectra in the range 900-1400 cm^{-1} from each iron phosphate glass. The peak positions are (□) 930-980 cm^{-1}, (○) 1010-1100 cm^{-1}, (■) 1140-1200 cm^{-1}, (●) 1240-1310 cm^{-1}. Lines are guides for the eye.

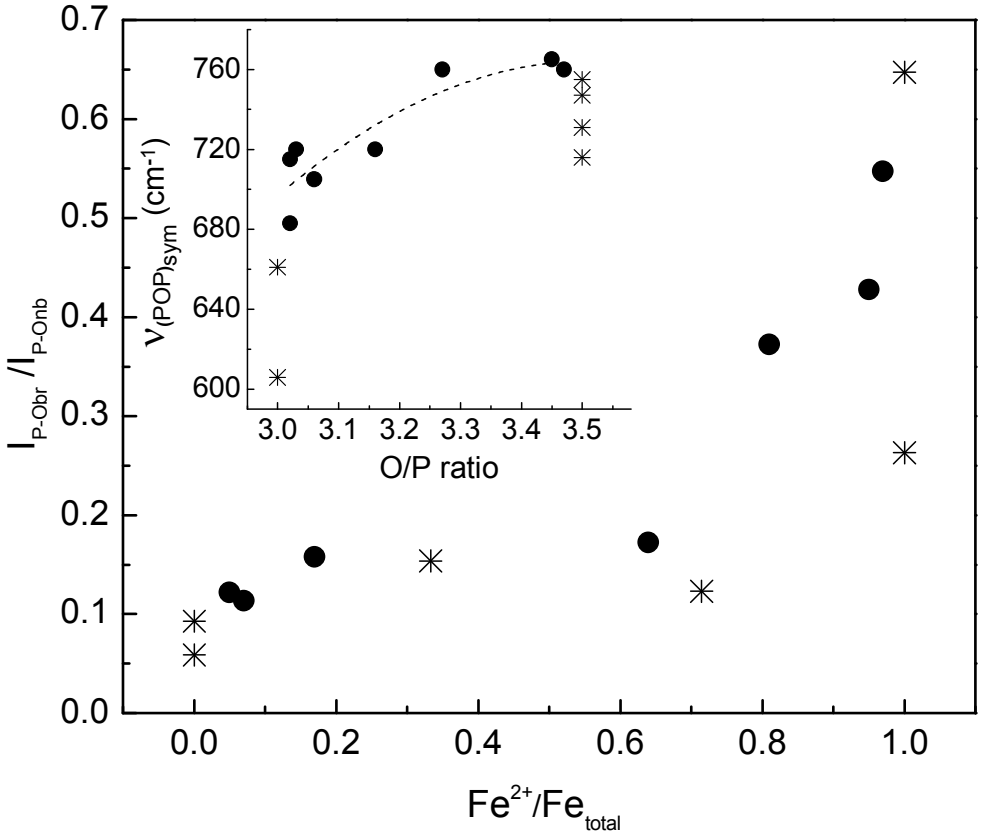

Figure 7: Intensity ratios for the P-O-P and P-O_{nb} symmetric stretching Raman peaks for iron phosphate compounds (*) and glasses (●) as a function of the fraction of ferrous ions. The inset shows the frequency of the $(POP)_{sym}$ peak as a function of composition. The dashed line is a guide for the eye.

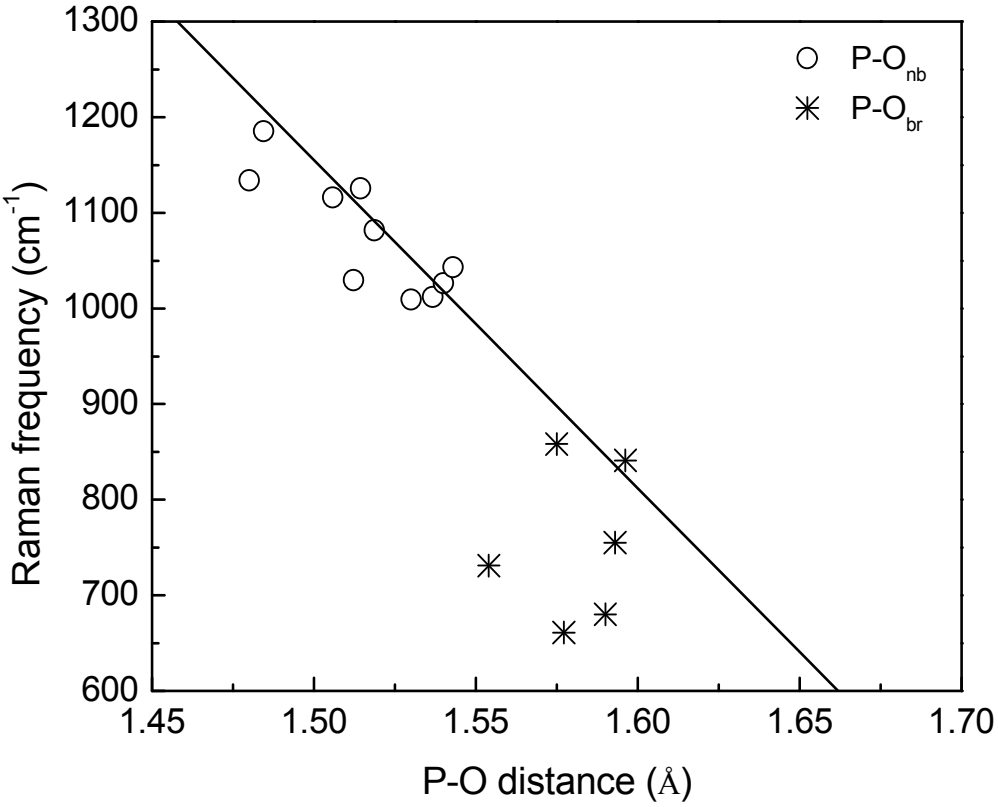

Figure 8: The average positions of the Raman peaks for the P-O_{nb} (o) and P-O_{br} (*) stretching modes, compared to the average respective bond distances, for the iron phosphate compounds studied in this work. The line is the empirical correlation (equation 2) proposed by Popović.[16]

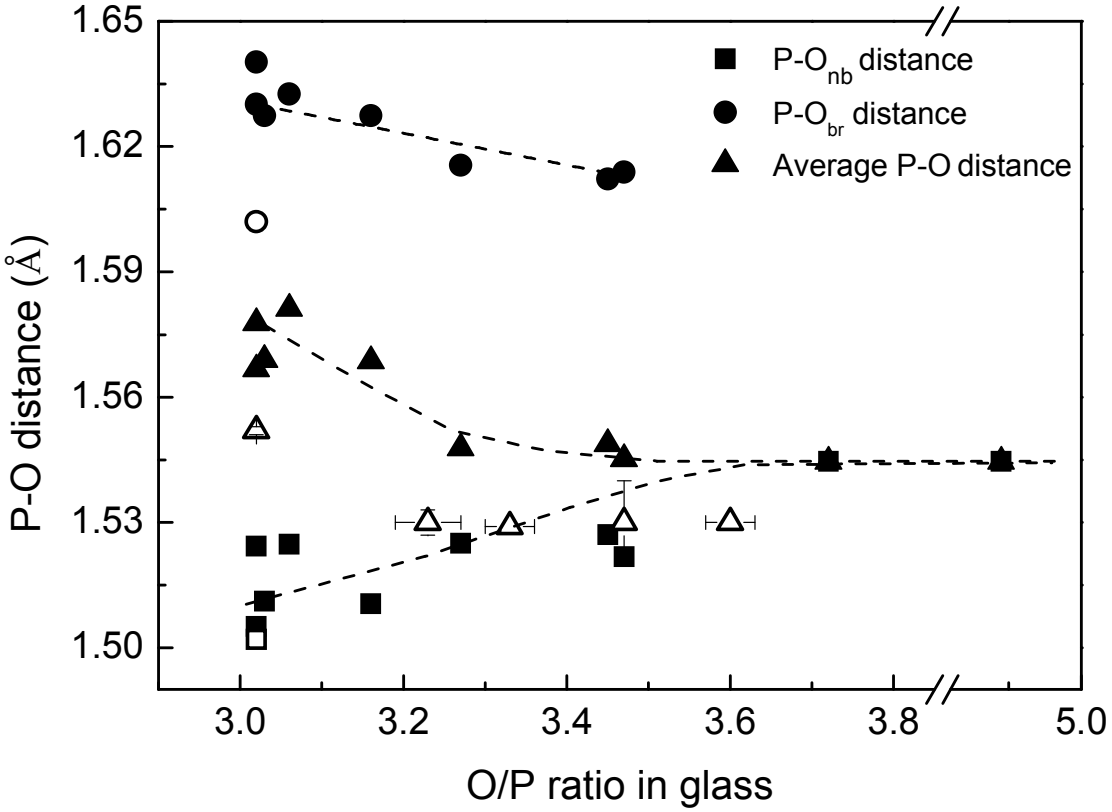

Figure 9: P-O bond distances (closed symbols) for the iron phosphate glasses calculated from Raman peak positions using equation 2. The open symbols are bond distances reported in the literature.[39-41] Dashed lines are guides for the eye.

APPENDIX A

SYNTHESIS AND CHARACTERIZATION OF IRON PHOSPHATE COMPOUNDS

A. SYNTHESIS AND CHARACTERIZATION OF IRON PHOSPHATE COMPOUNDS

Liying Zhang, Mark E. Schlesinger, Richard K. Brow

Department of Materials Science and Engineering, Missouri University of Science and Technology, Rolla, MO 65409, USA

ABSTRACT

Iron phosphate compounds were prepared using $FePO_4 \cdot xH_2O$, Fe, Fe_2O_3, Fe_3O_4 and $NH_4H_2PO_4$. X-ray diffraction, SEM and DTA/TGA were used to characterize the products. The preparation recipes are summarized. Ferric phosphate compounds were made in air by controlling the solid reaction temperature and time; ferrous and mixed-valence iron phosphate compounds were made at specific temperatures in sealed tubes or in reducing gas. The melting or decomposition characterization temperatures were determined. Laboratory experience in preparation and characterization of iron phosphate compounds were also summarized.

1. INTRODUCTION

Transition metal phosphates have been extensively studied due to their potential applications as catalysts, food additives and fertilizer. Iron phosphates have drawn extensive attention due to their optical, electrical and magnetic properties [1-7]. $FePO_4$, $Fe_2P_2O_7$, $Fe_3(P_2O_7)_2$ and $Fe_4(P_2O_7)_3$ are well-known for their use in oxidative

dehydrogenation [4-6]. Fe_3PO_7 can be used as an electrode material for lithium secondary batteries [7].

Based on the PDCP database, there are thirteen iron phosphate compounds [4]. Among them, four are ferric phosphates (Fe_3PO_7, $FePO_4$, $Fe_4(P_2O_7)_3$ and $Fe(PO_3)_3$), four are ferrous phosphates ($Fe_4P_2O_9$, $Fe_3(PO_4)_2$, $Fe_2P_2O_8$ and $Fe(PO_3)_2$), and the others (Fe_9PO_{12}, Fe_2PO_5, $Fe_7(PO_4)_4$, $Fe_3(P_2O_7)_2$ and $Fe_7(P_2O_7)_4$) are mixed–valence compounds. Four other compounds were mentioned in the literature, but without information on preparation details, characterization, or XRD references. They are $Fe_4P_6O_{21}$, $Fe_5(PO_4)_3O$, $Fe_5P_2O_{11}$, and $Fe_5P_4O_{16}$. $Fe_4P_6O_{21}$ and $Fe_5P_4O_{16}$ were mentioned by Wentrup in 1935 [8]. However, $Fe_4P_6O_{21}$ was proven to not exist and in the phase diagram should be Fe_3PO_7 [9]. Gleitzer and his colleagues investigated solid-state equilibria in the Fe-P-O system at 900°C under a range of oxygen partial pressure, and did not report any information about $Fe_4P_6O_{21}$ [10,11]. Wentrup included $Fe_5P_2O_{11}$ and $Fe_5P_4O_{16}$ in the composition map after Schenck reported the compounds in 1932 [8], but did not make or study them. The mixed-valence iron oxy-phosphate $Fe_5(PO_4)_3O$ was reported by Gleitzer [10] to have a triclinic cell, but without any XRD data. In addition, $Fe_4P_2O_9$, i.e., $Fe_4(PO_4)_2O$, was prepared by Gleitzer and his colleagues in vacuumed silica ampoules at 900°C [11,12]. However, it was hard to obtain pure $Fe_4P_2O_9$ due to its domain of stabilities in a narrow p_{O2} range. $Fe_4P_2O_9$ was reported to be a metastable phase in H_2-H_2O mixtures [11].

Various experiments were also designed to prepare $Fe_4P_2O_{11}$, $Fe_4P_2O_9$ and $Fe_5P_3O_{13}$ compounds as well as other compounds with XRD data. The preparation and discussion about $Fe_4P_2O_{11}$ can be referred to [13].

1.1. Ferric phosphates preparation

Hong, et al., used Fe_2O_3 and $(NH_4)_2HPO_4$ as starting materials to prepare Fe_3PO_7 by solid-state reactions. $FePO_4$ was made at 950°C by the reaction of Fe_2O_3 and $(NH_4)_2HPO_4$, and then Fe_3PO_7 was synthesized from the reaction of $FePO_4$ and Fe_2O_3 at 1050°C for twelve hours [7]. $Fe_4(P_2O_7)_3$ was discovered by D'Yvoire [14] by heating a mixture of $FePO_4$ and $Fe(PO_3)_3$ to 950°C. JCPDS card 36-0318 provides the only crystallographic information about this compound (PCPDFWIN version 2.1 (JCPDS-International Centre for Diffraction Data)). Elbouaanani[15] prepared $Fe_4(P_2O_7)_3$ by heat-treating a mixture of $Fe(PO_3)_3$ and $FePO_4$ at 940°C for 72 hours in oxygen. $Fe(PO_3)_3$ can be synthesized by heating a mixture of $Fe(NO_3)_3$ and $NH_4H_2PO_4$ first at 300°C for four hours and then at 800°C following by a rapid cooling to room temperature[16,17].

1.2 Ferrous phosphate preparation

The general way to prepare ferrous phosphates is to reduce the corresponding ferric phosphate in a reducing atmosphere. Zheng et al. prepared β-$Fe_2P_2O_7$ by solid state reaction of FeC_2O_4 and $NH_4H_2PO_4$ at 630-700°C in argon [18]. Reduction of corresponding ferric phosphates in H_2 was used to prepare $Fe_3(PO_4)_2$ and $Fe(PO_3)_2$. The determination of experimental conditions will be discussed.

1.3. Mixed-valence iron phosphates preparation

The mixed–valance compounds can be prepared in sealed silica tubes at 900°C or by carefully reducing Fe-P-O batch mixtures. Gleitzer prepared $Fe_9(PO_4)O_8$, Fe_2PO_5, $Fe_7(PO_4)_6$, $Fe_3(P_2O_7)_2$ and $Fe_7(P_2O_7)_4$ by heat-treating samples at 900°C and annealing with a trace of $FeCl_2$ as mineralizing agent [19-23].

To our knowledge, melting temperatures for the above compounds have rarely been reported. $Fe_7(PO_4)_6$ was reported to melt at 996°C but the author did not mention the experimental conditions [24]. In this paper, the preparation methods for iron phosphates are discussed and summarized, and their melting behavior is studied.

2. MATERIALS AND METHODS

2.1 Preparation and studies about liquidus temperatures

Iron phosphates can be made using commercially available $FePO_4 \cdot xH_2O$ (Alfa Aesar, 100%), Fe_2O_3 (Alfa Aesar, ≤45μm, ≥99%), $NH_4H_2PO_4$ (Alfa Aesar, 98%), Fe_3O_4 (Fisher Chemical, ≥99%) and Fe (Fisher Chemical, 99%). The batch materials were thoroughly mixed before heat treatment. By controlling the atmosphere, temperature and time of heat-treatment of different starting materials, corresponding iron phosphates can be made. 10-30 grams batches were heat-treated in air for ferric phosphate preparation. For ferrous and mixed-valence iron phosphates, one– to two–gram batches were heat treated in sealed silica tubes. The heating rate of 5°C/min and cooling rate of 2°C/min were used for all experiments. Table I shows the recipes used in our experiments for the compounds with XRD data.

A stoichiometric mixture of $Fe_3(PO_4)_2$, Fe and Fe_2O_3 was used as raw materials, or an $FePO_4$–Fe_2O_3 mixture. The thoroughly mixed batch was sealed in a silica ampoule under vacuum or in the flow of forming gas (10% H_2 and 90% Ar). Table II shows the experimental conditions that were used to make this compound.

In this work, many experiments were designed to prepare single–phase $Fe_5P_3O_{13}$. Heat-treatment at 900°C, 1000°C and 1500°C after long dwelling (24 hours ~ 5 days) and long annealing (1~7 days) were used to prepare $Fe_5P_3O_{13}$.

Final materials were ground to –53 μm for the following experiments. XRD (Scintag 2000) and SEM-EDS (Hitachi S4700) were used to identify phases and observe morphology. The compounds were studied by DTA (Perkin Elmer DTA7) or DTA/TGA (Netzsch STA 409C) at the heating rate of 10°C/min in different atmospheres. The liquidus temperatures of iron phosphate compounds were obtained by DTA/TGA in air or quenching experiments. The quenching experiments were done on samples sealed in silica tubes under vacuum. The samples were held at temperatures between 900 and 1200°C for around twelve hours and then quenched in water. Samples were selected to be titrated by $KMnO_4$ (2 mM) for $Fe(II)/Fe_{tot}$ ratio determination; the results and discussion refer to the reported work in [13,25].

2.2 Characterization

Other laboratory experiences have been presented in this section. The experience in XRD characterization of iron phosphates was summarized through the comparison of XRD patterns from different equipment. The confirmation of melting temperature of $FePO_4$ was done by observing the melting process of $FePO_4$ in tube furnace.

The Raman spectra (Horiba Jobin Yvon LabRam HR) studies of $Fe_3(P_2O_7)_2$ from different recipes were discussed to present some questions for the future work. To study the structure of crystalline $Fe_3(P_2O_7)_2$, the compound was made by the two batch mixtures #A($Fe_4(P_2O_7)_3$+$Fe_2P_2O_7$) and #B($Fe(PO_3)_3$+Fe_2PO_5). The samples were first ground to powder for XRD identification. All XRD patterns matched with 80-2315.

3. EXPERIMENTAL RESULTS AND DISCUSSION

3.1. Ferric phosphates

Figures 1 and 2 show XRD patterns and SEM images collected for ferric phosphates Fe_3PO_7, $FePO_4$, $Fe_4(P_2O_7)_3$ and $Fe(PO_3)_3$. The samples obtained by the above experimental procedures were all polycrystalline. $FePO_4$, $Fe_4(P_2O_7)_3$ and $Fe(PO_3)_3$ are laminate, while Fe_3PO_7 are more three-dimensional grains.

The reduction of Fe(III) starts for the four ferric phosphate compounds at different temperatures when they are heated in air. The DTA/TGA patterns of Fe_3PO_7 and $FePO_4$ in air were reported in [13]. Fe_3PO_7 decomposes around 1100°C. The reduction of Fe(III) causes weight loss due to the release of O_2. After that the heat capacity changes, which causes the shift of the DTA baseline. There is no obvious peak for the incongruent melting of this compound, estimated to be 1380°C [13]. $FePO_4$ loses weight above 1000°C, due to the reduction of Fe(III) [13]. $FePO_4$ melts at 1208°C in air from DTA.

Figure 3 shows the DTA and TGA of $Fe_4(P_2O_7)_3$ in air. The melting temperature of this compound is around 900°C. Around its melting temperature weight loss begins, which means that reduction of Fe(III) starts around the compound's melting temperature. Mössbauer shows 1.5% Fe(II) in the sample after heat-treatment at 950°C for six hours (see Fig. 4). Based on our experiments, this compound does not lose much phosphorus during heating to 950°C. Quenching method was also used to study the melting temperature of $Fe_4(P_2O_7)_3$, which gives 945±8°C. Clearly, the quenching method gives a higher melting temperature (~40°C for $Fe_4(P_2O_7)_3$) due to the competition between the quench rate and crystallization.

Figure 6 shows the DTA and TGA patterns for $Fe(PO_3)_3$ in air. The DTA “hump" at around 1200°C corresponds to a big weight loss indicated by TGA. When $Fe(PO_3)_3$ was heat–treated below 1100°C at the heating rate of 10°C/min, XRD traces continued to show pure $Fe(PO_3)_3$. The reduction of Fe(III) happens above 1200°C in air (Mössbauer in Figure 5 shows the Fe(II) ratio is around 11.8% when $Fe(PO_3)_3$ is heated at 1200°C after six hours).

Meanwhile, $Fe(PO_3)_3$ has phosphorus loss above 1100°C. For example, we heated $Fe(PO_3)_3$ in Al_2O_3 crucible at 1100°C for 12 hours following by cooling at 1°/min. The crucible was crushed and analyzed in the Hitachi S4700. Figure 7 shows a porous deposit on the surface of the Al_2O_3 crucible; and EDS analysis of the deposit indicates phosphorus. No quantitative studies of phosphorus volatilization were carried out in the present work.

3.2 Ferrous phosphates

3.2.1 Determination of preparation procedures for ferrous phosphates

Several experiments were done to determine the optimum temperature for making ferrous phosphates. When temperatures were too low, the Fe (III) in the mixture was not fully reduced, and if temperatures were too high, the Fe(III) phosphate reduced to phosphide. A series of XRD and experiments with various temperatures were carried out in order to determine the proper reducing temperature for the preparation for each ferrous phosphate compound. Figure 8 shows the XRD collected for determination of the optimum reducing temperature for generating $Fe_3(PO_4)_2$. At 900°C the Fe(III) was reduced to FeP, at 700°C the product was $Fe_3(PO_4)_2$ with a little Fe_2P, and below 600°C some unreduced $FePO_4$ remained, along with some unreacted Fe. Based on these results,

the appropriate reducing temperature was 600 – 700°C. Using the same method, we determined the optimum reducing temperature in forming gas was between 680 and 690°C. Figure 9 gives XRD confirmation of the reducing temperatures.

The same method was used to determine the optimum preparation temperatures for $Fe_2P_2O_7$ and $Fe(PO_3)_2$, which are 560° and 650°C, respectively.

3.2.2 Characterization of ferrous phosphates

In the preparation of $Fe_4P_2O_9$, the most frequently detected phase in the samples after heat-treatment was $Fe_3(PO_4)_2$. Based on the experimental results, the heat-treatment of samples in Al_2O_3 crucible with $FeCl_2$ as the mineralization agent and sealed in silica ampoules yielded some product with an XRD pattern closest to the standard $Fe_4P_2O_9$ XRD patterns. Figure 10 shows the XRD pattern which is closest to pure $Fe_4P_2O_9$. It indicates that at least two phases of $Fe_4P_2O_9$ exist in the product. Based on that, modified experimental conditions, including longer heat-treatment time, slower cooling rate or higher temperature were used to prepare single phase of $Fe_4P_2O_9$. However, none of them worked well.

Figure 11 shows the SEM images of the ferrous phospahte powders. They show that the samples reduced in forming gas are porous and one morphology resulted for each compound.

Figure 12 shows the DTA and TGA patterns for $Fe_2P_2O_7$ and $Fe(PO_3)_2$ in Ar. Based on the TGA patterns of the two ferrous phosphate compounds, it is clear that weight gain due to oxidation happens between 400 and 800°C. $Fe_2P_2O_7$, above 400°C, oxidizes to form $FePO_4$ which starts to be reduced back to $Fe_2P_2O_7$ above 1000°C and

melts around 1208°C. The oxidation and reduction are corresponding to the weight gain and loss in TGA patterns of $Fe_2P_2O_7$ in Fig. 11 (a).

To prevent the ferrous phosphate compounds from oxidizing during heating, various DTA settings were tried. Figure 13 shows the DTA and TGA patterns of $Fe_2P_2O_7$ run in Ar with different settings (like changing to high purity Ar, increasing purging time (by 0.5 hr to one night) before experiments start). TGA for both experiments showed a ~5% weight gain at 800°C, which corresponds to ~90% oxidation of Fe(II). Forming gas (5% H_2 and 95% Ar) was used to control the atmosphere of the DTA, but again the results showed almost the same weight gain (~5%). For reaction (1), all Fe ions are in solid state. When the equipment or the gas flow contains sufficient p_{O2} to drive the reaction, the oxidation occurs. Since the thermodynamic data for iron phosphates at different temperatures has not been reported, the critical oxygen partial pressure cannot be obtained.

$$Fe(II)+(1/4)O_2 \rightarrow Fe(III)+(1/2)O^{2-} \quad \ldots\ldots(1)$$

Sealed tubes were used to control the atmosphere, prevent the valence change of iron and minimize loss of phosphorus. Figure 14 shows XRD patterns collected for $Fe_2P_2O_7$ after being heated at 1065°C and $Fe(PO_3)_2$ after being heated at 920°C for twelve hours in sealed tubes. The results show that the use of sealed tubes under vacuum prevented Fe(II) oxidation. By quenching experiments using sealed tubes, the melting behavior and temperature of the ferrous phosphates were studied.

3.3 Mixed-valence iron phosphates

The means of producing mixed-valence iron phosphates have been previously discussed [20-24]. XRD was used to characterize the phases after preparation. DTA/TGA in Ar or forming gas did not prevent the valence change of iron above 400°C (see Fig. 12). Finally, mixed-valence iron phosphates were studied using the same methods used for ferrous phosphates. In this work, we did not use temperatures above 1500°C for a long time to prevent deformation of the silica tube. Table III summarizes the thermal characterization temperatures of iron phosphates studied in this work.

The experiments to grow $Fe_5P_3O_{13}$ single crystal failed in this work. We noticed much more mutual diffusion and interaction between silica tube and samples for 1000° and 1500°C samples, which can be observed through the weakened and colored silica tube wall where samples touched silica tube. Meanwhile, the CTE of the sample was quite different from that of fused silica, and the silica tube cracked easily during cooling if the samples were heated above 1000°C for 24 hours. In the end, the single crystalline phase of $Fe_5P_3\ O_{13}$ was not obtained in this work.

All 17 iron phosphate compounds were marked and listed in Fig. 15. Of these, 13 were been prepared successfully, which are marked in green. The reported iron phosphates which were not prepared successfully in this work are marked in grey. The lines are connecting the compositions.

3.4 Characterization experience

FeK fluorescence when CuKα is used for XRD causes background uniformly increased over the entire angular range. In this work, a low scanning rate (1~2 minutes per degree for Scintag XDS 2000, which can decrease the signal intensity) was used for

most of the samples, considering the cost and convenience to the authorized user. For the samples that have very low signal/noise ratio, are present in very small amounts or need quantitative studies of phases, the thin film XRD (Philips X-Pert) diffractometer was used. Figure 16 shows the comparison of XRD collected on the sample powder $Fe_3(P_2O_7)_2$, but obtained from two methods. The XRD patterns obtained using the two methods show no difference when used in phase identification, although the signal/noise ratio and signal intensity in powder XRD is not as good as that of thin film XRD.

Raman spectra were collected for both powder and bulk $Fe_3(P_2O_7)_2$, since the Raman spectra show some difference in relative intensities in one powder. Figure 17 shows the Raman of $Fe_3(P_2O_7)_2$ powder made from mixtures #A($Fe_4(P_2O_7)_3$+$Fe_2P_2O_7$) and #B($2FePO_4$+$Fe(PO_3)_2$). From the comparison, we can see that the peaks at lower wave-number range (<1000 cm^{-1}) are very reproducible, and the four peaks at ~1033, ~1100, ~1150, and ~1190 cm^{-1} are also repeatable. However, the peaks at 1000 cm^{-1} and 1200 cm^{-1} don't exist in the spectra of #A $Fe_3(P_2O_7)_2$, but in the spectra of #B $Fe_3(P_2O_7)_2$. Based on our experiment about the Raman of iron phosphate compounds, the peak ~1000cm^{-1} and ~1200cm^{-1} can be assigned to the Q^0 and Q^2. Since $Fe_3(P_2O_7)_2$ decomposes to $FePO_4$ above 925^oC, meanwhile we found that the peak around 1000 cm^{-1} usually comes with the color change after Raman detection. It is indicated that the ~1000cm^{-1} peak may arise from the phase change induced by the laser. For the peak around 1200 cm^{-1}, it is probably partially from the residual $Fe(PO_3)_3$ in the final product or the phase change induced by laser. The explanation of the other peaks is given in Table IV.

The bulk of $Fe_3(P_2O_7)_2$ made from batch #A was studied by Raman. Figure 18 shows the two kinds of Raman spectra for the same $Fe_3(P_2O_7)_2$ sample. It is shown that the peaks exist at the same positions. However, the relative intensity of the peaks between 1000-1200 cm^{-1} is not exactly the same. The different intensity could be induced by the possibility difference of electrons at some energy level, which need to be further studied through collecting more series of spectra. The assignments in Table IV are also valid for these patterns.

The melting process of $FePO_4$ was observed in a tube furnace in air. Figure 19 shows the images captured around the melting temperature. The melting temperature was determined by the lowest temperature that the hill shape starts to get flat. The observation method gives the comparable melting temperature of $FePO_4$: 1200±5°C (1208±5°C from DTA/TGA). However, DTA/TGA cannot be used to determine the melting temperature of the compounds which have incongruent melting behavior or serious evaporization. This experiment confirms the results from DTA/TGA studies.

4. SUMMARY AND DISCUSSION

We have successfully prepared 12 iron phosphates that exist in the XRD database by controlling the conditions of solid reactions. The methods of determining the melting temperature of ferric, ferrous and mixed-valence iron phosphates were discussed and summarized. Of the iron phosphate compounds, Fe_3PO_7 and $Fe_3(P_2O_7)_2$ decompose during heating, and the others melt congruently. The thermal characterization temperatures of those iron phosphates were determined. Quench methods provide higher

characterization temperatures due to the competition between quench rate and crystallization, whose quantitative effect should be studies in the future.

ACKNOWLEDGEMENT

This work was supported by the National Science Foundation, grant DMR-0502463.

REFERENCES

[1] A.Q. Yuan, J. Wu, Z.Y. Huang, K. Wu, S. Liao, Z.F. Tong, "Synthesis of $NH_4FePO_4H_2O$ Nano-plates via Solid-State Reaction at Low Temperature and its Thermochemistry Properties," Mater. Res. Bull. 43 (2008) 1339–1345.

[2] S. Boudin, K.H. Lii, "Ammonium Iron(II, III) Phosphate: Hydrothermal Synthesis and. Characterization of $NH_4Fe_2(PO_4)_2$," Inorg. Chem. 37 (1998) 799-803.

[3] Y.G. Ko, U.S. Choi, B.G. Ahn, D.J. Ahn, "Study on Syntheses of Phosphates and Transition-metal Complexes on Viscose Rayon Felt for Flame Retardancy," J. Polym. Sci. A: Polym. Chem. 38 (2000) 2815-2823.

[4] Y. Wang, X.X. Wang, Z. Su, Q. Guo, Q. Tangm Q. Zhang, H. Wan, "SBA-15-Supported Iron Phosphate Catalyst for Partial Oxidation of Methane to Formaldehyde," Catal. Today 93-95 (2004) 155-161.

[5] G.O. Alptekin, A.M. Herring, D.L. Williamson, T.R. Ohno, R.L. McCormick, "Methane Partial Oxidation by Unsupported and Silica Supported Iron Phosphate Catalysts: Influence of Reaction Conditions and Co-Feeding of Water on Activity and Selectivity," J. Catal. 181 (1999) 104-112.

[6] M. Ai, K. Ohdan, "Effects of Differences in the Structures of Iron Phosphates on the Catalytic Action in the Oxidative Dehydrogenation of Lactic Acid to Pyruvic Acid," Appl. Catal. A 165 (1997) 461-465.

[7] Y-S Hong, Y.J. Park, K.S. Ryu, S.H Chang, "Crystalline Fe_3PO_7 as an Electrode Material for Lithium Secondary Batteries," Solid State Ionics, 156 (2003) 27-35.

[8] H. Wentrup. "Beitrag zum System Eisen-Phosphor-Sauerstoff," Arch. Eisenhuttenw, 9 (1935) 57-60.

[9] J. Korinth, P. Royen, "Reaction in the System $Fe_2O_3/FePO_4$ (in Ger.)," Z. Anorg. Allg. Chem, 313[3-4] (1961) 121-37.

[10] A. Modaressi, J.C. Kaell, B. Malaman, R. Gérardin, C. Gleitzer, "Study of the System Fe-P-O (for Fe/P ≥1) and its Compounds: the Oxyphosphates of Iron (in Fr.)," Mater. Res. Bull, 18 (1983) 101-109.

[11] J. C Kaell, F. Jeannot, and C. Gleitzer, "Study of the Progressive Reduction of $Fe_3(PO_4)_2$ and $Fe_9(PO_4)O_8$ (in Fr.)," Ann. Chim., 9 (1984) 169-80.

[12] M. Bouchdough, A. Courtois, R. Gerardin, J. Steinmetz, C. Gleitzer, "Preparation et Etude d`un Oxyphosphate $Fe_4(PO_4)_2O$ (Fr.)," J. Solid State Chem. 42 (1982) 149-157.

[13] L. Zhang, M.E. Schlesinger, R.K. Brow, "Phase Eqilibria in the Fe_2O_3-P_2O_5 System," under review.

[14] F. D'Yvoire, "Etude des Phosphates D'Aluminum et de Fer Trivalent I-L'Orthophosphate Neutre d'Aluminum," Bull. Soc. Chim. Fr. (1962) 1224-1236.

[15] L.K. Elbouaanani, B. Malaman, R. Gérardin, M. Ijjaali, "Crystal Structure Refinement and Magnetic Properties of $Fe_4(P_2O_7)_3$ Studied by Neutron Diffraction and Mössbauer Techniques," J. Solid State Chem. 163 (2002) 412-420.

[16] C. Gleitzer, "Anhydrous Iron Phosphates and Oxyphosphates," Eur. J. Solid State Inorg. Chem. 28 (1991) 77-91.

[17] J.M. Rojo, J.L. Mesa, L. Lezama, T. Rojo, "Magnetic Properties of the $Fe(PO_3)_3$ Metaphosphate," J. Solid State Chem. 145 (1999) 629-633.

[18] W. Zheng, R. Guo, D. Zhong, K. Du, G. Xu, "Solid State Synthesis and Characterization of Iron(II) Pyrophosphate $Fe_2P_2O_7$," Chinese Chem. Letters 18 (2007) 1525-1527.

[19] C. Gleitzer, A. Modaressi, R.J.D. Tilley, "Intergrowth Phases in the Fe_9PO_{12}---Fe_7SiO_{10} System," 59(3) (1985) 362-370.

[20] A. Modaressi, A. Courtois, R. Gerardin, B. Malaman, C. Gleitzer, "Fe_2PO_5, un Phosphate de fer De Valence Mixte. Préparation et études Structurale, Mössbauer et Magnétique (in Fr.)," J. Solid State Chem., 40(3) (1981) 301-311.

[21] M. Ijjaali, G. Venturini, B. Malaman, C. Gleitzer, "Préparation et Étude d'un Disphosphate de Fer de Valence Mixte $Fe_3(P_2O_7)_2$, Premier cas de Fe^{2+} en Coordinence Trigonale Prismatique dans un Oxide (In Fr.)," Eur. J. Solid State Inorg. Chem. 310 (1990) 1419-1423.

[22] M. Ijjaali, G. Venturini, R. Gerardin, B. Malaman, C. Gleitzer, "Synthesis, Structure and Physical Properties of a Mixed-Valence Iron Diphosphate $Fe_3(P_2O_7)_2$: First Example of Trigonal Prismatic Fe^{2+} with O^{2-} -ligands (in Fr.)," Eur. J. Solid State Inorg. Chem. 28 (1991) 983-998.

[23] B. Malaman, M. Ijjaali, R. Gerardin, G. Venturini, C. Gleitzer, "$Fe_7(P_2O_7)_4$, A Mixed-Valence Iron Diphosphate, the Missing Link Between $Fe_2P_2O_7$ and $Fe_3(P_2O_7)_2$ (in Fr.)". Eur. J. Solid State Inorg. Chem. 29 (1992) 1269-1284.

[24] Yu. Gorbunov, B. Maksimov, Yu. Kabalov, A. Ivashchenko, O. Mel'nikov, N. Belov, "Crystal Structure of $Fe^{2+}{}_3Fe^{3+}{}_4(PO_4)_6$," Dokl. Akad. Nauk SSSR, 254 (1980) 873-877.

[25] L. Zhang, M.E. Schlesinger, R.K. Brow, "The Liquidus Surface of the $Fe_2P_2O_7$ – $Fe(PO_3)_2$ System," to be submitted.

Table I. Preparation recipes for iron phosphate compounds.

Compound	Batch materials	Preparation recipe
Fe_3PO_7	$FePO_4$, Fe_2O_3	950°C for 12 hours, then 1050 for 72 hours
$FePO_4$	$FePO_4 \cdot xH_2O$	Raw materials, 880°C for 12 hours
$Fe(PO_3)_3$	Fe_2O_3, $NH_4H_2PO_4$	Ammonia burn-off at 500°C overnight, thoroughly milled and then cooked at 800°C for 12 hours
$Fe_3(PO_4)_2$	$FePO_4$, Fe_2O_3	Reduced in forming gas at 680–690°C for 6 hours [*2]
$Fe_2P_2O_7$	$FePO_4$	Reduced in forming gas[*1] at 560°C for 6 hours[*2]
$Fe(PO_3)_2$	$FePO_4$, $NH_4H_2PO_4$	Ammonia burn-off at 500°C overnight, after thoroughly milled and then reduced in forming gas[*1] at 650 for 6 hours[*2]
Fe_9PO_{12}	Fe_2O_3, Fe, $FePO_4$	900°C for 12 hours in sealed ampoule
Fe_2PO_5	Fe_2O_3,$Fe_2P_2O_7$	900°C for 12 hours in sealed ampoule
$Fe_7(PO_4)_6$	Fe_2O_3, FeP_2O_6	900°C for 12 hours in sealed ampoule
$Fe_3(P_2O_7)_2$	$Fe(PO_3)_3$, Fe_2PO_5	900°C for 12 hours in sealed ampoule
$Fe_7(P_2O_7)_4$	$Fe_2P_2O_7$, $Fe_3(P_2O_7)_2$	900°C for 12 hours in sealed ampoule

*1: Forming gas is 10% H_2 and 90% Ar.
*2: Reducing time is related to the reducing gas flow and sample size.

Table II. Experimental conditions in the preparation of $Fe_4P_2O_9$.

Sealed conditions	**Heat-treatment**
$Fe_3(PO_4)_2$ +Fe +Fe_2O_3 in tubes	900°C (24 hr), cooled at 2°C/min
$Fe_3(PO_4)_2$ +Fe +Fe_2O_3 in tubes	700°C (24 hr), cooled at 2°C/min
$Fe_3(PO_4)_2$ +Fe +Fe_2O_3 in tubes	1000°C (24 hr), cooled at 2°C/min
$Fe_3(PO_4)_2$ +Fe +Fe_2O_3 in Al_2O_3 crucible	900°C (6 hr), cooled at 2°C/min
$Fe_3(PO_4)_2$ +Fe +Fe_2O_3 in Al_2O_3 crucible	900°C (5 days), cooled at <2°C/min
$Fe_3(PO_4)_2$ +Fe +Fe_2O_3 in Al_2O_3 crucible, with ~40mg $FeCl_2$ as mineralization agent	900°C (24 hr), cooled at 2°C/min
$Fe_3(PO_4)_2$ + Fe_2O_3	900°C (6 hr) in forming gas, cooled at 2°C/min

Table III. Thermal characterization temperatures of the compounds obtained in this work.

Composition	Melting (°C)	Decomposition (°C)	Method
	1380±24 [13]		Extrapolating
Fe_3PO_7		1090±5[13]	Quenching experiments +SEM/EDS
$FePO_4$	1208±5		DTA
$Fe_4(P_2O_7)_3$	910±5 945±8		DTA Quenching experiments+ OM/Raman
FeP_3O_9	1205±8		Quenching experiments +OM/Raman
$Fe_3P_2O_8$	>1200		Quenching Experiments +XRD
$Fe_2P_2O_7$	1100±8		Quenching Experiments +XRD
FeP_2O_6	945±8		Quenching Experiments +XRD
Fe_9PO_{12}	>1200		Quenching experiments +XRD
Fe_2PO_5	1145		Quenching Experiments +XRD
$Fe_7(PO_4)_6$	>1200		Quenching experiments +XRD
$Fe_3(P_2O_7)_2$		925±8	Quenching experiments +XRD
$Fe_7(P_2O_7)_4$	1015±8°C		Quenching experiments +XRD

Table IV. Assignment of the Raman spectra of $Fe_3(P_2O_7)_2$ compound in the range of 600-2000 cm^{-1}.

Raman	1140-1186 m	1100 vs	1035-1045s	759 vw	660 w	482 m
Assignment	$\nu_{as}(Q^1)$	$\nu_s(Q^1)$	$\nu_{as}(Q^1)$	ν_s(P-O-P)	$\delta_{as}(Q^1)$	$\delta_s(Q^1)$

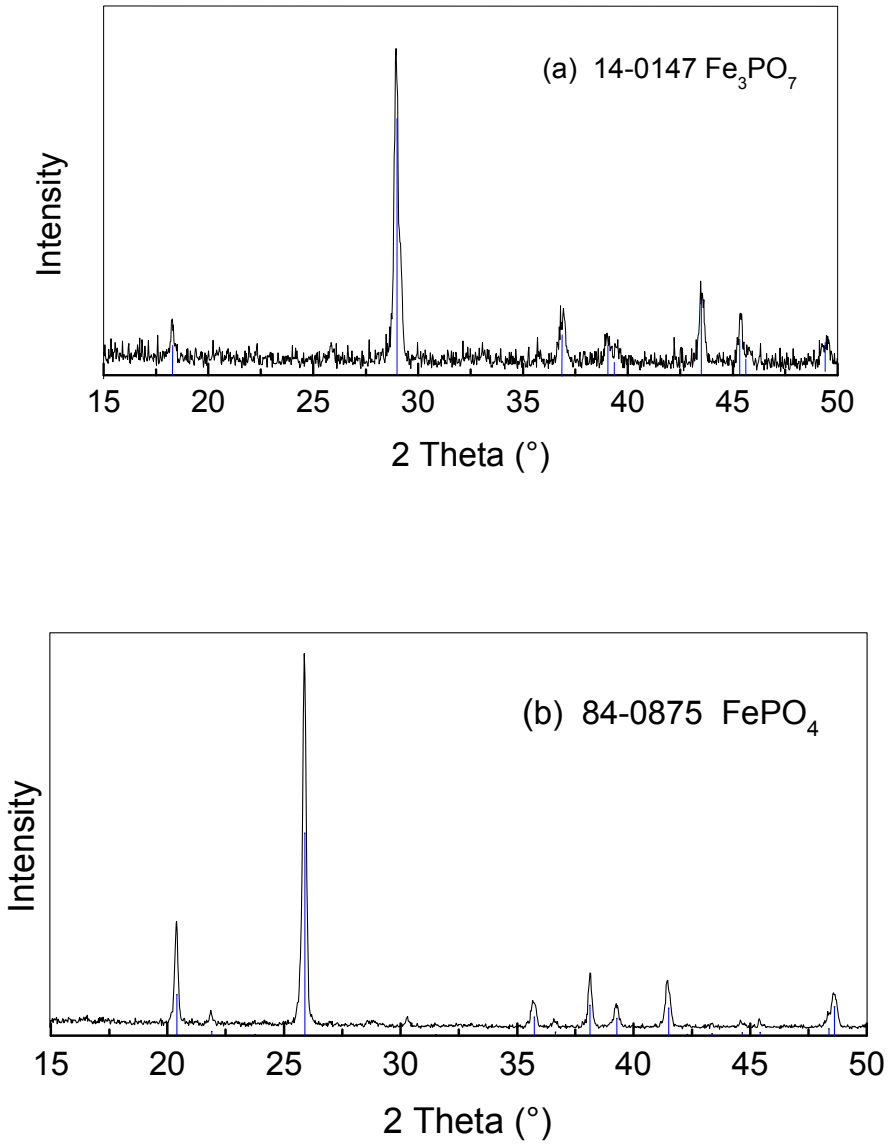

Figure 1: XRD patterns for ferric phosphate compounds.

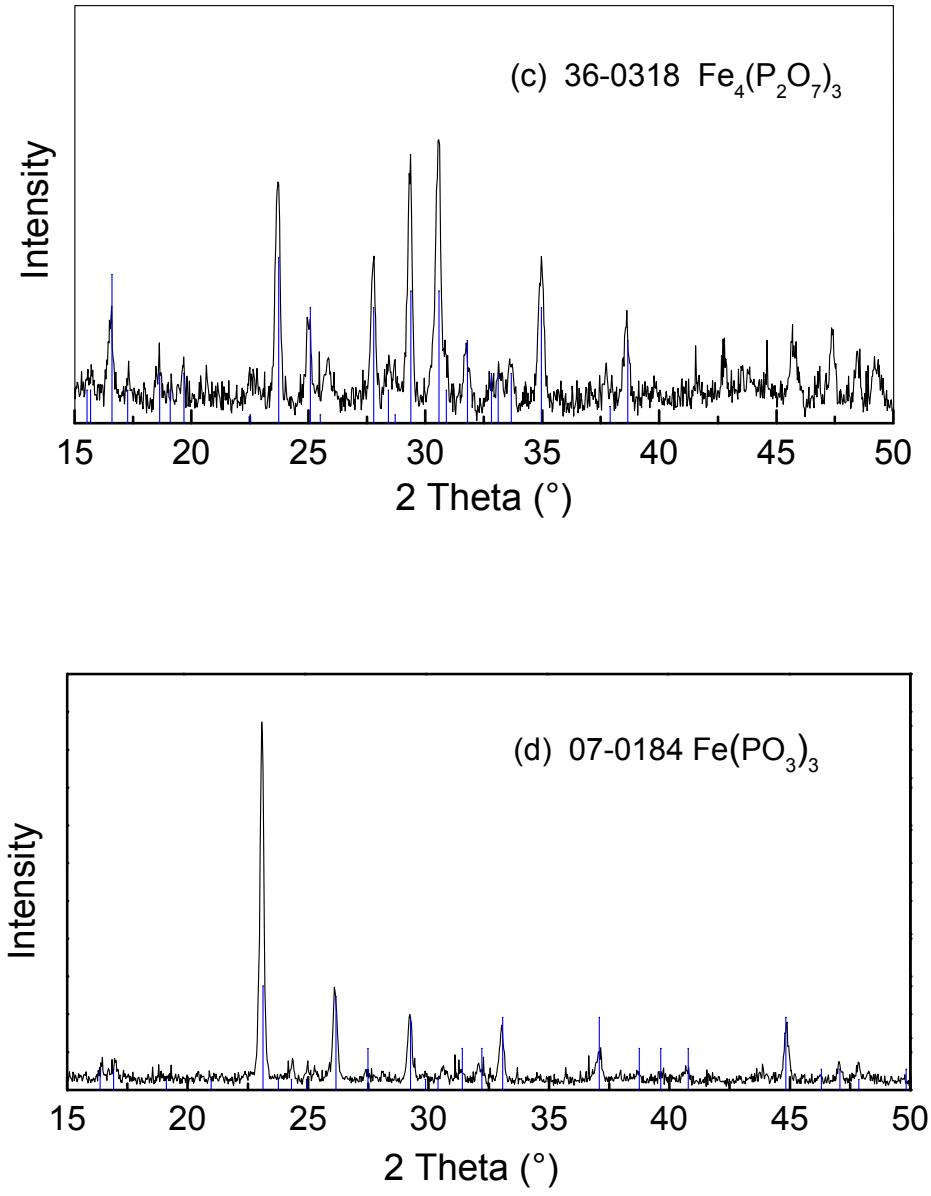

Figure 1: XRD patterns for ferric phosphate compounds.(cont.)

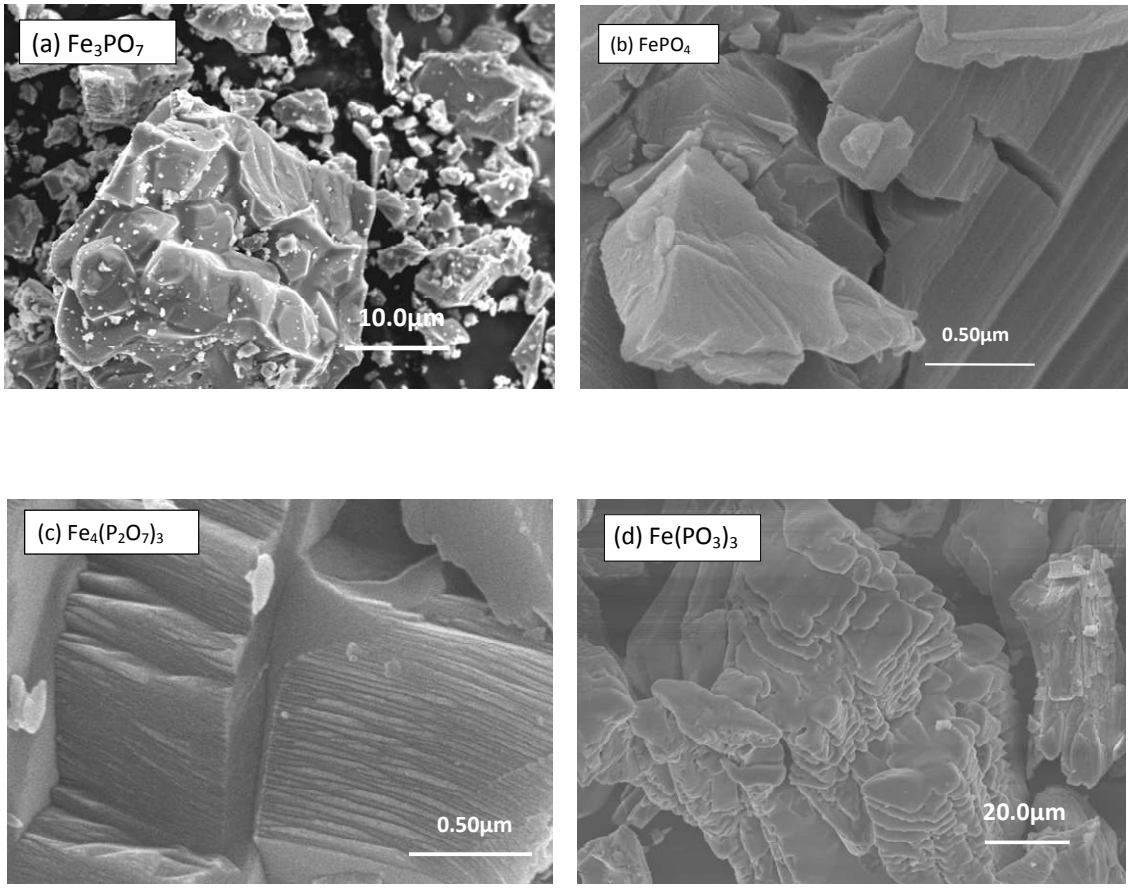

Figure 2: SEM images of the powders of ferric phosphate compounds.

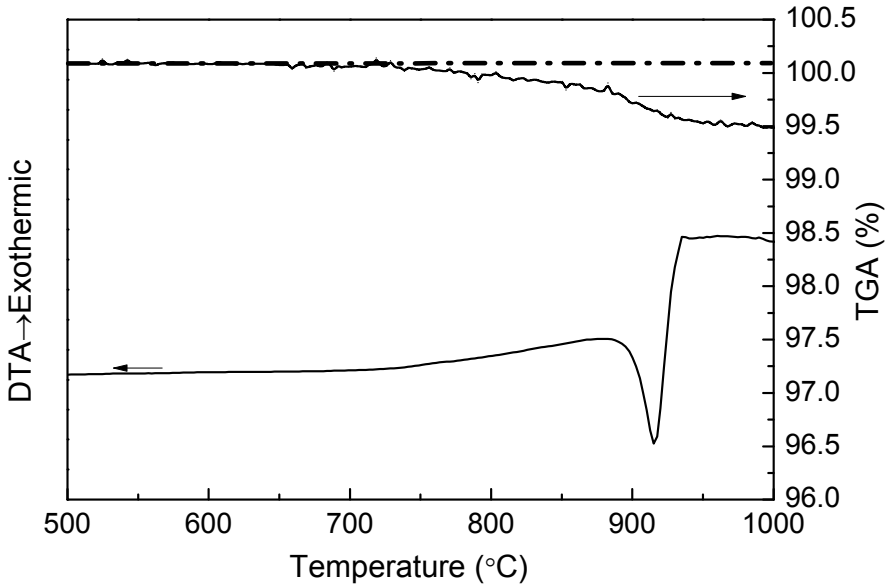

Figure 3: DTA and TGA of $Fe_4(P_2O_7)_3$ (in air).

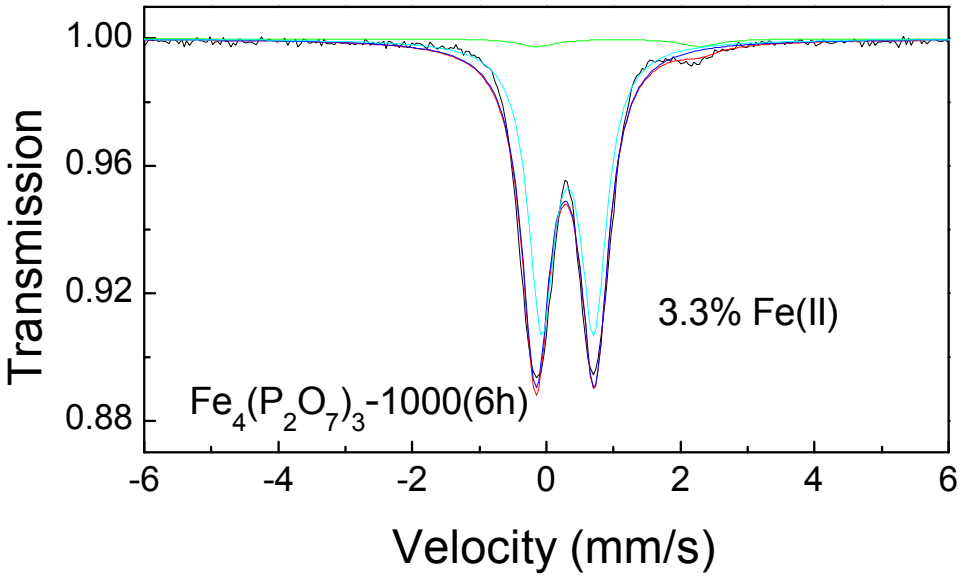

Figure 4: Mössbauer spectra of $Fe_4(P_2O_7)_3$ quenched after being heated at 1000°C for six hours.

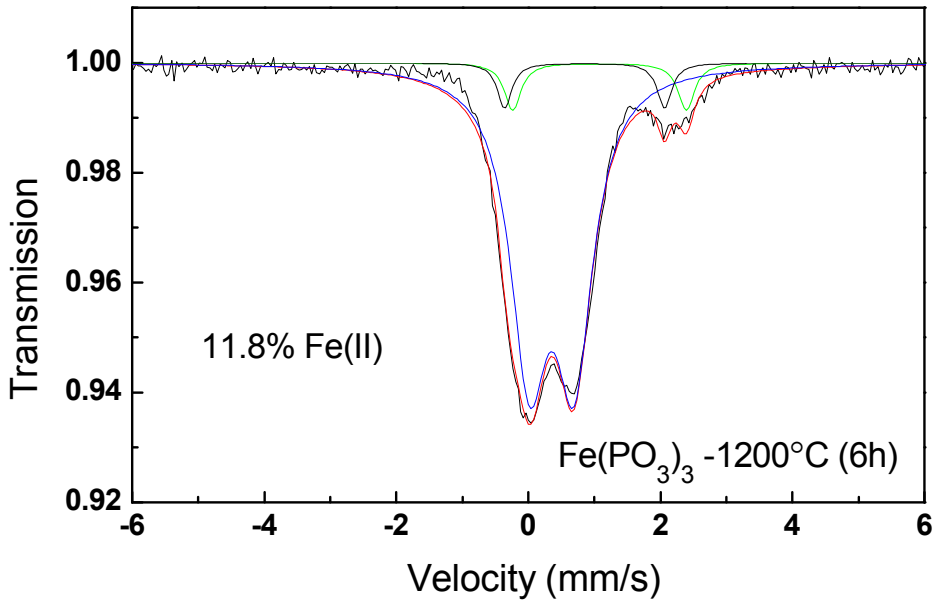

Figure 5: Mössbauer spectra of $Fe(PO_3)_3$ quenched after being heated at 1200°C for six hours.

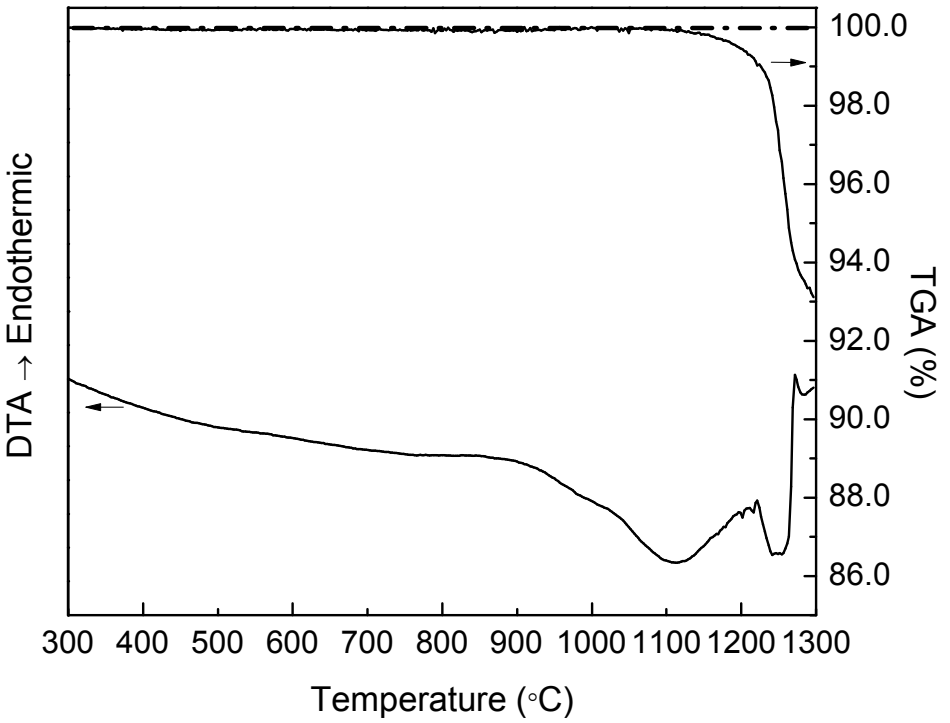

Figure 6: DTA and TGA of $Fe(PO_3)_3$ (in air).

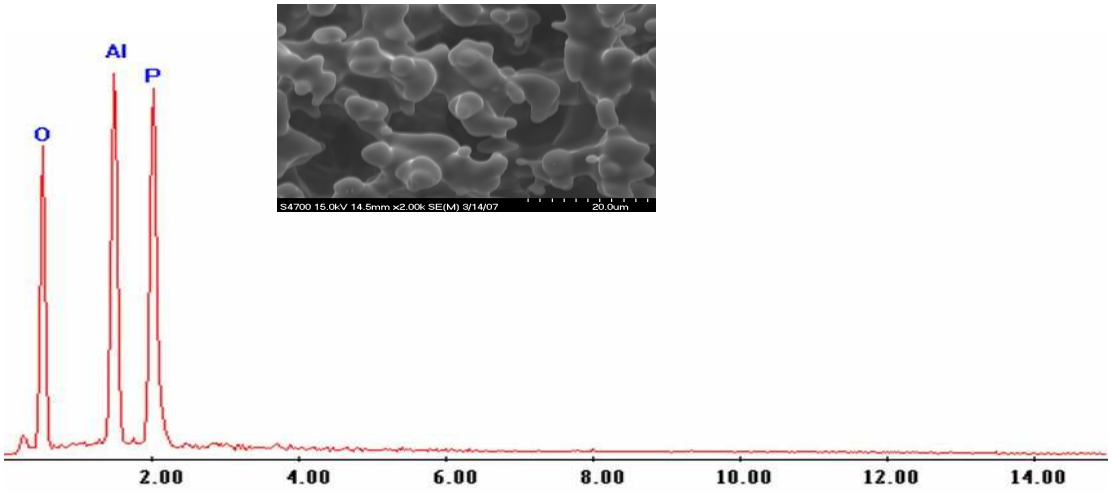

Figure 7: EDS captured at 15KV on the area shown in image.

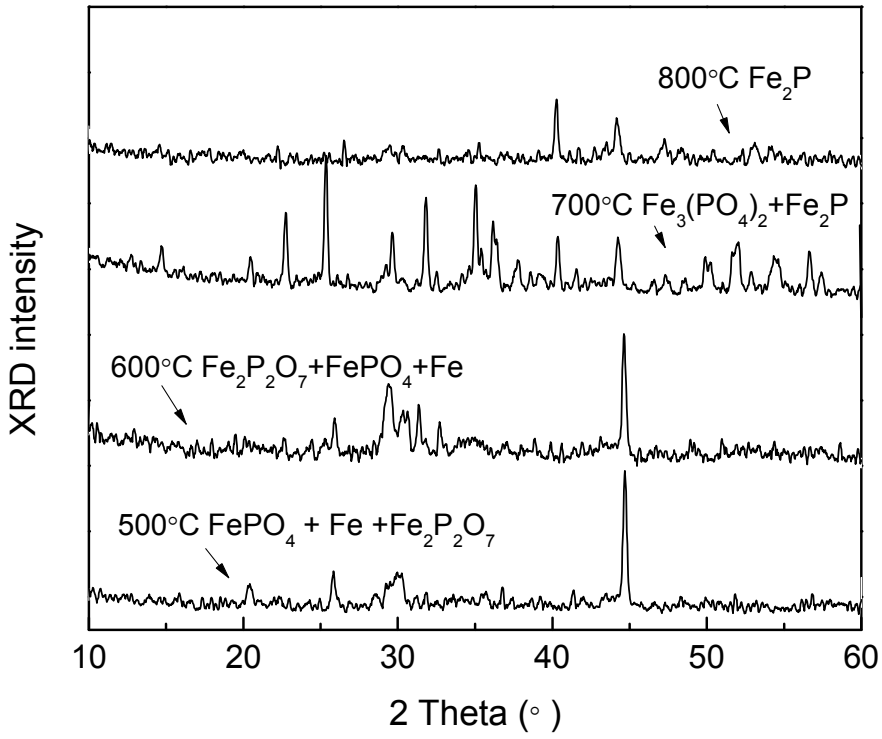

Figure 8: XRD collected for determination of the optimum reducing temperature range for producing compound $Fe_3(PO_4)_2$.

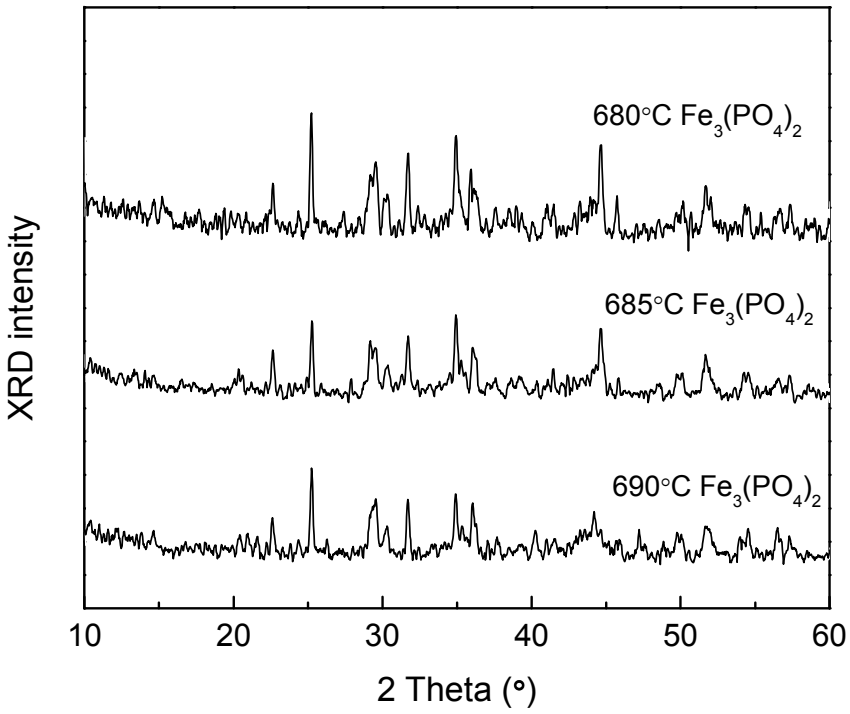

Figure 9: XRD collected to confirm the optimum reducing temperature for $Fe_3(PO_4)_2$.

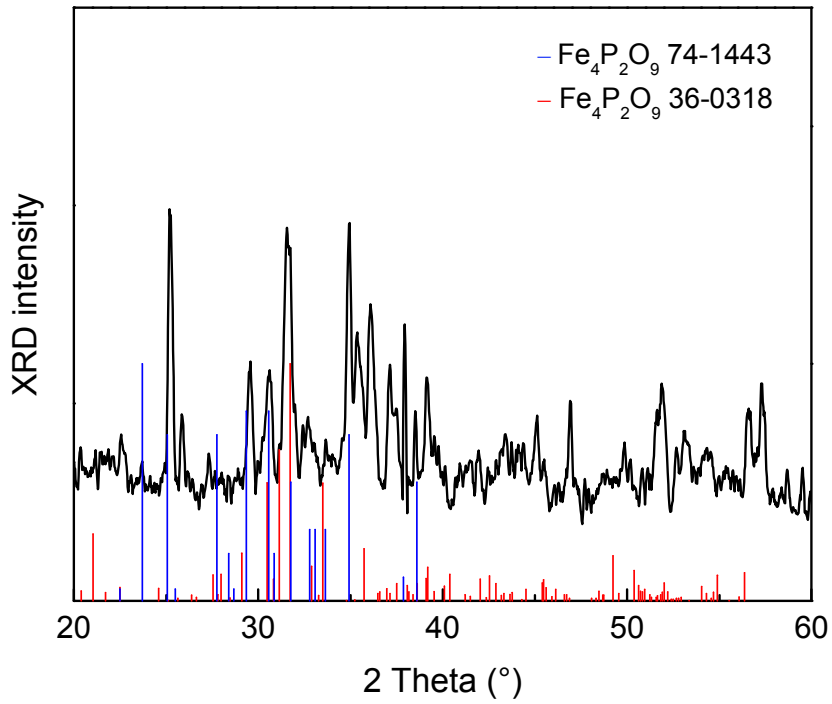

Figure 10: XRD of the samples with the composition as $Fe_4P_2O_9$ after being heated at 900°C for 24 hour in an Al_2O_3 crucible sealed under vacuum with $FeCl_2$ as mineralization agent.

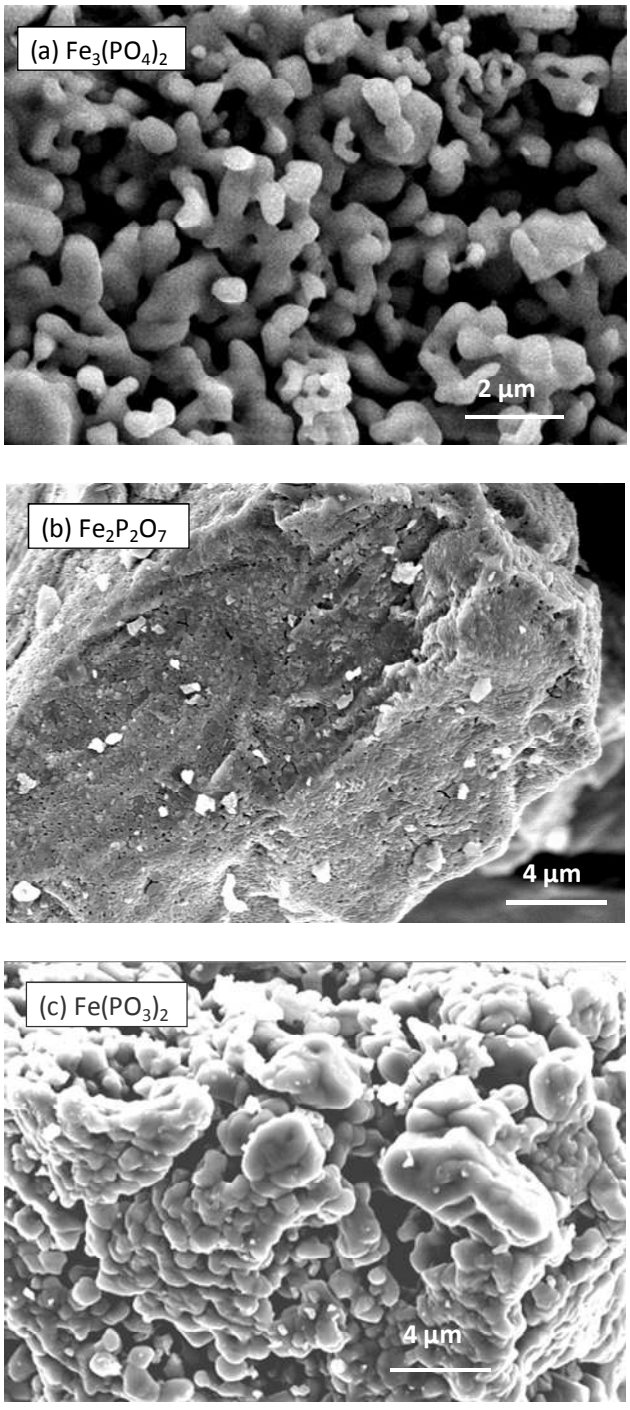

Figure 11: SEM images of the powder ferrous phosphates obtained by reducing ferric counterparts in forming gas (10%H_2+90%Ar).

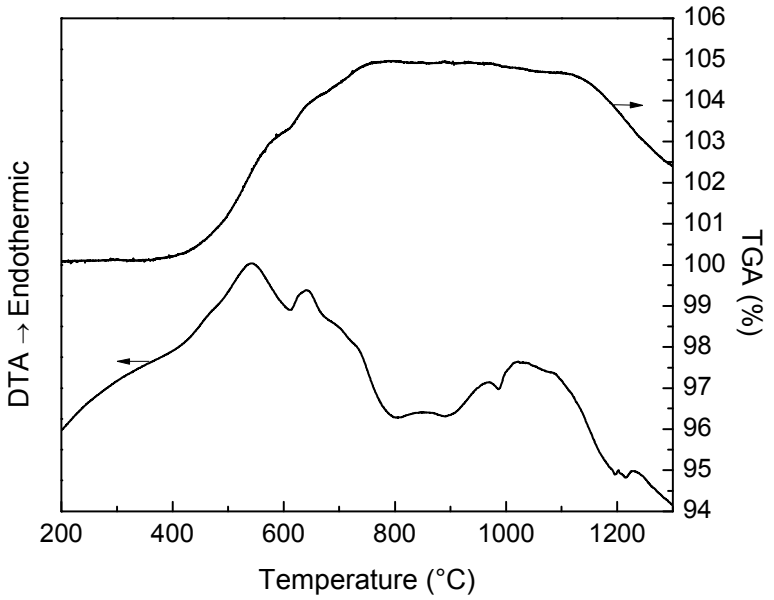

(a)

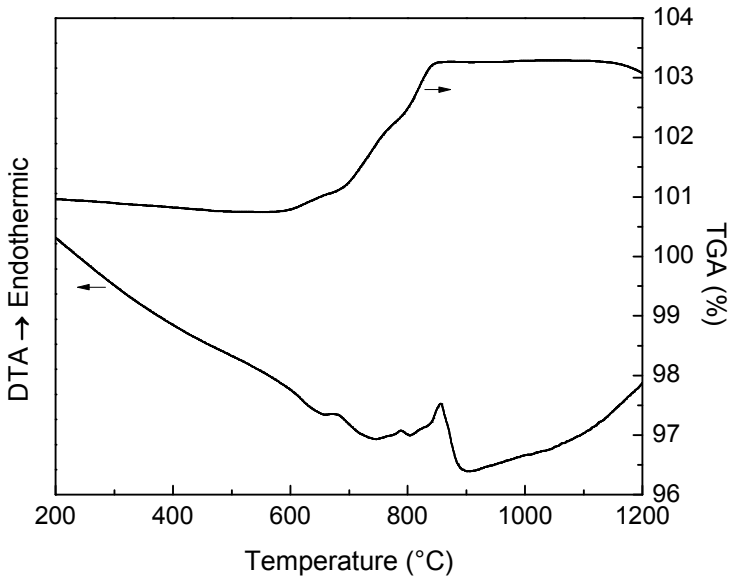

(b)

Figure 12 DTA and TGA patterns of (a) $Fe_2P_2O_7$ and (b) $Fe(PO_3)_2$ in Ar.

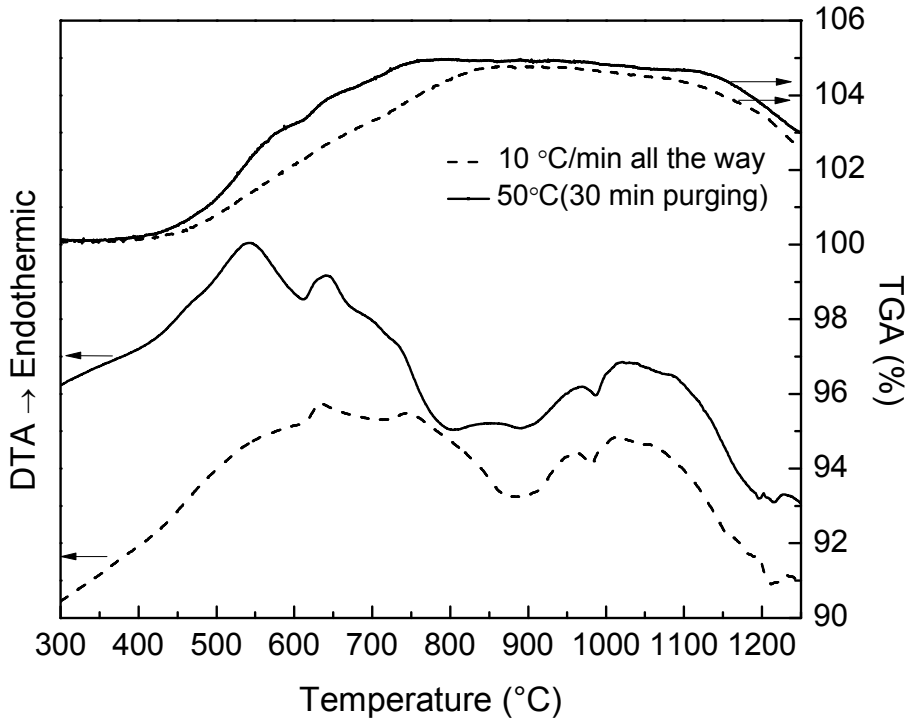

Figure 13: DTA and TGA of $Fe_2P_2O_7$ run at different settings (in Ar).

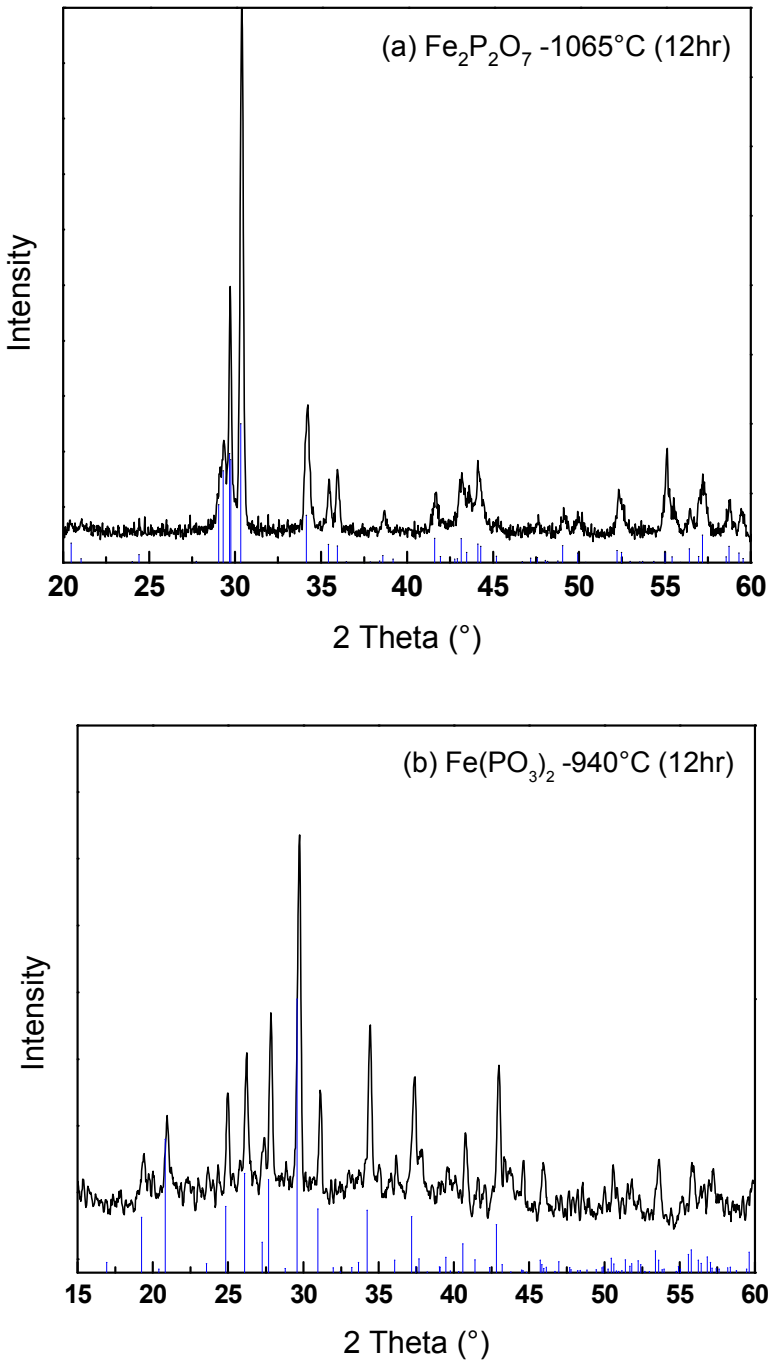

Figure 14: XRD patterns collected on the sealed samples (a)-$Fe_2P_2O_7$ and (b)-$Fe(PO_3)_2$. The blue ticks represent the position and intensity of standard phases.

#	Compound composition
#1	Fe_3PO_7
#2	$Fe_4P_2O_{11}$
#3	$FePO_4$
#4	$Fe_4(P_2O_7)_3$
#5	$Fe(PO_3)_3$
#6	$Fe_4P_2O_9$
#7	$Fe_3(PO_4)_2$
#8	$Fe_2P_2O_7$
#9	$Fe(PO_3)_2$
#10	Fe_9PO_{12}
#11	$Fe_5P_2O_{11}$
#12	Fe_2PO_5
#13	$Fe_5P_3O_{13}$
#14	$Fe_5P_4O_{16}$
#15	$Fe_7(PO_4)_6$
#16	$Fe_3(P_2O_7)_2$
#17	$Fe_7(P_2O_7)_4$

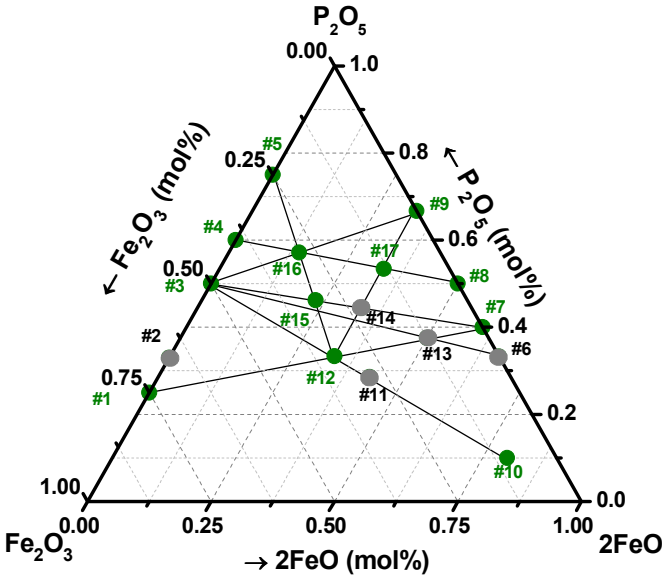

Figure 15: Ternary composition diagram with corresponding iron phosphate compounds.

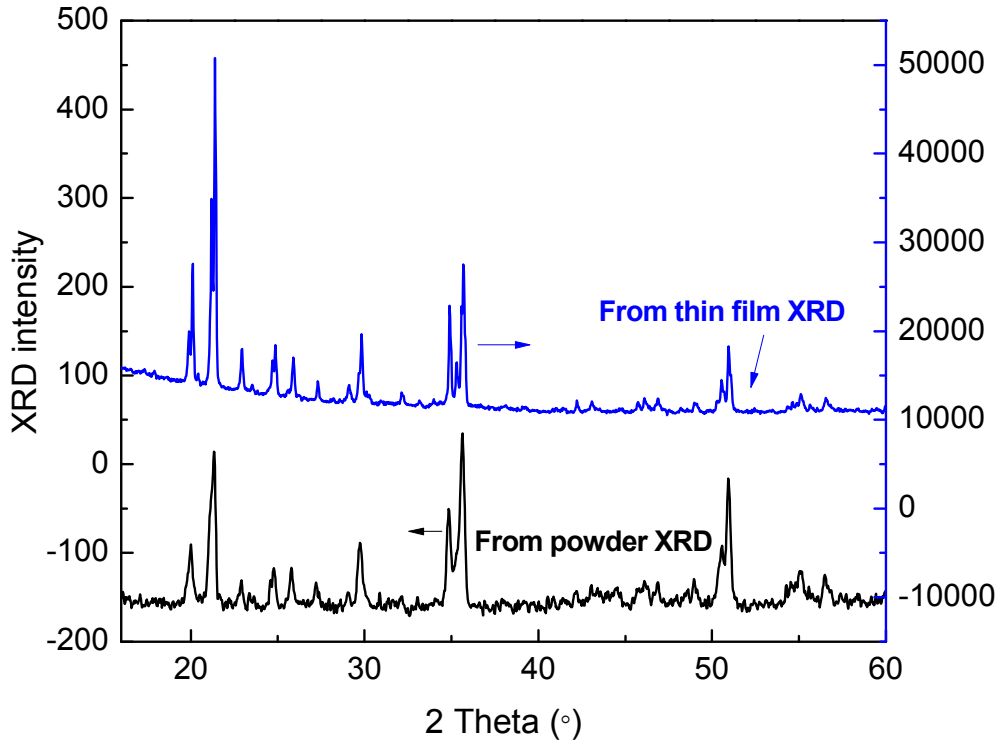

Figure 16: XRD patterns of powder $Fe_3(P_2O_7)_2$ [5] collected by two methods.

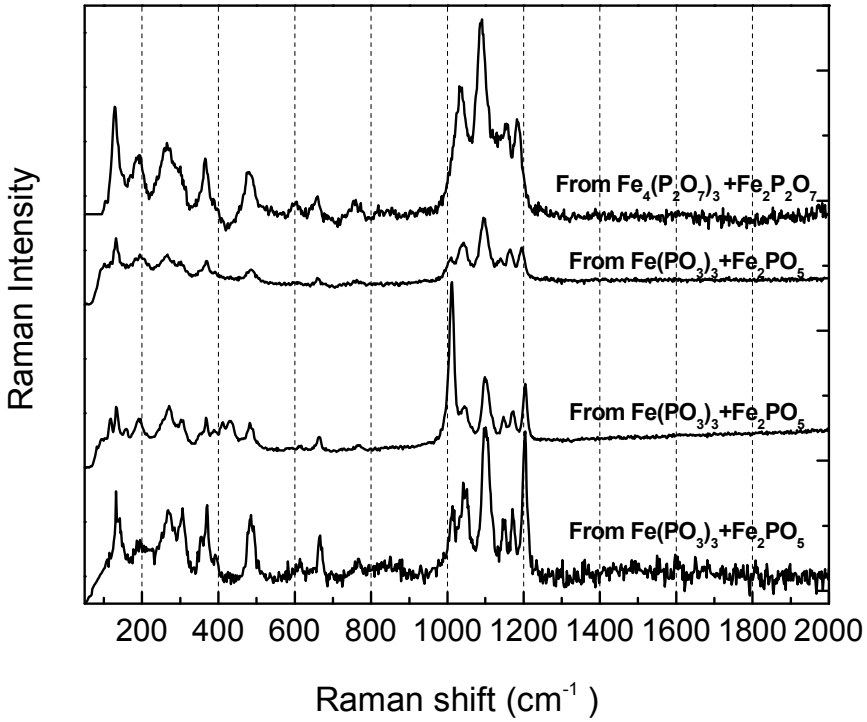

Figure 17: Raman spectra of $Fe_3(P_2O_7)_2$ crystalline powder from different batches.

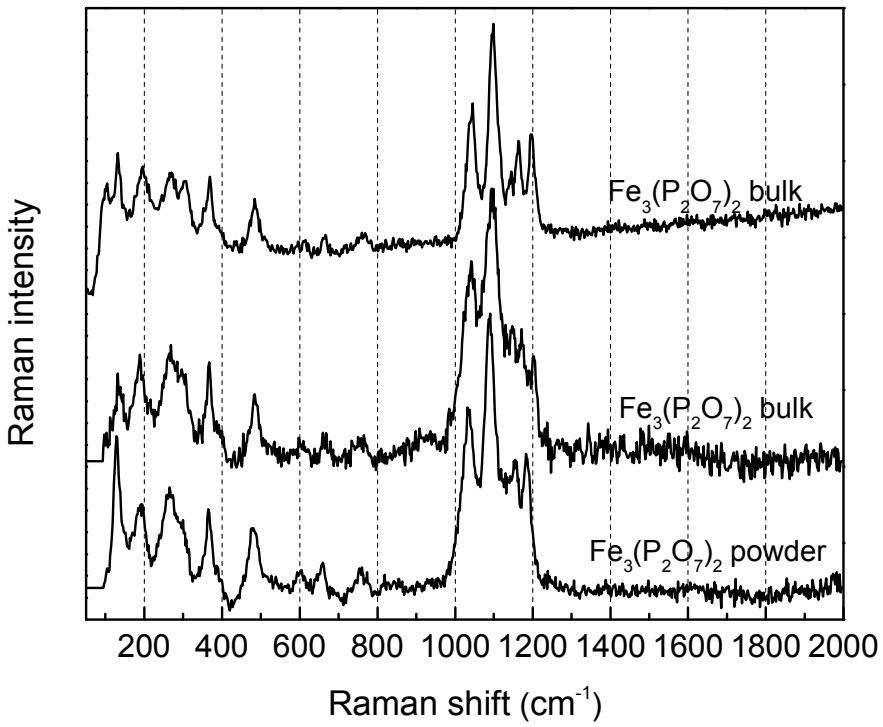

Figure 18: Raman spectra of $Fe_3(P_2O_7)_2$ bulk made from #A.

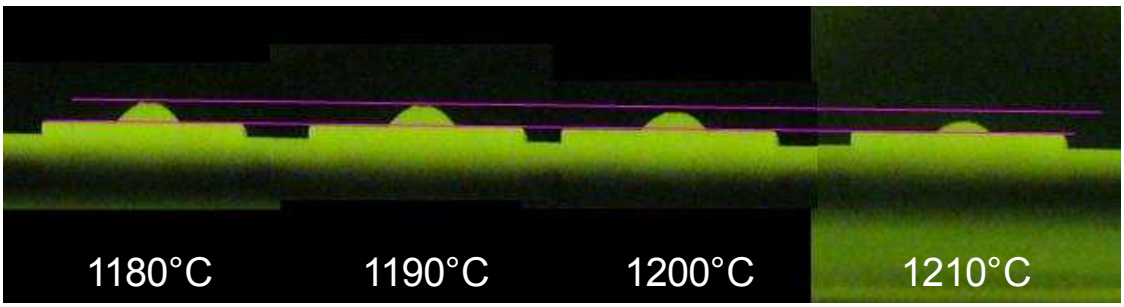

Figure 19: Images captured by digital camera on $FePO_4$ during heating in air at 2°C/min

APPENDIX B

THE LIQUIDUS SURFACE OF THE $Fe_2P_2O_7$ –$Fe(PO_3)_2$ SYSTEM

B. THE LIQUIDUS SURFACE OF THE $Fe_2P_2O_7$-$Fe(PO_3)_2$ SYSTEM

Liying Zhang[1], Mark E. Schlesinger[1*], Richard K. Brow[1]

[1]Department of Materials Science and Engineering, University of Missouri, Rolla, MO 65409

ABSTRACT

To determine the liquidus surface of the $Fe_2P_2O_7$-$Fe(PO_3)_2$ system, the ferrous phosphate compounds $Fe_2P_2O_7$ and $Fe(PO_3)_2$ were synthesized. Quenching experiments were used to determine liquidus temperatures, and a eutectic point at 52.8±0.5 mole% FeO and 935±8°C was determined.

1. INTRODUCTION

Four ferrous phosphate compounds, $Fe_4P_2O_9$, $Fe_3(PO_4)_2$, $Fe_2P_2O_7$ and $Fe(PO_3)_2$ are reported to exist in the FeO–P_2O_5 system [1,2,3,4]. Wentrup presented a phase diagram for the FeO-$Fe_3(PO_4)_2$ system [4] by recording the heating and cooling curves when heat-treating sealed samples under vacuum. A eutectic at ~81.8 mole% FeO and 1008°C was reported between FeO and $Fe_3(PO_4)_2$, and a solid–state transformation for $Fe_3(PO_4)_2$ was found at 942°C. Wentrup did not obtain the liquidus temperature of $Fe_3(PO_4)_2$ experimentally, but curve–fit the liquidus line to estimate a melting temperature of ~1230°C for $Fe_3(PO_4)_2$. Trömel and coworkers published a partial phase

* Corresponding author: Mark E. Schlesinger (mes@mst.edu)

diagram for the iron–rich end of "$FeO\text{-}P_2O_5$" in 1965[5], and this diagram is useful for the phase equilibria study of Fe-P-O slags in the metallurgical industry. They also did some isothermal studies of ferrous-rich phosphate melts. In this paper, the ferrous-rich phosphate system was not studied due to the difficulties in making glasses from those melts at the laboratorial quench rate. However, the $Fe_2P_2O_7$-$Fe(PO_3)_2$ system was studied in this work.

Hoggies mentioned that $Fe_2P_2O_7$ melts around 1200°C, without providing detailed information [6]. Glass formation in the ferrous phosphate system in the $xFeO \cdot (1\text{-}x)$ P_2O_5 ($0 \leq x \leq 0.50$) composition range melted at 1100°C was reported by Karabulut, et al. [7]. Those glasses melted in sealed ampoules under vacuum contained 6-18% $Fe(III)/Fe_{total}$. The melting conditions provide some information about the liquidus surface of those compositions. In this paper, the liquidus surface of the $Fe_2P_2O_7$–$Fe(PO_3)_2$ system was determined by quenching sealed samples from different temperatures and analyzing the results.

2. EXPERIMENTS

$Fe(PO_3)_2$ and $Fe_2P_2O_7$ were prepared by reducing ~20 grams of raw materials of the corresponding ferric phosphates under forming gas (10% H_2 and 90% Ar) at 560°C and 650°C for six hours [3]. The final products were characterized by X-ray diffraction (XRD Scintag XDS 2000). Compound powders (<53 μm) were used in the following experiments. The Fe/P ratio in several samples was analyzed using EDS to study the composition uncertainty, as described by [8].

Samples containing 0.6–1.0 g of mixture of $Fe(PO_3)_2$ and $Fe_2P_2O_7$ with different FeO content were sealed and heat-treated at different temperatures for 10-12 hours, followed by a fast quench into water. The samples were sealed under vacuum (< 0.07 atm) in 11 mm × 13 mm silica tubes. Table I shows the experimental temperature ranges for the compositions in this system. The quenched samples were pulverized and prepared for powder XRD. The liquidus temperatures were determined by characterizing samples from temperatures that bracket the expected liquidus temperature. The samples with 54.5 mol% FeO quenched from 940 and 970°C and samples with 64.1 mol% FeO quenched from 1050 and 1100°C after being heated for ~12 hours were pulverized to < 53 μm and dissolved into H_2SO_4 solutions (~5 M) for titration by $KMnO_4$ (2 mM) [9] to determine the Fe^{2+} content.

3. RESULTS

The XRD patterns in Fig. 1 indicate that the congruent melting temperature of $Fe(PO_3)_2$ is 945 ± 8°C. Combined with the measurement uncertainty, the error in the melting temperature is estimated to be ≤ 8°C. Using the same method, the congruent melting temperature of $Fe_2P_2O_7$ was determined to be 1105 ± 8°C.

Figure 2 shows the XRD patterns collected from several compositions quenched from temperatures below their respective liquidus temperatures, compared with the XRD patterns of crystalline $Fe_2P_2O_7$ and $Fe(PO_3)_2$. The crystalline phases identified in the quenched samples show which solid phase the melt was in equilibria with at the experimental temperatures. These results can be used to determine the liquidus temperatures and eutectic point of the $Fe_2P_2O_7$-$Fe(PO_3)_2$ system.

Figure 3 shows the liquidus curves obtained by fitting the experimental points. The $Fe_2P_2O_7$–$Fe(PO_3)_2$ system has a eutectic point at 52.8±0.5 mol% FeO and 935°C. The uncertainty in composition was estimated based on EDS analysis of several samples, and temperature uncertainty results from the combination of furnace and measurement uncertainty. To our knowledge, it is the first time to report the liquidus surface of $Fe_2P_2O_7$–$Fe(PO_3)_2$ system. The glass of $Fe(PO_3)_2$ in sealed ampoules can be melted at 1100°C [10], which is consistent with the results form this work. However, more work need to be done to evaluate the liquidus surface determined in this work.

4. DISCUSSION

In this work, the atmosphere in the sealed ampoules sets p_{O2} at ~0.01 atm at room temperature. Fe(II) and Fe(III) form an equilibria with oxygen at high temperature in sealed ampoules. From titration and mössbauer results, 5% of the Fe(II) in $Fe_2P_2O_7$ oxidized to Fe(III) after being heated at 1200°C for ~2 hours; and 3% and 19% of the Fe(II) in $Fe(PO_3)_2$ oxidized to Fe(III) after being heated at 1200°C for ~0.5 and 2 hours respectively [11].

The effects of the sealed atmosphere in this work on the iron oxidationstate after some heat-treatment were studied by titrating some quenched samples which are quenched from different temperatures. Table II lists the Fe(II)/ Fe_{tot} from titration as a function of temperature, and the corresponding liquidus temperatures obtained from this work. Based on these results, less than 15% of the Fe(II) in the samples oxidized during the process.

Partial oxidization (10 – 15 mol%) of Fe(II) changes the liquidus temperature by < 50°C, estimated based on our laboratory experience in quenching samples in sealed ampoules or in air. On the other hand, since crystallization happens during quenching and the crystal size depends on the quench rate and crystal growth kinetics, the liquidus temperature provided by the quench method could be higher than the ideal situation. The quantitative analysis might be done in the future.

ACKNOWLEDGEMENT

This work is supported by the National Science Foundation (U.S.A.) under Grant DMR-0502463.

REFERENCES

[1] M. Bouchdoug, A. Courtois, R. Gerardin, J. Steinmetz, C. Gleitzer, "Preparation et Etude D`un Oxyphosphate $Fe_4(PO_4)_2O$," J. Solid State Chem. 42 149-157 (1982).

[2] M. Ai, K. Ohdan, "Effects of Differences in the Structures of Iron Phosphates on the Catalytic Action in the Oxidative Dehydrogenation of Lactic Acid to Pyruvic Acid," Appl. Catal. A., 165 461-465 (1997).

[3] L. Zhang, M.E. Schlesinger, R.K. Brow, "Synthesis and Characterizations of Iron Phosphate Compounds," to be submitted.

[4] H. Wentrup, "Contribution on the System Iron-Phosphorus-Oxygen," Arch. Eisenhut. 9 57-60 (1935).

[5] G. Trömel, K. Schwerdtfeger, "A Study of the System Iron-Phosphorus Oxygen," Arch. Eisenhüt., 34 (1963) 55-59.

[6] J.T. Hoggins, "Crystal Structure of $Fe_2P_2O_7$," J. Solid State Chem. 47 278-283 (1983).

[7] M. Karabulut, E. Metwalli, D.E. Day, R.K. Brow, "Mössbauer and IR Investigations of Iron Ultraphosphate Glasses," J. Non-Cryst. Solids 328 199-206 (2003).

[8] L. Zhang, M.E. Schlesinger, R.K. Brow, "Phase Equilibria in the Fe_2O_3-P_2O_5 System," accepted, Apr. 2010.

[9] S. I. Grishin, J. M. Bigham, O. H. Tuovinen, "Characterization of Jarosite Formed upon Bacterial Oxidation of Ferrous Sulphate in a Packed-Bed Reactor," Appl. Environ. Microbiol. 54 3101-3106 (1988).

[10] U. Hoppe, M. Karabulut, E. Metwalli, R.K. Brow and Póvári, "The Fe-O Coordination in Iron Phosphate Glasses by X-Ray Diffraction with High Energy Photons," J. Phy.: Condens. Matter. 15 6143-6153 (2003).

[11] L. Zhang, R.K Brow, M.E. Schlesinger, "A Raman Study of Iron-Phosphate Compounds and Glasses," J. Am. Ceram. Soc., submitted in Jun. 2010.

Table I Quench temperatures for each composition in $Fe_2P_2O_7$-$Fe(PO_3)_2$ system.

FeO mol%	Temp. range (°C)
50	900, 1000, 950, 940
50.9	900, 960, 930, 950, 940
52.1	920, 950, 930, 940, 935,945
52.3	920, 960, 940, 930
52.6	930, 970, 940, 950, 945, 955
53.1	930, 970, 940, 950
54.5	930, 970, 950, 960
56.5	950, 1050, 1000, 1010
58.8	1000, 1050, 1020, 1030
64.1	1050, 1100, 1080, 1090
66.47	1050, 1140, 1090, 1110, 1100

Table II Titration results and liquidus temperatures obtained from this work.

Initial FeO (mol%)	Heat treatment	Fe(II) /Fe_{tot}	Liquidus temperature
50.0	1200°C (0.5hr)	0.97 ± 0.01	945°C
50.0	1200°C (2hr)	0.89 ± 0.04	
54.4	940°C (12hrs)	0.85 ± 0.01	955°C
54.5	970°C (12hr)	0.86 ± 0.01	
64.1	1050°C (12hr)	0.86 ± 0.01	1085°C
64.1	1100°C (12hr)	0.89 ± 0.01	
66.7	1200°C (2hr)	0.95 ± 0.04	1105°C

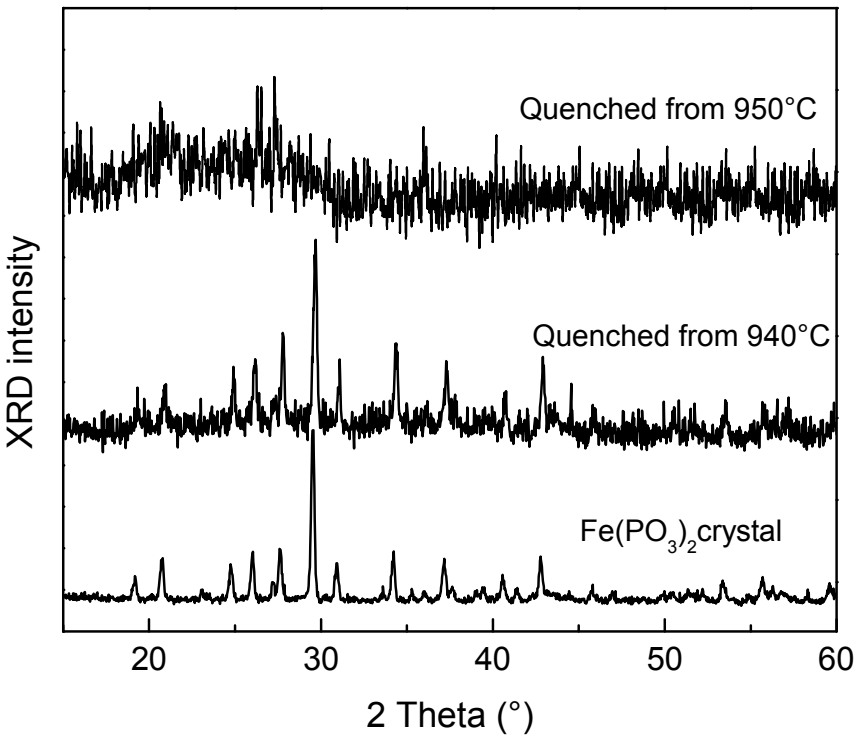

Figure 1: XRD patterns of $Fe(PO_3)_2$ crystals and samples quenched from 940 and 950°C.

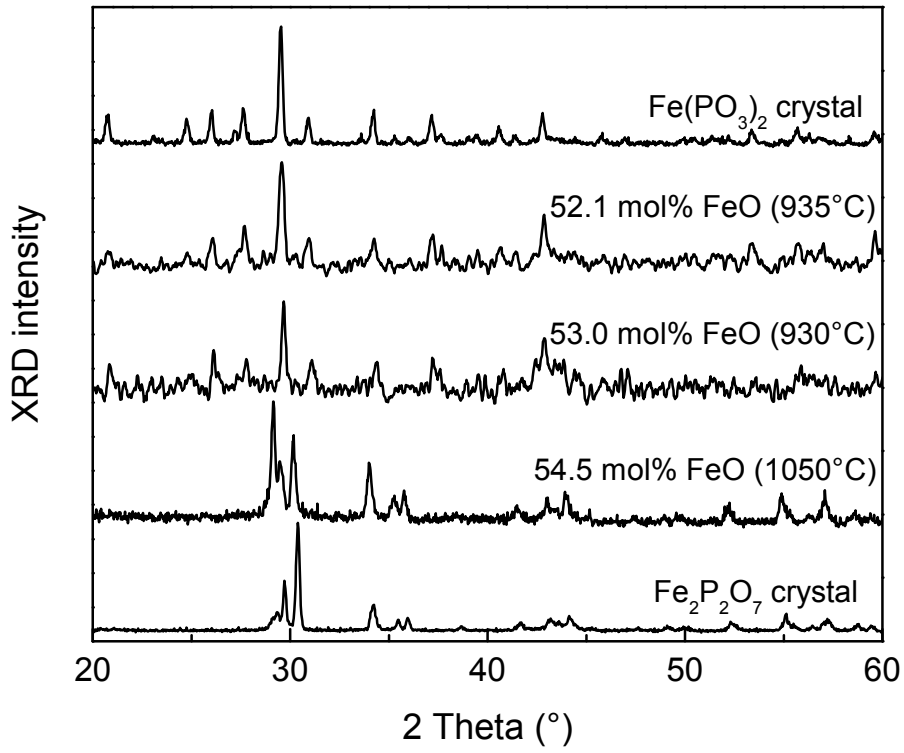

Figure 2: XRD patterns of the samples after heat-treatment at various temperatures, compared with the patterns for $Fe_2P_2O_7$ and $Fe(PO_3)_2$.

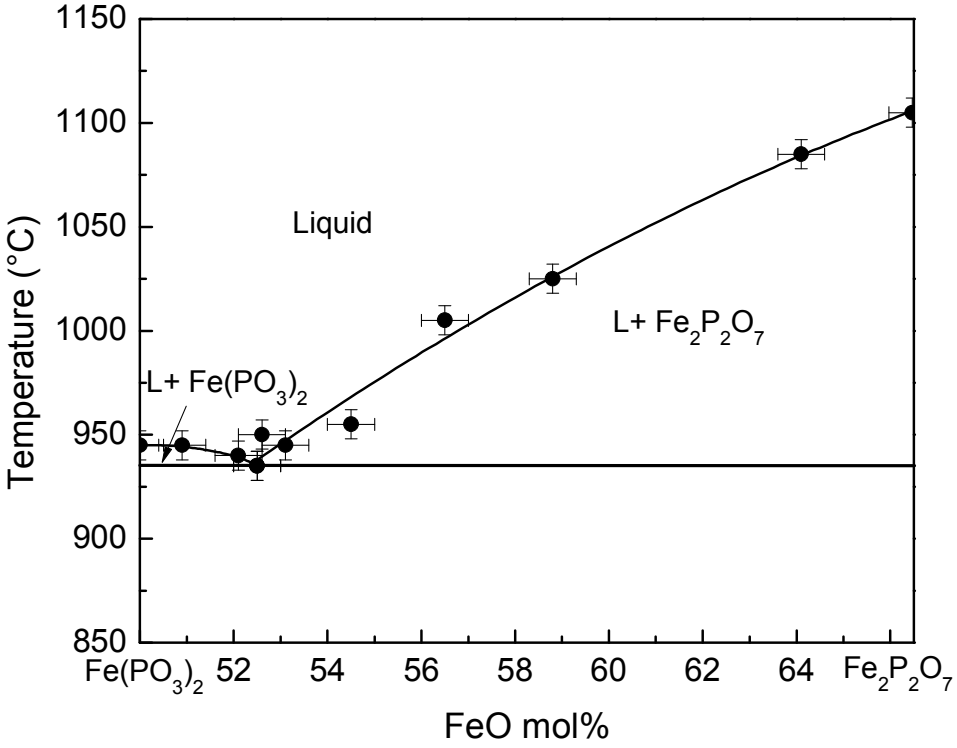

Figure 3: Liquidus surface obtained by analysis of quenched samples.

SECTION

3. SUMMARY AND AFTERWORDS

This section summarizes the overall conclusions drawn from the research reported in this dissertation. After this summary, suggestions for future experiments are provided.

1. The liquidus surface of the Fe_3PO_7–$Fe(PO_3)_3$ system was re-determined using sample preparation techniques that minimize the effects of sample volatilization and reduction. Four ferric phosphate compounds were identified: Fe_3PO_7, $FePO_4$, $Fe_4(P_2O_7)_3$ and $Fe(PO_3)_3$. Fe_3PO_7 is the only ferric oxo-phosphate compound detected and it decomposes in air at 1090°C. The congruent melting point of $FePO_4$ (1208°C) is similar to what has been reported, but $Fe_4(P_2O_7)_3$ melts congruently at 945°C, about 300°C lower than claimed by Wentrup. $Fe(PO_3)_3$, whose melting temperature has not been previously reported, melts congruently at 1205°C. Eutectic points exist at 58.0 mole% Fe_2O_3 (1070°C), 42.7% Fe_2O_3 (925°C), and 37.0% Fe_2O_3 (907°C). These results are consistent with reports in the literature for the thermal behavior of ferric phosphate crystalline compounds and for the formation of glasses from ferric phosphate melts.
2. The development of new information about the liquidus surface of the Fe_3PO_7–$Fe(PO_3)_3$ system has made it possible to extend studies of glass formation and structure to iron-rich compositions, with nominal Fe/P ratios in the range 1.0-1.6. Critical cooling rates estimated from characteristic temperatures obtained by differential thermal analyses, as well as the liquidus temperatures, are at least 10^3 times greater for the new iron-rich compositions than for the conventional iron phosphate melts (1-10°C/sec). These greater critical cooling rates are consistent

with lower melt viscosities at the respective liquidus temperatures, and are consistent with glass (and melt) structures that are based on isolated phosphate tetrahedra (Q^0) linked to the Fe(II) and Fe(III) polyhedra.

3. The stability against crystallization of glasses prepared in the course of the study of the liquidus surface of the $Fe_4(P_2O_7)_3$- $Fe_3(PO_3)_3$ system was investigated. These compositions are similar to those under investigation for use as hosts for nuclear wastes. Characteristic temperatures (glass transition temperature, T_g and crystallization temperature, T_x) obtained by differential scanning calorimetry, were used with the respective liquidus temperatures (T_L) to calculate stability parameters as a function of glass composition. In general, these stability parameters decrease with increasing O/P and Fe/P ratios, meaning that the glasses more easily crystallize as the nominal composition changes from $Fe_3(PO_3)_3$ to $Fe_4(P_2O_7)_3$ and the average polyphosphate chain length decreases. Thus, predictions about glass-forming tendency in the iron phosphate system require more than information about eutectic compositions, where the differences between T_L and T_g are expected to be least, but also on the viscosities of melts near T_L, which will depend on the glass structures.
4. Raman spectra were collected from iron ortho-, pyro- and metaphosphate compounds, and compared to those collected from glasses with similar nominal compositions. Complex spectra from many of the crystalline compounds showed multiple peaks due to symmetric and asymmetric vibrational modes associated with inequivalent bond distances, and these spectra help interpret similar features in the spectra of the relevant glasses. Decomposition of the Raman spectra from

the polyphosphate glasses suggests that the distributions of phosphate anions are generally broader than expected simply from the nominal O/P ratio, and this greater structural complexity is likely related to enhanced glass-forming tendency of the iron phosphate compositions, compared with other phosphate melts. A correlation reported in the literature between the Raman peak position for P-O stretching modes and the average P-O bond for crystalline phosphates was shown to hold for the crystalline iron phosphates prepared in this study, and this same correlation provides an estimate of the average P-O bond distances in the iron phosphate glasses that is in good agreement with reports in the literature from high energy diffraction studies of similar glasses.

5. Quenching experiments were used to determine liquidus temperatures, and a eutectic point at 52.8±0.5 mole% FeO and 935±8°C was determined.

The research presented in this dissertation provides much information about the phase equlibria in iron phosphate system, and glass forming ability, stability and structures of iron phosphate glasses. However, there are many unanswered questions that could be addressed in future studies.

1. The determination of thermal parameters of iron phosphate compounds: In this work, efforts were made to control the valence change from initial composition caused by redox reaction and phosphorus loss. The redox reaction is affected by atmosphere, composition and temperature. Some studies of Fe(II) /Fe_{total} ratio as a function of temperature and composition under atmospheric pressure were carried out for glasses from the Fe_3PO_7-$FePO_4$ and $Fe_4(P_2O_7)_3$-$Fe(PO_3)_3$ systems (see

paper II and III). However, that work is limited and a more systematic study of iron redox reactions, including thermodynamic modeling, in the iron phosphate system is needed. The thermodynamic data, including Gibbs energy of fusion, entropy and enthalpy, have rarely been reported for the iron phosphate system, which makes the theoretical calculation of phase equilibria or liquidus surface difficult. Therefore, experiments for the determination of above thermal parameters of iron phosphate compounds will help verify the phase diagram determined in this work.

2. Quantitative studies and control of phosphorus loss: The present study observed that the Fe/P ratio changes with composition, time, and temperature. Generally, Fe/P ratio increases with heat-treatment time and temperature. Phosphorus loss starts significantly around the melting or decomposition temperature of phosphate compounds. Sealed tubes help to prevent the loss of phosphorus at high temperature based on the results reported in the paper 1 and in Appendix A. Based on the laboratory experience, when melting phosphate glass, the glass composition changes from the original batch due to Fe(III) reduction and phosphorus loss. DTA/TGA with mass spectrometry can provide much information about the gas released from the sample at different temperature, providing information about thermal capacity of the compound, which is very helpful to determin the reaction and thermal parameters about phosphorus volatility. About the control of phosphorus loss, phase stability experiments in a (P_2O_5) vapor atmosphere will be very intresting to do. Before setting up melting experiments in a P_2O_5 atmosphere, the calculation about the equilibrium partial

pression of P_2O_5 for iron phosphates using thermaldynamic data such as Gibbs free energy of initial compound and o f final product at different temperatures will be very helpful. A similar approach can be used to control the redox reaction of iron, like setting up property partial pressure of O_2 at different temperature based on the modeling or calculation for the compounds.

3. Purification of iron phosphate compounds made in this work: Powder XRD analysis was the principal way that iron phosphate compounds were identified in this work. The resolution of powder XRD (Scintag XDS 2000) cannot detect ~2% impurity if any other crystal as impurtiy exists in the compound. However, in some of the future studies, like Raman spectra and Mössbauer studies, impurities could make the spectral interpretation more difficult. The iron phosphate compounds prepared in this work are not single crystals, and could be different from what is reported based on XRD database in terms of crystalline parameters. Therefore, when Raman spectra are used to predict structure parameters, some of the bands cannot be easily assigned to exact bonds, which makes the prediction of P-O distance in glasses less precise. In the future, attempts could be made to grow single crystals of iron phosphate compounds to support studies of crystal and glass structures.
4. Extend the current liquidus surface: In the present work, the studies of ferrous phosphate system are focused on the glass forming area ($Fe_2P_2O_7$ – $Fe(PO_3)_2$ system). Sealed tubes were used to reduce the effect of valence change of iron and loss of phosphorus. But heat conduction takes some time (<10 seconds for the sample quenched below 1250°C based on laboratory experience) when quenching

samples, although very thin (~1 mm) silica glass tubes were used in this work. In the future, experiments that can reduce or eliminate the above effects, need to be designed for the determination of ferrous, and mixed-valence phosphate systems, based on the results in this dissertation.

5. Need to sort out the role of melt viscosity, structure and glass-forming tendency…

VITA

Liying Zhang was born on Nov 19th, 1979 in Xinle, Hebei Province, P.R. China. Liying did a good job in coursework and after-class activities. Before entering university, Liying was the monitor in high school and elementary school. Liying won a third prize in Hebei Youngsters' paper contest with her small paper on noise pollution in 1996. Holding fast to her dreams, Liying entered Tongji University, Shanghai and started her bachelor's study on Materials Science and Engineering in 1998. Due to her hard work, Liying received six honors and awards during her undergraduate studies. In 2002, Liying got her Bachelor's degree with "the simulation of gas flow in annealing kiln" and was recommended for Master's candidate without taking any tests. Liying continued her master's study in materials on simulation of tin flow and temperature distribution in float glass process. Her hard work produced three journal publications.

After her graduation, Liying was employed by SMIC (Semiconductor Manufacturing International Corporation), Shanghai and worked as a Customer Quality Engineer. Following her husband to Rolla, U.S. in 2006, Liying found her real interest still in materials. So in the summer of 2006, Liying applied and was accepted by the Department of Materials Science and Engineering, Missouri University of Science and Technology. She started her Ph.D. study under the supervision of Drs. Schlesinger and Brow. During her Ph.D studies, Liying worked on the phase diagram of iron phosphate and glass studies based on phase diagram. Her doctoral work led to four peer-reviewed journal papers, three posters and four oral presentations at U.S. or international conferences.